Lottah Mining Pty Ltd

Annual Report

for

EL18/2007

For the period

July 2015 - July 2016

Prepared by:

Andrew Rae: Geologist

Lottah Mining Pty Ltd

15 Anglesea Street

Wivenhoe, Tasmania 7320

1. Foreword

1.1 Function of the Annual Report

This Annual Report has been prepared as a public document for submission to Mineral Resources Tasmania (MRT). The report provides a summary of the exploration activities undertaken by Lottah Mining Pty Ltd on EL18/2007 during July 2015 - July 2016.

1.2 Role in the Regulation Process

This document fulfils the role of an Annual Report on EL18/2007 for the period July 2015 - July 2016, as required under Section 28 of the *Mineral Resources Development Act 1995*.

1.3 Datum

Geocentric Datum MGA94, zone 55 has been used for this report unless otherwise stated.

Distribution

1 x Mineral Resources Tasmania

1 x Lottah Mining Pty Ltd – Sydney Office

1 x Lottah Mining Pty Ltd – Wivenhoe Field Office

Executive Summary

This report covers exploration activities completed on EL18/2007 for the period July 2015 – July 2016. The EL forms part of a tenement package prospective for Magnetite and Tungsten mineralisation around the House Top Granite in NW Tasmania.

During the term the company continued assessment of existing geological data on the remainder of the tenement outside of the now granted mining lease. Three project areas were chosen to focus on, based on the available magnetic surveys, indicating magnetic highs, for potential magnetite. These were;

1) The L13 deposit. This deposit exhibits a strong magnetic high and sits north of and along strike from the existing Kara orebody giving it a high priority rating for the company. During the period the company had a UAV magnetic survey completed as well as a ground based gravity survey. Potential drill sites were discussed for future work with an initial drill proposal being submitted to MRT. However, the approval was put on hold at the company's request.
2) The Rogetta South deposit. This deposit is also represented by a magnetic high and located near to Kara Mines deposit number 2. A first pass reverse circulation drill program had already been completed at the deposit in the previous reporting year and a gravity survey was completed to help delineate the deposit as the company had access to a gravity machine.
3) The Suttons Skarn deposit. To date the company has done little work on this deposit but it was decided to complete a gravity survey over the deposit as a first pass due to the availability of the gravity machine. During this survey the gravity machine was irretrievably damaged with most of the data being lost and the survey not completed.

Contents

Table & Figure Contents

1 INTRODUCTION

The Blythe River Iron Project (BRIP) consists of a number of small to medium size magnetite skarn deposits located in NW Tasmania, approximately 30km south of Burnie. Exploration is focused on resource delineation of semi massive to massive magnetite deposits to provide a resource base for a magnetite mining operation for the iron ore market.

Work Completed on EL18/2007 during the period of July 2015 – July 2016 was mostly focused on the potential magnetite deposit known as L13. Work completed on L13 included conducting a gravity survey, UAV magnetic survey, geophysical modelling, the planning of a drilling program and general ground reconnaissance. However, two other deposits, Rogetta South and Suttons Skarn were also targeted for the completion of gravity surveys during the period. Other work on EL18/2007 included historic drill core and data analysis, geological reconnaissance and minor track maintenance.

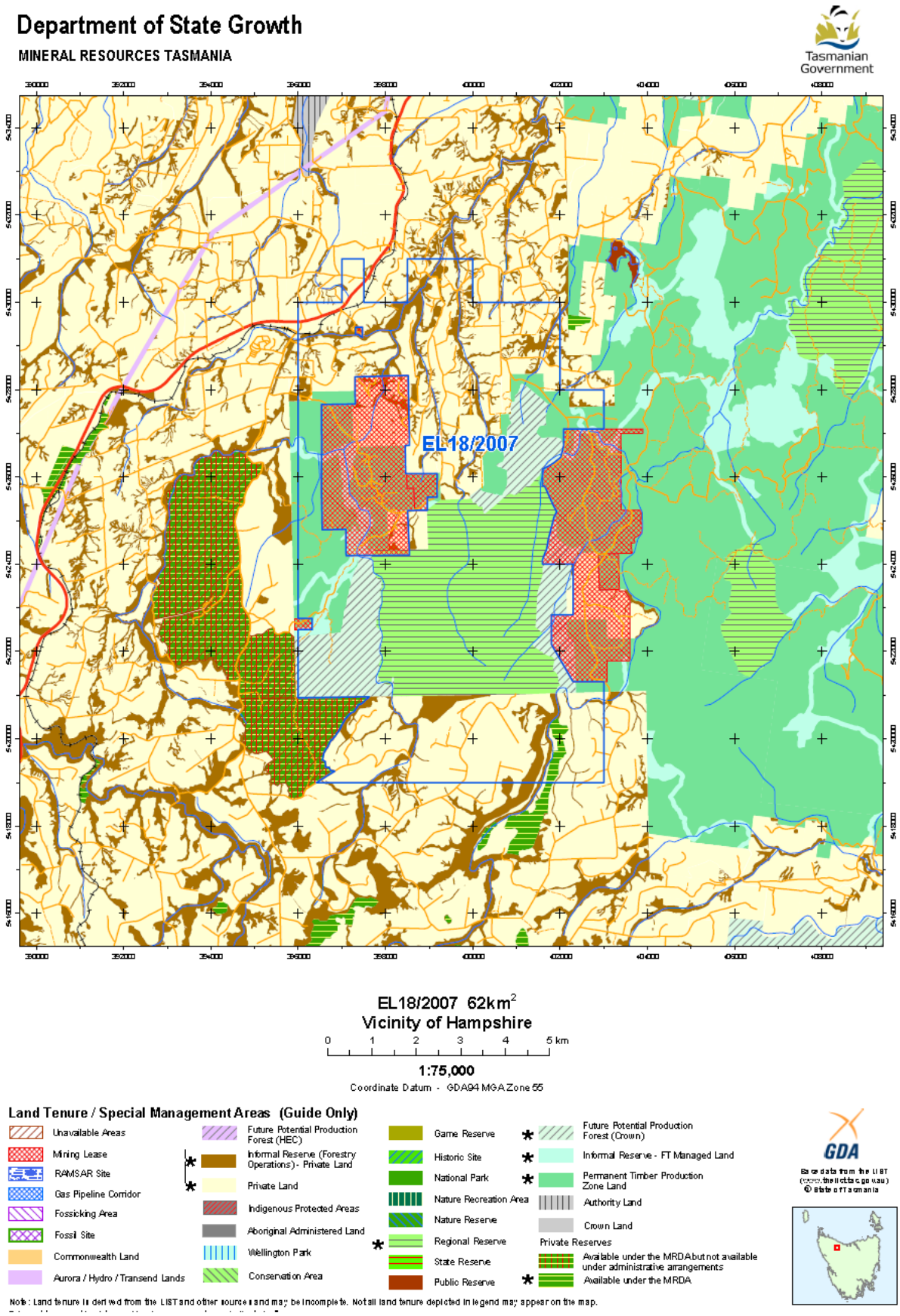

Figure 1: Map showing the land tenure of EI18/2007.

2 REGIONAL GEOLOGY

The Blythe River Iron Project is located on the western margin of the Dial Range Trough and is underlain by lithologies of the Late Proterozoic Oonah Formation, Owen Group Siliciclastics, Gordon Group Limestone, Devonian Granites and Tertiary Basalt (Figure 1). The Dial Trough is a structurally interesting basin that includes a possible Northern Extension of the Hellyer Fault, and significant basin bounding faults on the western and eastern sides. The Devonian post orogenic Housetop Granite dominates the geology to the south of the project area and is considered to underlie much of the southern Dial Trough. The Dial Trough has been poorly mapped and stratigraphic correlations are uncertain for many units.

Oonah Formation

The oldest rocks in the district are the Proterozoic Oonah formation, consisting of polydeformed quartzwacke, siltstone and pelite with lesser dolerite intrusives. These are overlain by a sequence of pelite-carbonate with minor mafic volcanics and conglomerate. This association is host to replacement deposits at Mt Bischoff and near Zeehan and consequently represents a potential host for similar styles of skarn mineralisation.

Mt Read Volcanics

Mt Read Volcanic associations have been correlated with the felsic volcaniclastics of the Western Volcano-sedimentary sequence and the Tyndall Group quartz-feldspar phyric volcaniclastics.

Owen Group

The Late Cambrian to Ordovician Owen Group overlies the Mt Read Volcanics and is comprised dominantly of siliciclastic conglomerate and sandstone. Locally volcanic derived conglomerates are associated with basal members. The Moina Sandstone, comprised of coarse to fine siliciclastic sandstone with minor intercalated conglomerate is the uppermost siliciclastic unit of the Owen Group and has a gradational contact with the overlying Gordon Group.

Gordon Group Limestone

Conformably overlying the Owen Group is the Gordon Group limestone and dolomite sequence which is the host of the Kara district magnetite skarns. The stratigraphic thickness of the limestone is regionally variable ranging between 50-1000m.

Housetop Granite

The Housetop granite outcrops in much of the Blythe River Prospect and is believed to extend below much of the area (Leaman, 1993). Leaman concludes that the Housetop granite is anomalously dense and highly magnetic, which may explain the abundance of iron metasomatism in the district. The granite is responsible for massive Magnetite-SnWO3 mineralisation of the Kara District. The association of Tasmanian Devonian granites with Magnetite, Sn-WO3, Pb-Zn-Ag and Au mineralisation is well documented.

Tertiary Basalt

Basaltic flows are widespread throughout the Blythe River Iron Project area, flooding Tertiary palaeo-topographic lows. The basalts vary widely in thickness and frequently have a high magnetic susceptibility creating difficulties for magnetite exploration below basaltic cover. Recent resource and exploration drilling at the Kara Mine indicates that the magnetite skarn extends below basalt cover.

2.1 LOCAL GEOLOGY

The Rogetta and other skarns in the area are hosted in folded roof pendants of Gordon Limestone and Moina Sandstone inliers within the Housetop Granite batholith. Magnetite skarns obviously have a very high magnetic susceptibility and form prominent magnetic highs so in theory should be simple to identify. Unfortunately, much of the area has been flooded with Tertiary Basalt, which has a relatively high magnetic susceptibility. Even though the magnetic susceptibility of the basalt is an order of magnitude less than that of the magnetite and magnetite skarn, it would appear from drill results that a number of magnetic highs may be basalt related.

Skarn mineralogy is complex; however, Zaw 2000 has identified a minimum of 4 stages of skarn formation at the Kara No1 deposit. The geology and morphology of the Rogetta and other skarns in the area are essentially identical in mineralogy and morphology to those at the Kara Mine operated by Tasmania Mines Ltd, Callaghan 2011 and Tasmania Department of Mines 1989.

Several major skarn facies have been highlighted in drill core and rock chips from drilling at Rogetta including:

Diopside skarn (SKPX)

Garnet skarn (SKGT)

Magnetite-diopside skarn (SKMG)

Magnetite-amphibole-epidote skarn (SKMG)

Calc-silicate skarn (calcite-epidote-chlorite and amphibole) (SKCS)

Marble (LMST)

The magnetite-diopside and magnetite-amphibole-epidote skarn assemblages form the basis of this resource estimate. Magnetite generally occurs as coarse disseminated euhedral crystals, veins and massive aggregates within a diopside or amphibole rich matrix. Mineralogical boundaries of skarn facies vary from sharp to more commonly gradational. While the dominant lithologies included in the resource are Magnetite diopside skarn and Magnetite-amphibole-epidote skarn some magnetite mineralisation does extend into the Garnet Skarn, the Calc Silicate Skarn and even the granite, typically as small veinlets of magnetite rich material suggesting that the magnetite mineralisation is a later stage alteration.

Figure 2. Rogetta North, Local Geology after Macintyre Mines and MRT Granite is represented by + symbol, calc - silicates as blocks and magnetite zones are shaded dark grey, other sediments in grey

Magnetite content is variable but where present generally occurs as coarse crystals of magnetite. Locally magnetite may become the dominant mineral with drill core showing several metre thick zones where magnetite is the dominant mineral.

Traditionally the magnetite skarns of the Kara / Rogetta area have been explored for Tin and Tungsten mineralisation. Zaw K. 2000 suggests W03 and Sn02 mineralisation is most commonly associated with the more hydrous magnetite-amphibole-epidote skarn phase. While there are historical references to scheelite and tin in the Rogetta area these minerals have not been evident in data collected during the most recent drilling campaign at Rogetta and are reported as minor in Tasmania Department of Mines 1989.

The Rogetta Skarns are located in relatively flat terrain dominated by low re-growth eucalypt forest on crown land managed by Forestry Tasmania. Access roads are well formed unsealed forestry roads.

The best drilled and largest deposit of the Rogetta Skarns is the Rogetta North Skarn. This is the only deposit of the Rogetta Skarns currently drilled to a sufficient density across the complete mineralised zone to allow estimation of a mineral resource classified as Indicated or Measured. The local Geology is shown in Figure 2.

The Rogetta North deposit consists of a north-south striking, gently south plunging asymmetric syncline of Ordovician Gordon Group limestone and much lesser Moina Sandstone lying directly on top of the Housetop granite. The western limb is vertical to sub vertical and the eastern limb is gently shelving (Figure 3).

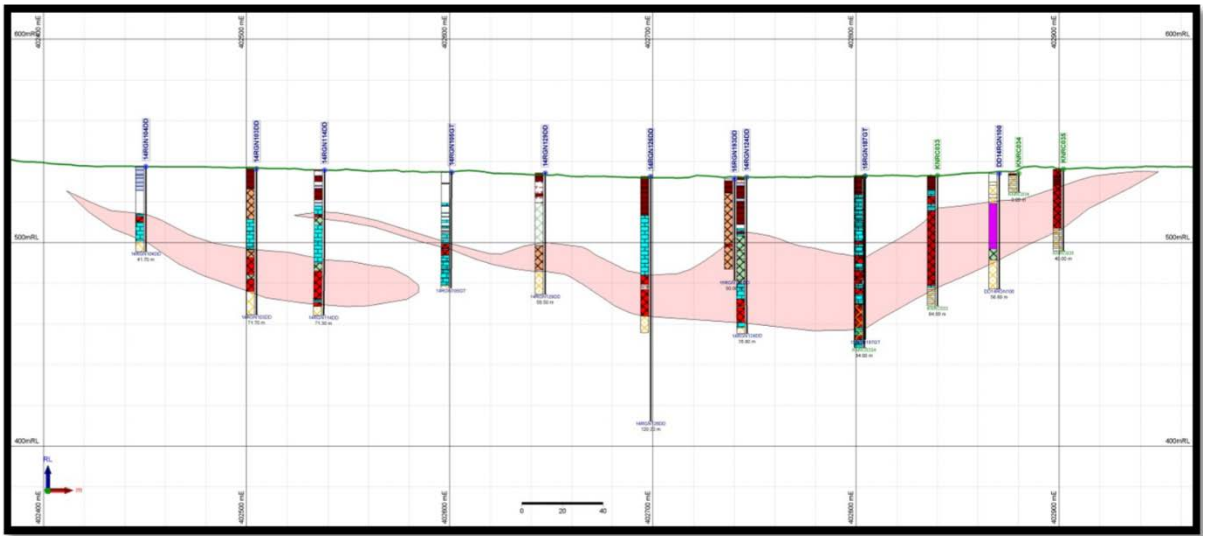

Figure 3. Section 5425400N looking North, Magnetite zone and drillholes

The deposit occurs over a strike length of almost 1000m and is approximately 100m wide at the shallow northern end, grading to in excess of 500m width as it plunges south. Mineralisation outcrops in the northern end and on the syncline limbs and extends to over 150m depth at the south end. The previous model (Callaghan 2011) shows the deposit as being largely closed off at the southern end, 5,425,400N. The recent drilling program has been able to extend the southern boundary 150m south to 5,425,200 N.

The 2011 Resource estimate (Callaghan 2011), observed that thick (10-60m) magnetite skarn mineralisation has been intersected in many drill holes, with a relatively consistent lens of mineralisation occurring directly over the granite, forming a shallow south plunging synform. Other less continuous lenses of magnetite skarn mineralisation are also present.

Current work suggests that the picture is more complex. Magnetically, as indicated by results of the high resolution aeromagnetic survey conducted in December 2014, the deposit is in two parts, magnetic imagery suggests that structural control has influenced the development of the magnetite alteration at Rogetta North. Internally while there is indeed an asymmetric synform shape to the granite pendant hosting the mineralisation, interaction with cross cutting structure and the magnetite alteration results in a very variable form to the mineralised body more reminiscent of a zone of hydrothermal alteration.

3 EXPLORATION HISTORY

The potential for economic deposits of Iron in the Northern part of Tasmania has been recognised for many years. The area to the south of Penguin hosted several small mines in the later 1800's. The Cuprona area along the Blythe River was considered as a possible source of iron for an Iron Ore Smelter in New South Wales (Twelvetrees 1901). Both areas are now covered by tenements managed by Lottah Mining. In the Hampshire area (30Km to the South of Burnie) a number of magnetite deposits were located, one of these is now the Kara Mine operated by Tasmania Mines Ltd. The remainder of these are on tenements controlled by Lottah Mining.

In the area controlled by Lottah Mining there has been various exploration programs conducted since the late 1950's by a number of exploration companies mainly looking for Tin, Tungsten and Base Metals. The companies working in the area have included, Shell, Billiton, CRA, Calminco, Macintyre Mines and the Tasmania Department of Mines.

More recently Red River Resources and Iron Mountain Mining acquired a number of tenements which now form the core of the group of tenements managed by Lottah Mining. Work by Iron Mountain Mining between 2007 and 2010 saw the Hampshire Iron occurrence drilled followed by the Rogetta North and Rogetta East deposits. (The Rogetta deposits were formally known as Kara 2 North and Kara 2 East respectively). While drill results were encouraging the management at Iron Mountain Mining did not see development of the Iron deposits in Tasmania as a priority and control passed to Forward Mining Ltd. Forward Mining conducted drilling on the Rogetta North and East deposits and followed that work with a mineral resource report that established an Inferred Resource of 16.6 Mt at 37.4% Fe with a 20% cut off for Rogetta North (Callaghan 2011). This work was reviewed as part of an IGR document prepared for Forward Mining by Hellman & Schofield Pty Ltd (Tear S 2011).

In early 2014 control of the tenements passed to Lottah Mining Pty Ltd. Since then Lottah Mining have been conducting a vigorous resource definition program over the Rogetta North area together with exploration and assessment of all the known Iron deposits in the area it has under tenement.

As part of the exploration work a number of new tenements have been acquired to follow up on exploration targets developed from reworked airborne magnetic survey work. This work is indicating that there are a number of unexplored targets for Iron in the area and has also started to quantify the potential of a number of the known iron deposits.

4 WORK COMPLETED

Work Completed on EL18/2007 during the period of July 2015 – July 2016 consisted of continued research of past work and assessment of geological potential for viable magnetite bodies that could be commercially exploited as further sources of ore for the Rogetta Mine Site.

In the first pass assessment of the tenement outside of the recently proved up Rogetta Ore Body, which is now contained wholly within the recently granted mining lease 1996P/M, the company chose three separate deposits to focus on based on preliminary investigations. They are;

- The L13 Deposit
- The Rogetta South Deposit
- The Suttons Skarn Deposit

A gravity survey was carried out over each of the deposits as a gravity machine was available to the company for short term use. A UAV magnetic survey was also completed over the L13 deposit. It should be noted that no geophysical interpretation has been carried out on the data recovered and that some of the data is incomplete due to the gravity machine being damaged beyond repair during the survey process.

All recovered data and plans of the proposed programs are included in the appendices section of the report.

A drill plan to test the iron at the L13 deposit was designed and submitted to MRT for approval, however, the company advised to hold the plan for the moment as further thought was being put into the project which may affect the drill program.

Other work on EL18/2007 included historic drill core and data analysis, geological reconnaissance and minor track maintenance.

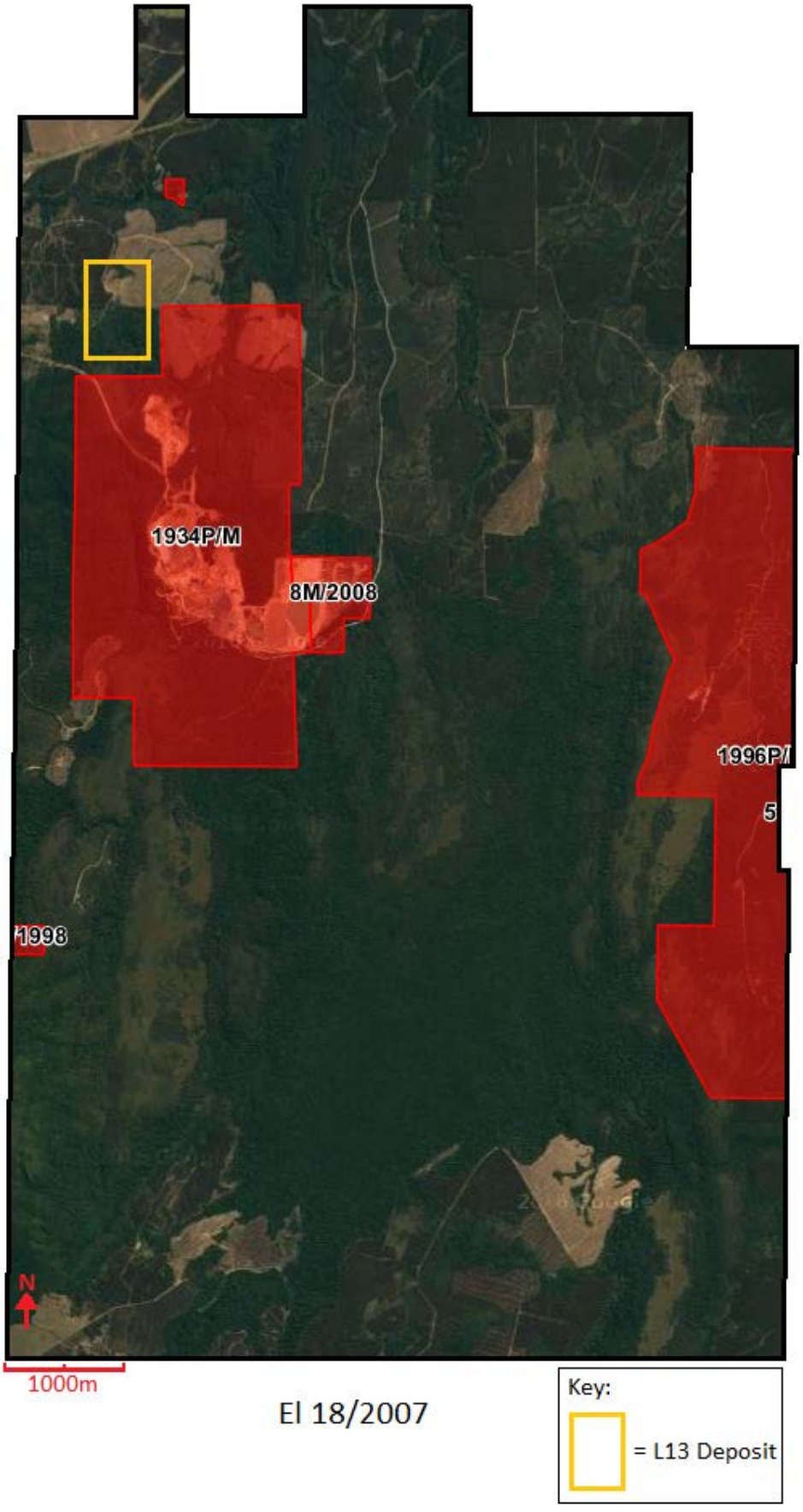

Figure 4: Map of EL18/2007 with the L13 Deposit Highlighted

5 DISCUSSION

The gravity survey on L13 was conducted as an Honours Project by Reuben McCormack organised by UTAS and GHD for Lottah Mining Pty Ltd. The project began in early 2015 and was completed in November 2015 (a copy of Reuben McCormack's thesis is attached in the appendix below).

The gravity survey was conducted on a 50×50 m grid (figure 5). Gravity data was tied to the base station at Natone Primary School. Two gravity meters were used; a Scintrex CG-3 and a Lacoste and Romberg G. A DGPS was used to pin point the location of each gravity reading.

Raw data was processed to generate simple Bouguer anomalies using the 1930 IGF formula (McCormack 2015). Terrain corrections were calculated based on the local LiDAR data and a regional DEM to generate a Complete Bouguer Anomaly dataset suitable for interpretation (McCormack 2015).

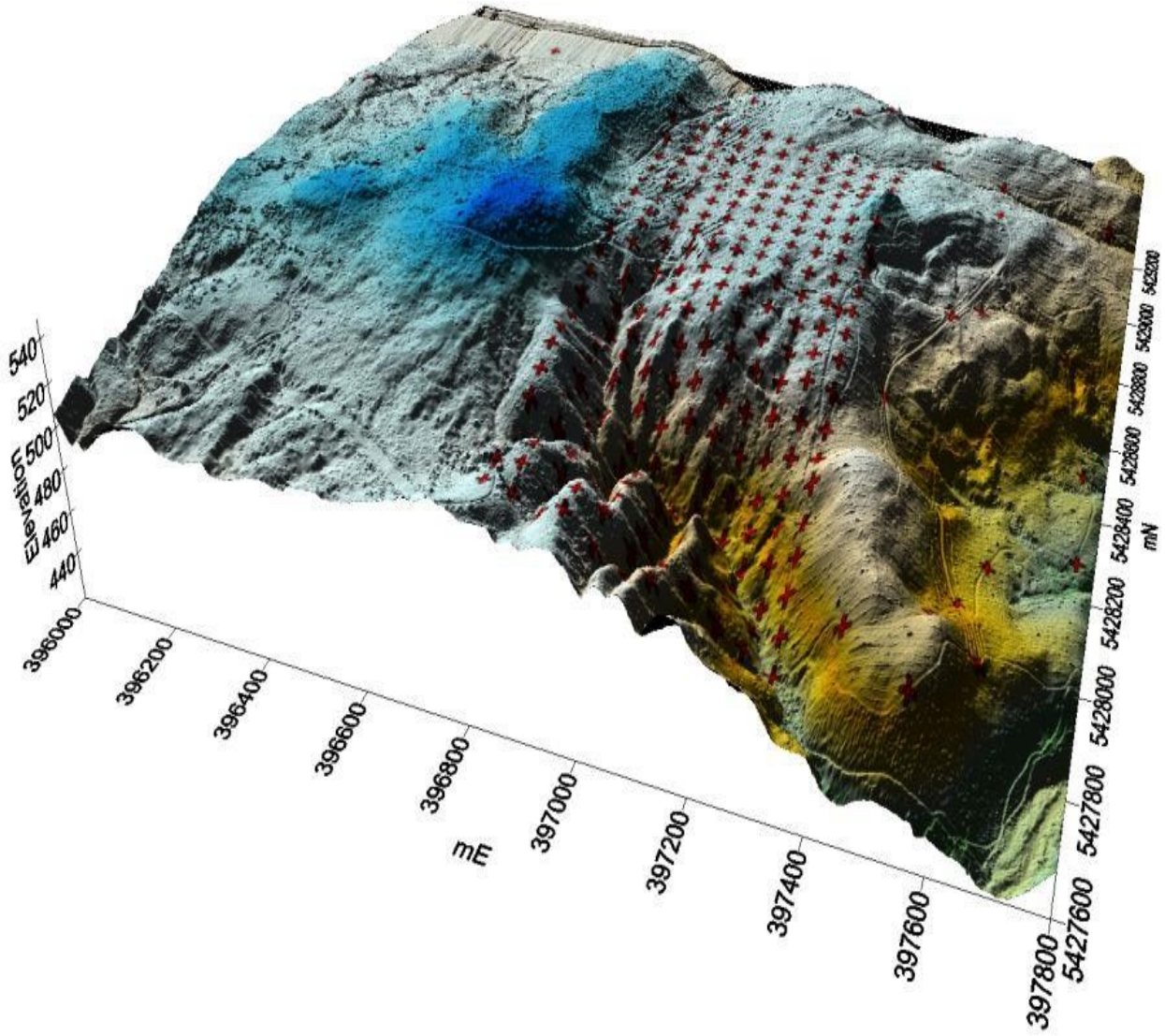

Figure 5: LiDAR elevation surface of L13 and the surrounding area, red crosses mark the gravity survey points (McCormack 2015).

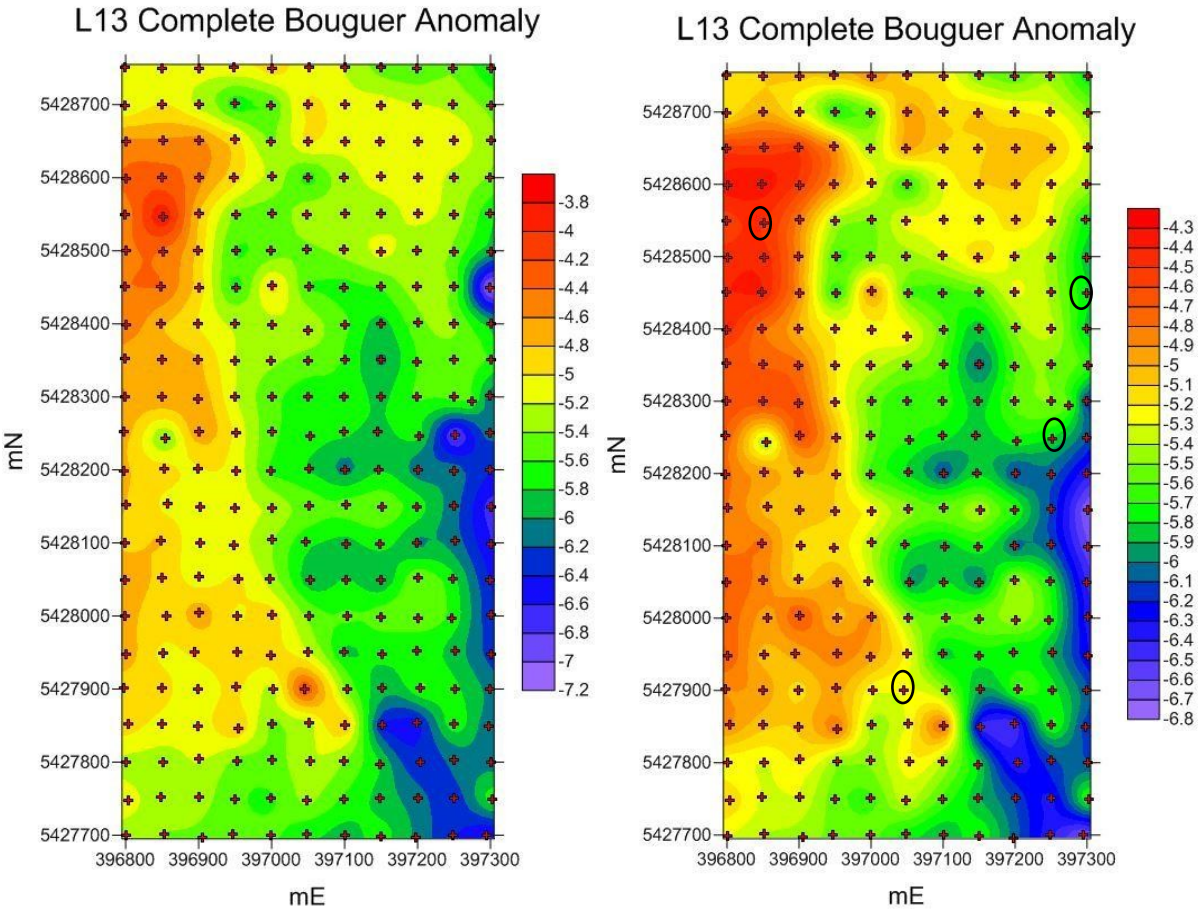

Figures 6 & 7: Complete Bouguer Anomaly (left), outlying points (circled in black) removed (right), units of mGals (McCormack 2015).

The magnetic survey covering the L13 prospect was collected by Rada Engineering Pty. Ltd using a three axes fluxgate magnetometer mounted on a multirotor UAV X4 drone. Flight lines were flown in an east-west direction separated by 25 metres with tie lines flown perpendicular every 100 metres (Figure 8). Sensor clearance was set to 20 metres and simultaneously collected elevation data with the magnetics. Processing of the raw data as also completed by Rada Engineering.

Magnetic data indicates a subsurface body of high magnetic susceptibility material at L13 but this is not matched by a corresponding positive residual gravity residual gravity anomaly. While numerical interpretation is affected by lack of constraints and hence significant ambiguity, it is considered unlikely that a large volume, high grade magnetite body exists at shallow depths at L13. Magnetite mineralisation is more likely present as small pods, veins or disseminated with an envelope of alteration (McCormack 2015).

LMPL devised a small scale drill plan (figure 9 and table 1) to test the observations and modelling produced by McCormack and Rada Engineering Pty. Density and magnetic susceptibility obtained from LMPL future drilling will be used to constrain the numerical interpretation of the geophysical data and therefore improve the understanding of the nature of the deposit.

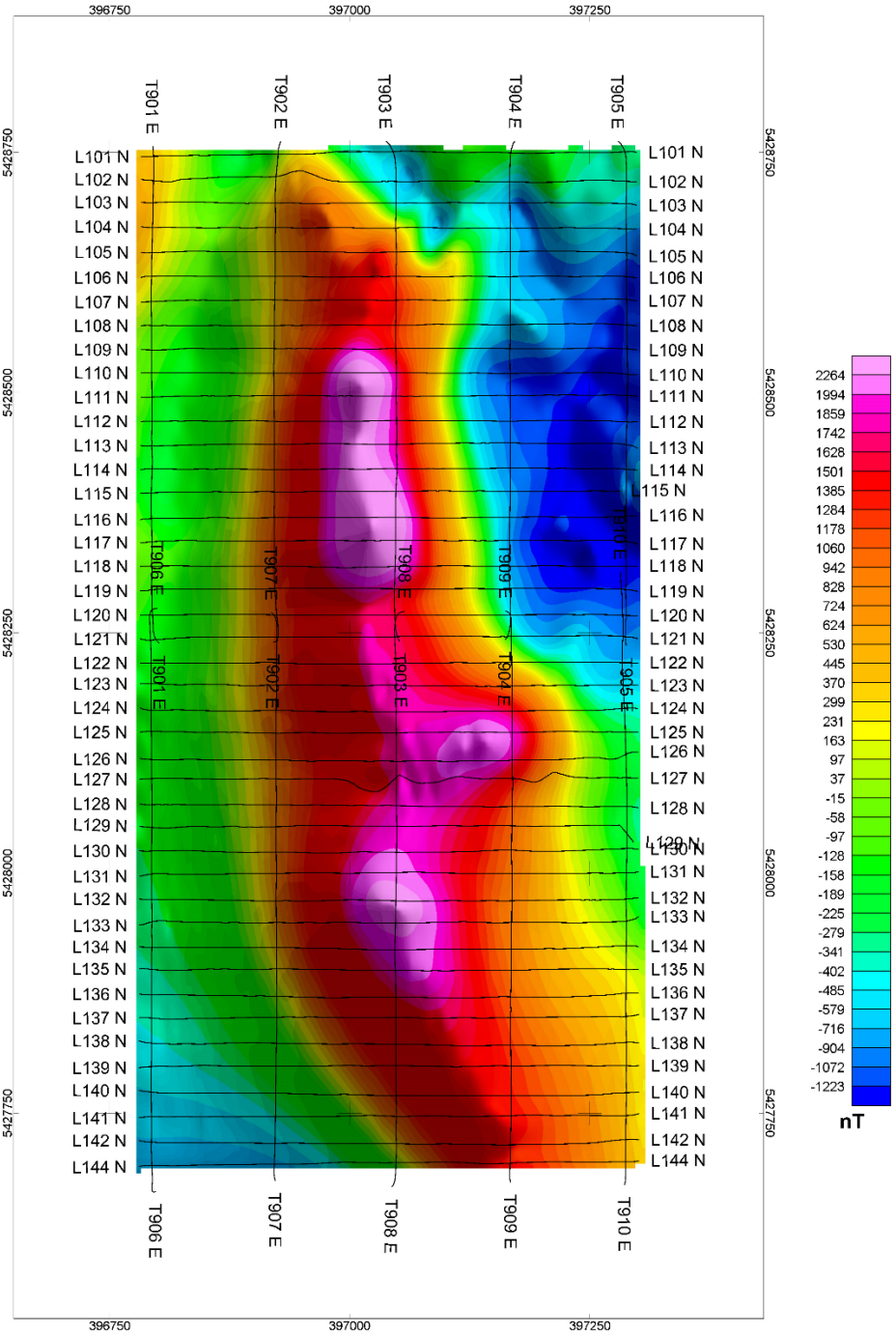

TMI Reduced To Pole

& Flight Path

50 0 50 100 150
(meters)
GDA94 / MGA zone 55

AREA : L13

UAV Magnetics survey Tasmania
Airborne Magnetic Survey Results
Flown for: Lottah Mining Pty Ltd

Figure 8: L13 TMI reduce to pole.

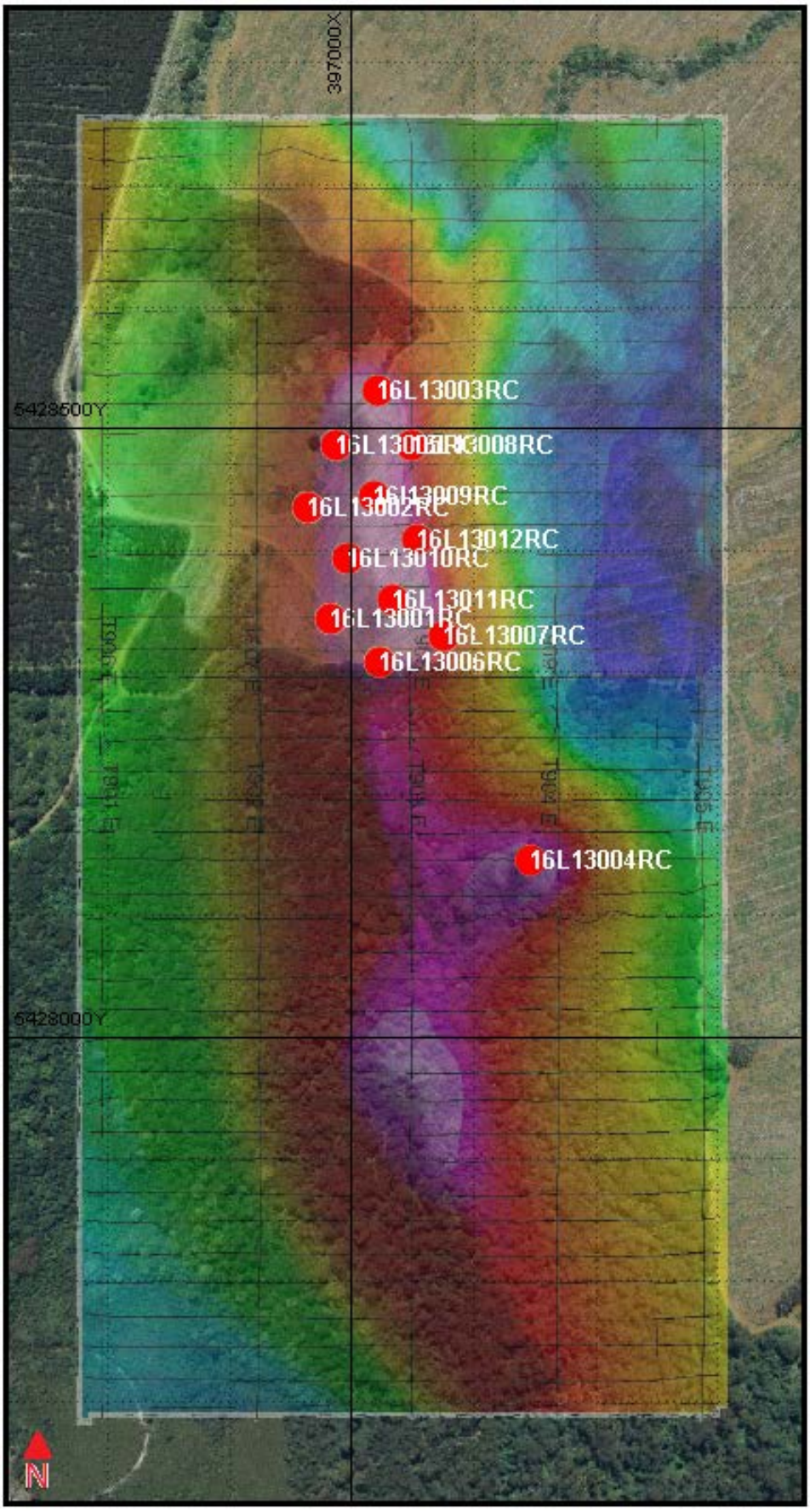

Figure 9: LMPL L13 Drill Plan overlying TMI and satellite images.

East	North	RL	HOLE ID	AZI	DIP	Depth
397145.8	5428146	488.5185	16L13004RC	0	-90	150
396982.8	5428343	488.5185	16L13001RC	90	-80	150
397022.4	5428309	488.5185	16L13006RC	0	-90	150
397034.1	5428359	488.5185	16L13011RC	0	-90	150
397075.5	5428329	488.5185	16L13007RC	0	-90	150
396996.8	5428393	488.5185	16L13010RC	0	-90	150
397053.3	5428408	488.5185	16L13012RC	0	-90	150
396964.2	5428435	488.5185	16L13002RC	90	-80	150
396986.9	5428487	488.5185	16L13005RC	90	-80	150
397049.2	5428486	488.5185	16L13008RC	0	-90	150
397020.7	5428531	488.5185	16L13003RC	0	-90	150
397017.1	5428445	488.5185	16l13009RC	0	-90	150

Table 1: LMPL proposed drill plan for L13

6 PROPOSED WORK PROGRAM

The proposed work plan for EI18/2007 for the 2016 – 2017 season will consist of work across the tenement to locate further targets including further desktop studies and field investigations. Work will also continue with the three deposits defined during this period.

- L13 – geological check mapping and detail if required. Assessment of drill plan prior to implementation of program
- Rogetta South – review of program to date and assessment of any further work to be completed.
- Suttons Skarn – geological check mapping and detail if required. Possible ground mag survey if deemed to be of value and planning of any drill program that may develop from the work completed.

7 EXPENDITURE

Expenditure for El18/2007 2015 – 2016 is presented below.

2015	Q3	$173,513.00
	Q4	$0.00
2016	Q1	$11,050.00
	Q2	$6,900.00
	TOTAL	$191,463.00

Table 2. El18/2007 2015-2016 quarterly expenditure

Expenditure for El18/2007 during the 2015-2016 year was $191,463.00.

8 ENVIRONMENTAL

Environmental disturbance on El18/2007 during the reporting period was minimal. Existing infrastructure access was utilised for site visits and surveys.

9 REFERENCES

Callaghan, TJ, 2011. Combined Annual Report for Blythe River Project EL6/2005, EL15/2006, EL18/2007, EL53/2007 and EL25/2009. Forward Mining Ltd. Unpub. Report.

Callaghan, TJ, 2011. Kara No. 2 North Mineral Resource Estimate NW Tasmania. Forward Mining Limited. Unpub. Report.

Callaghan, TJ, 2012. Blythe River Project Annual Report EL18/2007 Hampshire 2 NW Tasmania. Forward Mining Limited. Unpub. Report.

Callaghan, TJ, 2013. Blythe River Project Annual Report EL18/2007 Hampshire 2 NW Tasmania. Forward Mining Limited. Unpub. Report.

Callaghan, TJ, 2013. Blythe River Project Partial Relinquishment Report EL18/2007 Hampshire 2 NW Tasmania. Forward Mining Limited. Unpub. Report.

Kusnander K., Mayer A., Zlatkov G., 2009. Blythe Project Northern Tasmania Annual Report for EL18/2007 ("Hampshire 2"). Iron Mountain Mining Limited. Unpub. Report.

McCormack, R., 2015. Geophysical Assessment of Potential Magnetite Skarn Mineralisation at the L13 Prospect, Highclaire, Northwest Tasmania. UTAS Thesis.

Tear, S., 2011. Independent Geologist's Report Exploration Properties in NW Tasmania, Forward Mining Limited. Hellman & Schofield Pty Ltd., Unpub. Report

Whitehouse, G.K. 2015. Lottah Mining Pty Ltd Rogetta North Resource Assessment March 2015.

10 APPENDIX 1

L13 Gravity Data:

Station No.	Time	Gravity Reading	Easting	Northing	Elev+A1:F42ation
L13 Base	1429	3973.065	397275.1	5428294	517.485
1007	1542	3972.745	397299.6	5428301	510.588
1008	1558	3972.765	397301.1	5428350	511.578
1009	1608	3972.03	397300.1	5428400	514.28
1010	1615	3971.68	397250.4	5428400	518.59
1011	1623	3972.23	397250.4	5428351	515.188
1012	1631	3972.945	397250.4	5428300	512.614
L13 Base	1636	3972.88	397275.1	5428294	517.485
L13 Base	919	3973.19	397275.1	5428294	517.485
1017	932	3970.61	397300	5428449	514.159
1018	938	3971.52	397250.3	5428450	520.224
1019	947	3971.965	397199.8	5428500	518.384
1020	958	3972.353	397149.6	5428551	516.357
1021	1002	3972.28	397200.2	5428550	517.783
1022	1011	3971.3	397249.7	5428550	521.434
1023	1017	3971.16	397249.5	5428499	521.304
1024	1023	3970.165	397300.1	5428499	523.392
1025	1029	3969.295	397298.7	5428551	527.659
1026	1036	3971.425	397298.9	5428600	519.672
1027	1041	3972.285	397300.4	5428651	516.282
1028	1045	3972.8	397249.6	5428650	514.933
1029	1051	3971.905	397249.4	5428601	518.252
1030	1058	3972.565	397200.6	5428600	516.323
1021	1106	3972.295	397200.2	5428550	517.783
1032	1114	3972.455	397149.4	5428499	517.54
1033	1122	3971.95	397199.7	5428451	518.695
1034	1127	3972.045	397200.5	5428401	517.394
1035	1135	3972.23	397198.7	5428348	516.01
L13 Base	1140	3973.155	397275.1	5428294	517.485
L13 Base	1140	3973.155	397275.1	5428294	517.485
1037	1217	3973.25	397299.3	5428250	507.913
1038	1224	3973.76	397299.9	5428200	503.996
1039	1231	3974.765	397300.6	5428149	497.254
1040	1236	3976.59	397300.6	5428099	491.05
1041	1241	3977.72	397299.9	5428050	485.503
1042	1251	3978.09	397301.1	5428001	482.386
1043	1259	3979.705	397300.6	5427948	475.372
1044	1322	3981.2	397300	5427900	468.196
1045	1330	3982.485	397297.8	5427850	461.793
1046	1335	3983.975	397300.4	5427800	457.648
L13 Base	1350	3973.075	397275.1	5428294	517.485

L13 Base	1350	3973.075	397275.1	5428294	517.485
1048	1409	3972.935	397199.5	5428301	512.605
1049	1416	3971.755	397149.3	5428300	517.318
1050	1424	3971.135	397150.7	5428350	518.97
1051	1433	3971.41	397150.1	5428400	518.304
1052	1440	3971.8	397149.6	5428450	517.564
1053	1450	3972.28	397099	5428501	517.089
1054	1455	3972.38	397100.4	5428551	516.496
1055	1502	3972.49	397099.7	5428600	515.839
1056	1508	3972.75	397100.4	5428649	515.007
1057	1515	3972.675	397150.7	5428601	515.734
1058	1520	3972.765	397149.1	5428650	514.854
1059	1527	3972.98	397149.2	5428699	513.752
1060	1535	3972.915	397201	5428650	514.093
1061	1545	3972.915	397199.7	5428700	513.4
1062	1551	3972.735	397249.1	5428700	513.417
1063	1556	3972.315	397300.7	5428699	514.522
1065	1603	3972.58	397300.8	5428750	511.919
1066	1608	3972.835	397249	5428750	512.812
1068	1615	3972.615	397199.3	5428750	513
1059	1621	3972.975	397149.2	5428699	513.752
L13 Base	832	3980.37	397275.1	5428294	517.485
1083	910	3979.74	397299.5	5428301	510.992
1084	916	3980.36	397301.3	5428350	511.47
1085	921	3979.65	397250.3	5428351	515.992
1086	926	3980.31	397250.5	5428301	513.159
L13 Base	930	3980.57	397275.1	5428294	517.485
1088	949	3979.285	397099.3	5428300	519.703
1089	956	3979.415	397050.4	5428300	518.241
1090	1000	3979.92	397000.6	5428300	520.201
1091	1008	3980.6	396950.7	5428350	513.773
1092	1021	3981.075	396950.1	5428299	516.784
1093	1029	3982.41	396899.3	5428297	513.601
1094	1036	3979.95	396849.6	5428300	520.851
1095	1042	3979.38	396799.6	5428300	523.476
1096	1053	3979.405	396849.5	5428350	523.548
1097	1102	3979.025	396799.3	5428352	530.903
1098	1111	3979.79	396849.1	5428400	518.861
1099	1117	3980.43	396899.6	5428400	516.995
1100	1124	3981.065	396899.5	5428350	514.162
1091	1130	3980.665	396950.7	5428350	513.773
1102	1137	3980.285	396949.6	5428400	515.751
1103	1141	3980.05	397000.2	5428399	516.164
1104	1149	3979.425	396999.8	5428350	518.328
1105	1155	3979.225	397050.4	5428349	519.21
1106	1201	3979.73	397049.5	5428390	519.168

1107	1206	3979.355	397100.5	5428399	518.56
1108	1211	3979.235	397100.5	5428351	519.094
L13 Base	1217	3980.6	397275.1	5428294	517.485
1110	1312	3979.955	397051.5	5428450	517.067
1111	1317	3980.16	397048.7	5428501	516.886
1112	1323	3980.42	397049	5428550	516.705
1113	1329	3980.21	397050.6	5428600	515.297
1114	1336	3980.46	396999.9	5428650	514.489
1115	1345	3981.07	397049.3	5428650	515.466
1116	1357	3980.865	397049.9	5428700	516.532
1117	1405	3980.555	397050.9	5428751	516.801
1118	1411	3980.86	397001	5428750	517.003
1119	1417	3980.905	396948.2	5428750	516.454
1120	1423	3980.99	396901	5428750	515.751
1121	1428	3981.135	396850	5428749	514.734
1122	1440	3978.57	396798.8	5428751	527.359
1123	1449	3979.545	396798.8	5428699	524.078
1124	1508	3981.54	396850.6	5428700	516.08
1125	1516	3981.46	396900.2	5428701	514.175
1126	1522	3980.88	396950.1	5428701	515.046
1127	1528	3981.045	396999.3	5428699	515.554
1128	1532	3981.515	397000.3	5428650	514.894
1129	1546	3981.825	397000.3	5428601	514.06
1130	1555	3981.45	397000.7	5428551	515.481
1132	1600	3981.445	396950.8	5428550	516.411
1133	1607	3981.325	396951	5428500	515.863
1134	1619	3981.255	396999.8	5428501	517.077
1135	1623	3981.26	396951.2	5428450	515.982
1136	1627	3982.165	397000.7	5428452	516.296
L13 Base	1636	3982.37	397275.1	5428294	517.485
1138	1653	3984.85	397469	5428447	493.727
1139	1659	3982.65	397522.9	5428721	505.351
1140	1704	3983.82	397363.3	5428855	503.25
1141	1709	3981.635	397165.8	5428924	514.385
1142	1714	3982.615	396924.1	5428895	512.482
1143	1719	3978.695	396753	5429027	508.83
1144	1725	3985.79	396570.2	5429063	500.449
1145	1729	3986.675	396368.8	5429037	500.597
1146	1735	3987.545	396192.2	5428999	499.769
1147	1740	3987.89	395991.2	5429055	496.244
1148	1747	3982.72	396862.2	5428839	513.67
L13 Base	1756	3982.4	397275.1	5428294	517.485
L13 Base	850	3973.275	397275.1	5428294	517.485
1156	900	3972.74	396800	5428399	520.128
1157	904	3972.825	396798.7	5428451	518.325
1158	911	3972.905	396800.8	5428499	517.948

1159	918	3973.045	396799.5	5428550	517.309
1160	926	3973.32	396800.6	5428599	517.709
1161	934	3972.495	396800.1	5428649	519.294
1162	941	3973.425	396849.2	5428600	516.297
1163	950	3973.37	396851.2	5428651	516.402
1164	1000	3973.595	396900.1	5428651	516.472
1165	1005	3973.365	396949.3	5428653	514.111
1166	1019	3973.385	396949	5428600	518.033
1167	1026	3973.475	396900.3	5428599	514.853
1168	1032	3973.405	396848.8	5428599	516.452
1169	1114	3974.17	396850.9	5428546	515.518
1170	1125	3973.165	396900.5	5428550	514.311
1171	1132	3973.02	396899.6	5428500	515.452
1173	1141	3973.025	396900.8	5428450	515.009
1174	1148	3973.135	396849.1	5428450	516.862
1175	1154	3972.995	396851.5	5428499	517.459
L13 Base	1204	3973.185	397275.1	5428294	517.485
1177	1234	3977.36	396007.6	5428802	504.297
1178	1238	3975.17	396041.8	5428679	514.473
1179	1243	3974.725	396306	5428676	516.284
1180	1248	3971.65	396344.3	5428374	531.921
1181	1255	3971.535	396279.7	5428291	529.24
1182	1300	3972.355	395978.7	5428287	525.727
1183	1305	3970.705	395862.4	5428096	532.401
L13 Base	1320	3973.185	397275.1	5428294	517.485
L13 Base	930	3745.93	397275.1	5428294	517.485
1185	954	3745.28	397251	5428248	514.596
1186	1020	3746.49	397202	5428245	526.097
1187	1035	3745.67	397145.2	5428253	509.603
L13 Base	1043	3745.94	397275.1	5428294	517.485
1188	1109	3744.63	397098.7	5428252	527.608
1189	1116	3744.46	397053.7	5428246	522.617
1190	1129	3745.53	397000	5428252	531.879
1191	1137	3746.84	396951.4	5428250	523.055
1192	1146	3748.26	396900.8	5428252	513.407
1193	1208	3745.87	396854.5	5428244	523.799
1194	1217	3745.08	396797.7	5428253	526.595
1195	1233	3745.16	396798.1	5428198	522.635
L13 Base	1247	3745.93	397275.1	5428294	517.485
1196	1335	3746.72	397250.1	5428199	511.902
1197	1342	3747.22	397201.2	5428201	517.214
1198	1350	3746.74	397147.5	5428200	521.457
1199	1359	3745.19	397100.6	5428201	524.198
1200	1407	3744.78	397051.5	5428201	524.024
1201	1417	3745.89	396999.1	5428198	520.747
1202	1431	3747.18	396951.6	5428199	518.489

1203	1440	3748.06	396899.7	5428202	517.123
1204	1451	3748.01	396852.4	5428202	513.59
1205	1501	3745.99	396800.5	5428152	521.174
1206	1524	3748.6	396856.9	5428154	515.033
1207	1538	3748.06	396901.6	5428149	508.173
1208	1548	3748.22	396950.4	5428148	511.663
1209	1557	3747.98	397000.4	5428148	511.603
1201	1609	3745.94	396999.1	5428198	520.747
1210	1620	3747.08	397051.3	5428151	507.466
1211	1630	3747.08	397101.6	5428152	506.344
1212	1642	3748.42	397151	5428150	498.595
1213	1650	3748.79	397199.2	5428149	501.852
1214	1700	3747.44	397250.7	5428151	506.539
L13 Base	1708	3745.86	397275.1	5428294	517.485
L13 Base	840	3745.96	397275.1	5428294	517.485
1215	859	3749.51	397250.8	5428102	501.061
1216	908	3749.87	397199.3	5428099	511.957
1217	920	3750.15	397148.6	5428099	502.929
1218	928	3749.25	397102	5428099	513.887
1219	939	3748.67	397046.7	5428101	500.17
1220	949	3749.71	397000.3	5428105	507.962
1221	956	3749.23	396949.1	5428097	510.741
1222	1006	3748.44	396901.7	5428099	511.335
1223	1015	3748.33	396849.1	5428103	519.793
1224	1025	3746.36	396799.7	5428100	534.463
1225	1033	3745.83	396799.6	5428049	515.147
1226	1054	3748.52	396849.8	5428053	510.644
1227	1106	3749.08	396900.1	5428054	504.682
1228	1127	3750.97	396953.8	5428050	503.144
1229	1136	3751.94	396996.9	5428050	495.589
1220	1144	3749.66	397000.3	5428105	507.962
1230	1156	3749.93	397053.8	5428049	501.276
1231	1207	3750.86	397101.6	5428050	505.742
1232	1215	3751.94	397150.6	5428050	508.302
1233	1222	3752.45	397200.1	5428052	488.071
1234	1229	3751.48	397247.9	5428051	496.713
L13 Base	1237	3745.86	397275.1	5428294	517.485
1235	1326	3752.77	397247.7	5427997	475.217
1236	1335	3754.04	397201.4	5427997	475.798
1237	1342	3754.2	397149.5	5427999	480.952
1238	1351	3753.21	397104.3	5428000	482.605
1239	1358	3753.14	397051.4	5428000	489.397
1240	1411	3753.81	397000.2	5428001	478.427
1241	1422	3752.37	396952.9	5428000	476.945
1242	1437	3751.4	396900.5	5428004	489.296
1243	1454	3748.25	396856.8	5428000	516.28

1244	1503	3745.61	396799.7	5428000	514.121
1245	1513	3746.31	396800.3	5427948	521.467
1246	1527	3747.93	396851.6	5427949	510.555
1247	1607	3750.18	396895.1	5427951	504.434
1241	1621	3752.36	396952.9	5428000	476.945
1248	1640	3753.51	396952.9	5427951	481.78
1250	1706	3755.32	397049.7	5427951	471.677
1251	1714	3754.67	397099.4	5427951	464.737
1252	1721	3755.91	397150.9	5427948	466.881
1253	1729	3754.66	397198.6	5427952	469.447
1254	1737	3753.7	396999	5427946	479.759
L13 Base	1745	3745.74	397275.1	5428294	517.485
L13 Base	858	3745.73	397275.1	5428294	517.485
1255	925	3754.95	396999	5427946	479.759
1256	931	3756.22	396999	5427946	479.759
1257	942	3754.11	396999	5427946	479.759
1258	952	3753.26	396999	5427946	479.759
1259	1004	3753.69	396999	5427946	479.759
1260	1019	3750.7	396999	5427946	479.759
1249	1032	3752.67	396952.9	5427951	481.78
1261	1046	3753.06	396951.7	5427904	491.992
1262	1102	3750	396899.5	5427900	499.719
1263	1114	3749.29	396850.3	5427901	512.097
1264	1128	3747.08	396797.8	5427901	519.517
1265	1146	3748.83	396850.5	5427852	506.934
1266	1158	3748.87	396899.3	5427850	514.74
1267	1217	3752.01	396953.9	5427846	494.036
1261	1229	3753.04	396951.7	5427904	491.992
1268	1243	3749.71	397001.4	5427853	502.448
1269	1254	3752.88	397051.7	5427854	500.548
1270	1303	3754.21	397101	5427851	481.174
1271	1314	3752.81	397151.6	5427850	482.623
1272	1331	3755.14	397198.8	5427854	471.358
1273	1338	3756.87	397250.7	5427852	470.144
L13 Base	1351	3745.77	397275.1	5428294	517.485
L13 Base	916	3745.8	397275.1	5428294	517.485
1274	942	3756.3	397249.9	5427803	453.516
1275	950	3754.12	397203.8	5427800	474.675
1276	1000	3752.51	397148.9	5427797	481.268
1277	1006	3753.19	397099.7	5427801	481.62
1278	1017	3752.37	397053	5427801	488.219
1279	1035	3749.26	397000	5427804	495.369
u	1047	3748.35	396953.3	5427801	508.766
v	1104	3749.23	396900.4	5427805	504.308
w	1117	3746.63	396852.1	5427800	515.017
1283	1127	3749.54	396803.2	5427852	502.747

1284	1139	3747.76	396800.2	5427800	510.617
1285	1157	3746.65	396848.6	5427752	511.421
1286	1229	3746.99	396803.7	5427747	510.431
1287	1240	3746.92	396801.1	5427699	510.957
1288	1254	3747.36	396852.3	5427701	507.245
1289	1312	3749.38	396901.4	5427753	503.241
1290	1323	3747.08	396950.5	5427749	513.792
u	1329	3748.45	396953.3	5427801	508.766
1291	1350	3748.2	396999.6	5427750	506.871
1292	1400	3751.48	397049.1	5427748	488.021
1293	1414	3751.88	397099.7	5427750	480.752
1294	1426	3752.88	397148.8	5427751	482.866
1295	1433	3754.61	397201	5427750	477.369
1296	1438	3755.67	397249.9	5427750	482.518
1297	1443	3758.01	397302.3	5427750	452.645
L13 Base	1454	3745.92	397275.1	5428294	517.485
1298	1529	3755.28	397294.9	5427700	466.422
1299	1535	3754.74	397248.6	5427700	466.678
1300	1544	3752.87	397197.3	5427696	473.677
1301	1550	3753.58	397150.6	5427699	476.599
1302	1559	3750.38	397100.2	5427700	496.069
1303	1612	3750.8	397049.1	5427702	496.338
1304	1621	3749.37	396999.5	5427699	499.248
1305	1647	3746.99	396946.9	5427701	506.405
1306	1654	3748.23	396905.8	5427696	500.641
L13 Base	1722	3745.86	397275.1	5428294	517.485
L13 Base	855	3745.88	397275.1	5428294	517.485
1307	919	3744.68	397099.6	5428449	516.922
1059	930	3745.87	397149.2	5428699	513.752
1070	937	3745.34	397100.6	5428700	516.31
1072	944	3745.48	397101.5	5428750	514.862
1073	952	3745.45	397149.7	5428751	513.842
L13 Base	1006	3745.86	397275.1	5428294	517.485
1308	1027	3750.06	397379.9	5428245	482.138
1309	1033	3754.83	397580	5427937	459.736
1310	1040	3756.48	397616.1	5428068	453.45
1311	1046	3758.11	397767.1	5428173	442.574
1312	1054	3757.2	397756.9	5428354	448.101
1313	1102	3752.43	397694.7	5428517	472.311
1314	1109	3748.69	397522.9	5428493	491.323
1315	1119	3754.59	397633.6	5427832	460.07
1316	1132	3752	397540.6	5427693	474.171
1317	1140	3752.31	397413.9	5427776	473.624
1318	1146	3751.86	397547.4	5427846	474.257
1319	1157	3748.39	397510.3	5428870	495.014
1320	1207	3750.44	397739.9	5428882	484.599

1321	1216	3747.43	397442.6	5429022	501.255
1322	1222	3745.87	397234.5	5428979	511.837
L13 Base	1232	3745.87	397275.1	5428294	517.485
Natone					
P.S.	1343	3776.72			
Wivenhoe	1416	3829.39			
Natone					
P.S.	1434	3776.71			
Wivenhoe	1456	3829.46			
Natone					
P.S.	1514	3776.74			
Wivenhoe	1534	3829.49			

10 APPENDIX 2

Sutton Skarn Gravity Data:

Station	Easting	Northing	RL	Grav.
PRS32201112739	411292.6	5453432	13.508	
sutton base	399551.9	5426213	559.534	
3500				4005.095
3501	399551.9	5426213	559.534	3963.49
3502				4005.08
3503	399551.9	5426213	559.534	3963.49
3504				4005.055
3505	399551.9	5426213	559.534	3963.315
3506	399273.1	5427249	518.606	3971.7
3507	399270.6	5427301	519.491	3971.57
3508	399265.5	5427350	519.143	3971.515
3509	399259.3	5427401	521.331	3971.095
3510	399254.8	5427451	511.151	3970.935
3511	399254.6	5427501	516.348	3971.18
3512	399259.9	5427551	521.08	3971.23
3513	399275.3	5427601	521.35	3971.11
3514	399301.7	5427649	519.928	3971.185
3515	399317.8	5427701	518.424	3971.46
3516	399347.6	5427751	515.938	3971.54
3517				3963.27
3518				3962.955
3519	399318	5427250	519.766	3970.945
3520	399355.9	5427253	523.968	3970.58
3521	399398	5427246	527.508	3970.155
3522	399446.9	5427246	534.04	3969.835
3523	399453.4	5427301	533.474	3969.375
3524	399395	5427300	531.856	3969.795
3525	399354.3	5427303	530.376	3970.405
3526	399302.6	5427296	522.991	3970.795
3527	399304.1	5427350	519.286	3970.84
3528	399352.5	5427355	530.341	3970.27
3529	399400.7	5427359	534.118	3969.37
3530	399400.8	5427396	530.532	3969.635
3531	399353.8	5427402	528.7	3970.055
3532	399298.9	5427402	523.906	3970.595
3533	399302.2	5427453	525.366	3969.93
3534	399353	5427452	530.372	3969.455
3535	399402.1	5427452	550.28	3969.375
3536	399399.4	5427499	539.135	3968.555
3537	399352.9	5427500	540.858	3969.015
3538	399303.2	5427490	538.694	3970.03
3539	399319.8	5427536	531.48	3969.415
3540	399352	5427551	534.587	3968.645
3541	399400.4	5427552	546.514	3967.095
3542	399450.6	5427601	538.842	3966.365
3543	399476.8	5427550	534.727	3967.265
3544	399475.8	5427497	530.472	3968.52
3545	399449.8	5427450	529.582	3969.195
3546	399452.4	5427400	528.585	3969.455

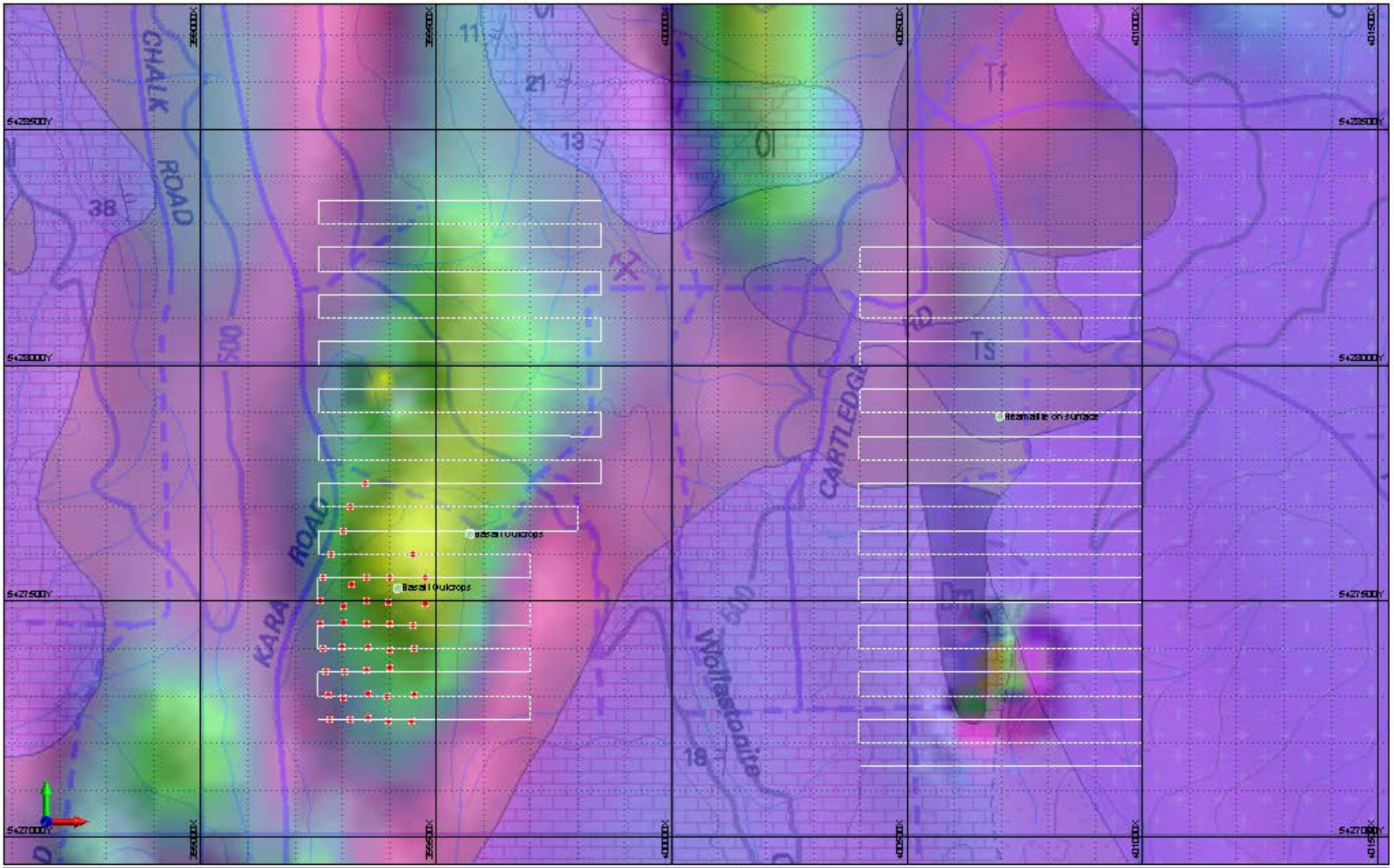

LMPL	White Grid = Planned Survey Area (50m Spacing) Red Dots = Completed Survey Points Green Dots = Field Notes	1:25,000 Geology Overlaying Regional Magnetics	Scale is Approximate	Plot Date: 02-Nov-2016 Plot File: Vizex	Sheet: 1 of 1 100 0 100m	**Sutton's Skarn Planned Gravity Survey**	Lottah Mining Pty Ltd

10 APPENDIX 3

Rogetta South Gravity Data:

Station ID	Easting	Northing	RL	Gravity
5000	402851.6	5423999	566.137	3962.26
5003	402847.2	5424256	547.565	3957.93
5004	402797.8	5424300	548.159	3958.21
5005	402851.9	5424196	554.067	3957.535
5006	402802.4	5424153	558.814	3953.395
5007	402699.4	5424205	553.944	3957.995
5008	402753.6	5424198	552.637	3958.175
5009	402751.2	5424251	544.325	3958.755
5010	402710.3	5424254	545.385	3959.07
5011	402800.2	5424252	548.668	3958.26
5012	402801.8	5424200	553.274	3958.195
5023	402851.7	5423999	566.197	3962.305
5024	402851.6	5423999	566.137	3962.475
5025	402802.9	5423998	565.795	3954.95
5026	402802.5	5423998	566.294	3955.255
5027	402754	5424051	567.511	3955.175
5028	402799.4	5424048	567.513	3955.3
5029	402800.1	5424048	567.082	3955.305
5030	402851.1	5424052	565.883	3955.27
5035	402852.5	5424153	559.931	3960.78
5036	402847.8	5424100	557.836	3960.345
5042	402799.1	5424103	564.903	3959.295
5043	402748.3	5424097	566.323	3958.88
5044	402746.2	5424150	560.233	3959.71
5045	402851.6	5423999	566.137	3966.105

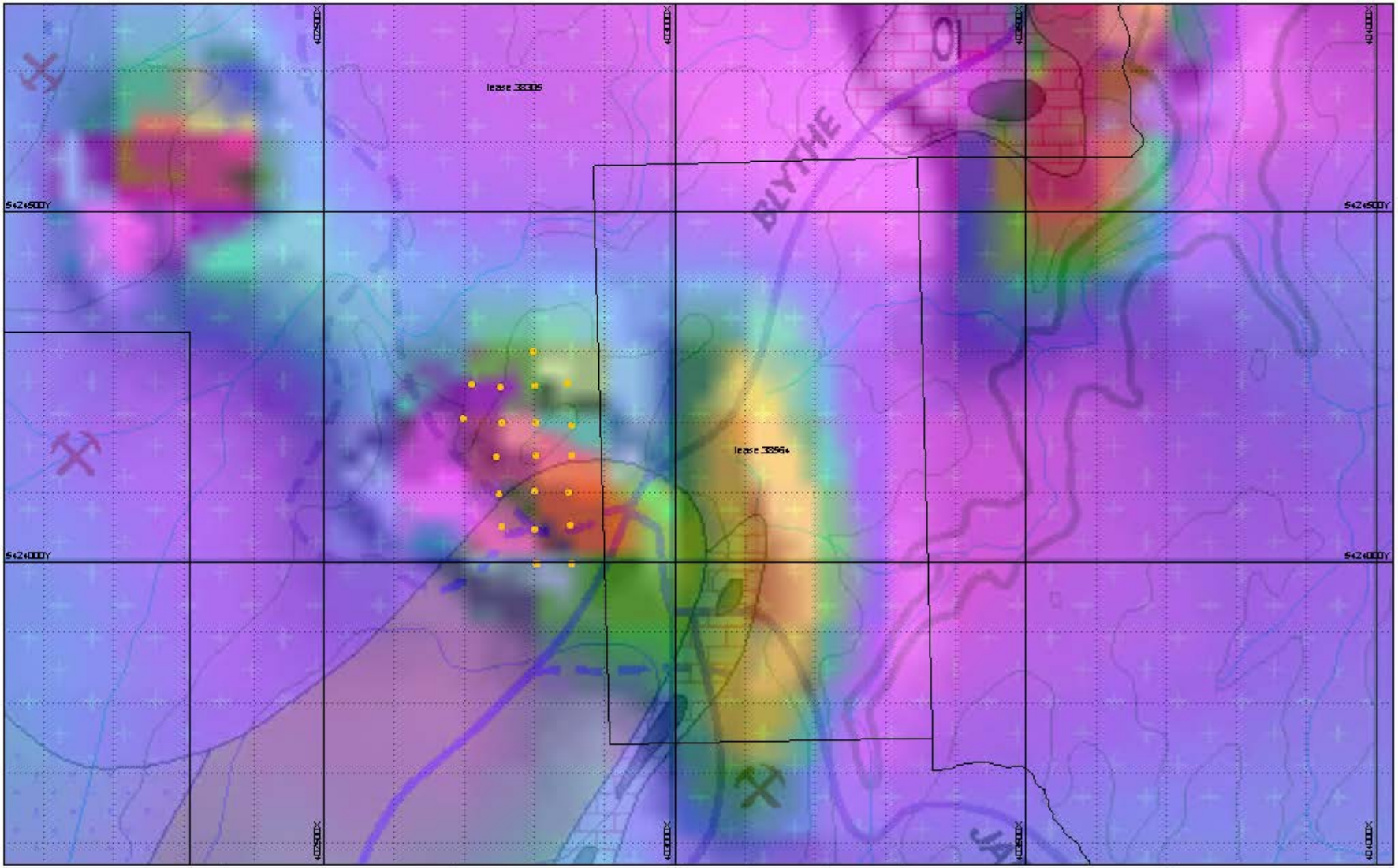

LMPL	Orange Dots = Gravity Points	1:25,000 Geological Map Overlaying Regional Magnetics	Scale is Approximate Plot Date 02-Nov-2016 Sheet 1 of 1 Plot File: Vizex 100 0 100m	**RGS Planned Gravity Survey**	Lottah Mining Pty Ltd

Geophysical Assessment of Potential Magnetite Skarn Mineralisation at the L13 Prospect, Highclaire, Northwest Tasmania

Reuben McCormack BSc

UNIVERSITY OF TASMANIA

A research thesis submitted in partial requirements of the degree of Bachelor of Science with Honours

Primary supervisor: Dr Michael Roach

Supported by

GHD

Mr Hugh Tassell & Mr Michael Anderson Project sponsor:

Lottah Mining Pty. Ltd

School of Physical Sciences, University of Tasmania November 2015

Abstract

Magnetite skarn deposits in northwest Tasmania are associated with Devonian granite intrusions. The L13 prospect is a potential magnetite deposit located approximately 30 km south of Burnie directly north of Kara mine. A high amplitude magnetic anomaly trends north-south through the L13 site and continues to the south over the Kara mine site. There is no outcropping geology or drilling at the site meaning there are no constraints on subsurface lithologies, geometries or of magnetite physical properties.

A ground gravity survey was conducted over the L13 prospect used in conjunction with a high resolution magnetic survey collected with a drone to assess the potential subsurface distribution of magnetite. A ~3000nT magnetic anomaly is present in the centre of the L13 site. Gravity data were processed and corrected for drift, elevation and large terrain variations. Removal of the regional field from the gravity data shows a broad area of low amplitude residual field corresponding to the area of the magnetic high. Forward and inverse modelling of the residual gravity and magnetic datasets illustrates that, in the absence of additional geological or petrophysical constraints, there is significant ambiguity in the position and characteristics of the causative magnetic body. The magnetic anomaly can be matched with a continuum of models ranging from a small deep massive magnetite body to a diffuse near surface zone of disseminated magnetite. The magnetic anomaly is not accompanied by a positive residual gravity anomaly and although gravity modelling is also non-unique, it tends to support the alternative that magnetite is disseminated in the subsurface. Magnetite may be present in conjunction with a low density alteration phase that is responsible for the slight negative residual gravity anomaly spatially coincident with the magnetic high.

Drilling at the L13 prospect is proposed to commence in the near future. It is imperative that petrophysical data are calculated from drillcore at an early stage to constrain the modelling and hence to better guide exploration at the site.

Declaration of Originality

No material presented in this thesis has been accepted for the ward of any other degree or diploma in any tertiary institution. To the best of my knowledge and belief, it contains no material previously published by any other person, except where due reference is made in the text of the thesis

Reuben McCormack BSc

6th of November 2015

Table of Contents

List of Figures

List of Tables

Acknowledgements

Firstly to my supervisor, Michael Roach, a big thank you for the last three years of geophysics at UTAS but especially for all your help and support this year from data processing to thesis writing.

I am very grateful to Lottah Mining for providing me with the opportunity of some industry experience. Thanks go to all the staff there that helped me during my weeks of field work and my stay in Burnie.

Thank you to GHD for handing this project on to me, especially to Hugh Tassell and Michael Anderson for providing me with data and tech support. Your help getting me ready for field work and support while collecting data was invaluable.

To my fellow Honours students both from UTAS and the MTEC courses, what more can I say other than it has been an honour! It has been great seeing a bit more of this country and stressing this year out together with an awesome bunch of fellow geos. A special shout out to fellow geophysics honours student Mark Smith our endless collaborations and sharing of ideas meant we (or at least you) got our daily exercise travelling between offices.

Thanks go to all my friends and family who have encouraged me through the year to keep pushing through to the finish. In particular to my parents whose endless supply of love, care and food packages have gotten me through the year, I could not have done it without you

Lastly to Dr Peter Smith, who although hasn't been a big part of this year was a friend and mentor through the first three years of my university degree sparking a love for science and the desire to investigate the unknown. Thank you for the scholarship you provided me and your every ready support and encouragement to pursue science, sorry it wasn't chemistry.

Chapter 1 Introduction

1.1 Background

Aeromagnetic surveys of northwest Tasmania show high amplitude anomalies around Devonian granite intrusions, in particular the Housetop Granite where heat and magmatic fluids from the intrusion have formed skarn mineralisations in Gordon Group limestone. Magnetite skarn is a common mineral in these deposits and is the primary cause of the high amplitude magnetic anomalies. The Kara deposit is the only skarn mineralisation associated with the Housetop Granite that is currently mined as a resource of magnetite and scheelite.

Other potential magnetite prospects have been identified by the exploration company Lottah Mining Pty. Ltd from aeromagnetic data and previous geological exploration. One of their tenements, named L13, covers a high amplitude, high frequency magnetic anomaly located immediately northwest of Kara mine. Lottah Mining are interested in the skarn mineralisation at this site as a potential source of magnetite. High resolution gravity and magnetic surveys were acquired at this site to gain a better understanding of the potential mineralisation.

1.2 Location

The L13 site can be accessed by forestry roads from the Ridgley Highway around 30 km south of Burnie. Access to the area was organised by Lottah Mining who had also marked the corners of the desired gravity survey area. L13 shares a tenement border with the Kara lease to the south and east. The northern part of the area is a eucalypt plantation, recently cleared and replanted with the remaining branches and other waste piled in long rows. There are some small areas of tea tree swamp and a young eucalypt plantation borders the western boundary of the northern half. The remainder of the L13 area is covered by native bushland. A clear boundary between the cleared and forested area can be seen in the Google Earth image shown in figure 1-1. The bushland is densely vegetated with steep topography exaggerated by a creek system in the south-east corner of the lease.

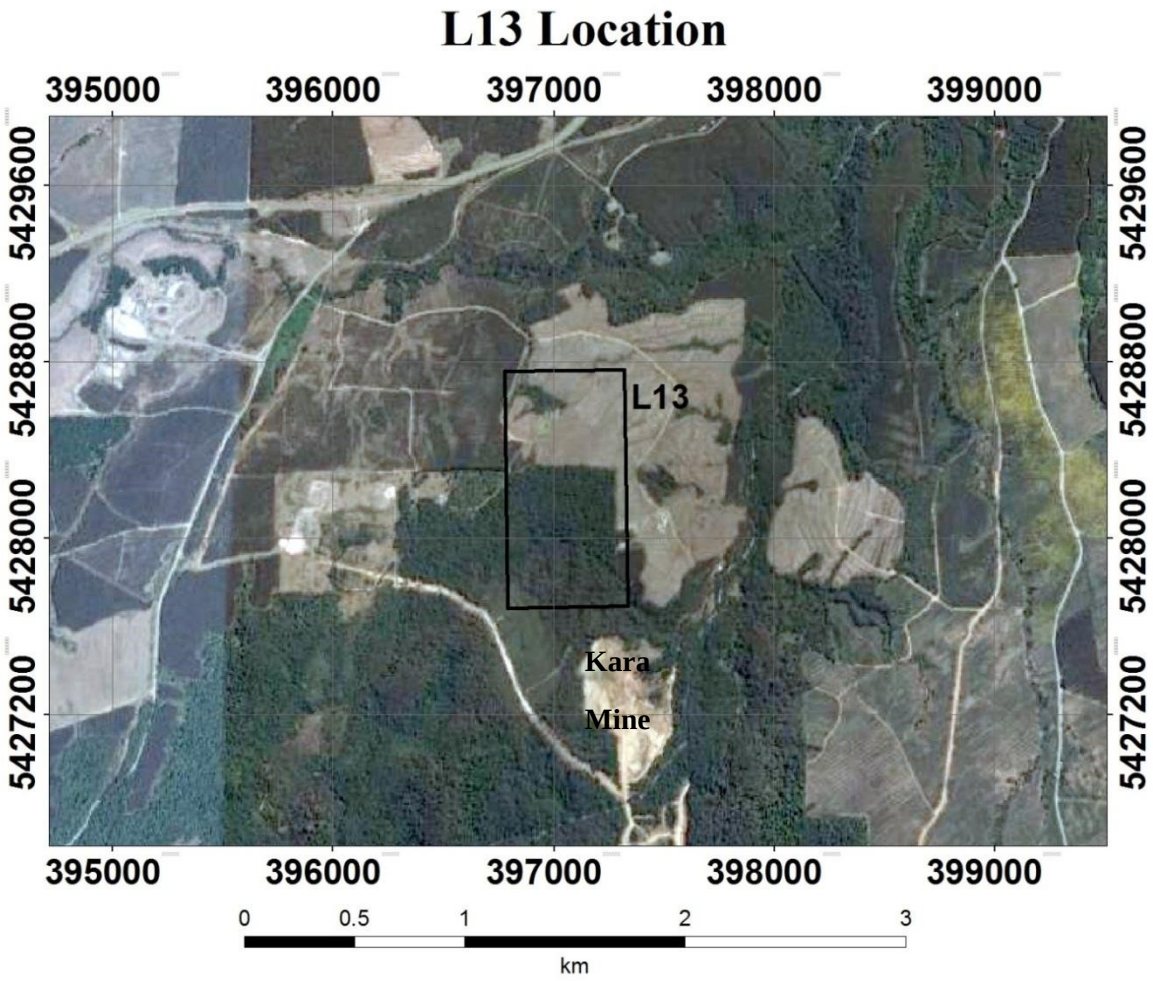

Figure 1-1: Goolge Earth image of L13 and the north extent of Kara mine.

1.3 Previous Work

The L13 tenement is owned by Lottah Mining Pty. Ltd. a geological exploration company based in Burnie on the northwest coast of Tasmania. L13 shares a tenement boundary with the Kara mine, a magnetite-scheelite deposit which has been operational since 1977 (Zaw 2000). A high amplitude magnetic anomaly associate with the Kara tenement trends to the north-northwest and into the L13 lease. In the absence of outcropping geology and drilling the mapping of geological boundaries around the L13 site is estimated from regional context and is poorly constrained.

1.3.1 Auger Drilling

The Australian and New Zealand Exploration Company conducted an auger drilling program during 1974 at the southern end of the L13 tenement. The survey was part of a larger investigation over a period of three years between 1971 and 1974. Auger holes were drilled on potential skarn mineralisation prospects searching for metallic minerals. Drill depths vary between 1.5 metres and 32.5 metres to auger refusal. The descriptions of the auger

locations and observations are qualitative only making them of little use for interpretation but they do provide limited indication of the distribution of magnetite and other lithologies. The majority of identified material is noted as clay with some magnetite skarn fragments as rubble. There are granite contacts at the base of at least two of the holes (not all basements rock types are identified) a unit which is not part of the surface geology at L13 but is integral to skarn formation (Whitehead 1974).

1.4 Other Prospects

Lottah mining also holds the tenements covering other magnetite prospects associated with the Housetop Granite including; Cuprona, Hampshire, Kiwi, Rogetta and Camena (figure 1-2). Mine construction is set to begin at Rogetta in early 2016. Other prospects were in a drilling phase or under assessment from high resolution geophysical investigations at the time of writing.

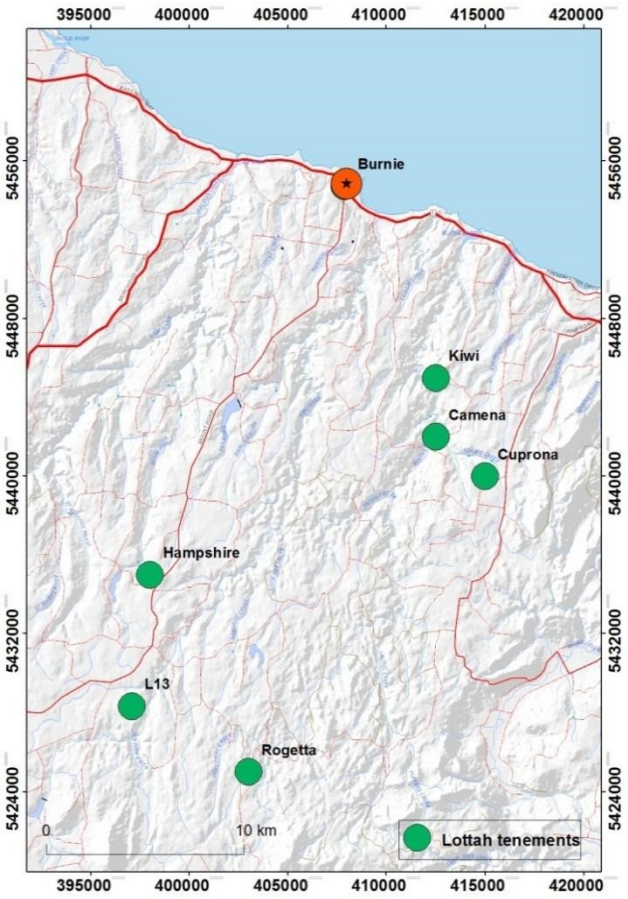

Figure 1-2: Location of tenements owned by Lottah Mining.

1.5 Methods

A gravity survey was conducted by the author over the L13 tenement on a 50×50 m grid.

Travel to the site was made from Burnie each day with a field hand from Lottah Mining. Gravity data was tied to the base station at Natone Primary School. Two gravity meters were used; a Scintrex CG-3 and a Lacoste and Romberg G. Raw data was processed to generate simple Bouguer anomalies using the 1930 IGF formula.

Terrain corrections were calculated based on the local LiDAR data and a regional DEM to generate a Complete Bouguer Anomaly dataset suitable for interpretation.

Magnetic data were collected by an external contractor, Rada Engineering Pty. Ltd, using a three axis fluxgate magnetometer mounted on a drone. Collected data from this survey was provided in a gridded format.

Gridded datasets were analysed and manipulated for display within ER Mapper 7.2 and ArcMap 10.3. Forward and inverse modelling was carried out on individual profiles in Potent and for the entire dataset in three dimensions using UBC-GIF inversion software.

1.6 Thesis Structure

This thesis is divided into seven chapters. A brief overview of the regional geology of northwest Tasmania focusing on the Burnie area and Housetop Granite intrusion, is provided in chapter two. Chapter two also discusses local geology and lithological units found near the L13 survey area. Chapter three focuses on the regional and local geophysical surveys conducted prior to this study and how the physical properties of different rock units affect the geophysical responses. Chapter four outlines the methods involved in the processing and display of collected data. Forward modelling and inversion techniques used to identify the possible locations of magnetite skarn bodies are discussed in chapters five and six respectively. The thesis concludes with a summary chapter discussing the findings and suggestions for further research.

Chapter 2 Geology

2.1 Introduction

North-West Tasmania has numerous magnetite skarn deposits within the Gordon Limestone formed by metamorphism during the intrusion of Devonian granite. The site investigated in this study is the L13 tenement held by Lottah Mining Pty. Ltd which is

located around 30 km South of Burnie close to the major magnetite skarn deposit at the Kara mine. Detailed geological studies of Precambrian rocks of the area surrounding Burnie have been described by (Spry 1957) with detailed studies of the geology of Kara mine described by Barrett (1980), Baillie (1986), Williams et al. (1986) and Williams, McClenaghan et al. (1989) summarised by Zaw and Singoyi (2000)

2.2 Regional Setting

The area containing the L13 prospect is bounded by two blocks of Precambrian rocks, the Tyennan block to the South and Rocky Cape block to the north (figure 2-1). Basement rocks in the study area are predominately comprised of the Precambrian Burnie and Oonah formations consisting of interbedded qurtzose lithic wake, phyllite and minor dolomite. These sediments are unconformably overlain by Cambrian to Early Devonian sequences of siliceous sediments, mafic volcanics, volcano-sedimentary rocks along with younger conglomerates, sandstone, siltstone and carbonates. Devonian granitoid bodies intruded into the volcano-sedimentary sequences including the Housetop Granite which crops out close to the study area. Granite intrusion is associated with multiple carbonate replacement deposits. Multiple Tertiary basalt flows form an extensive cover between the Rocky Cape and Tyennan Block.

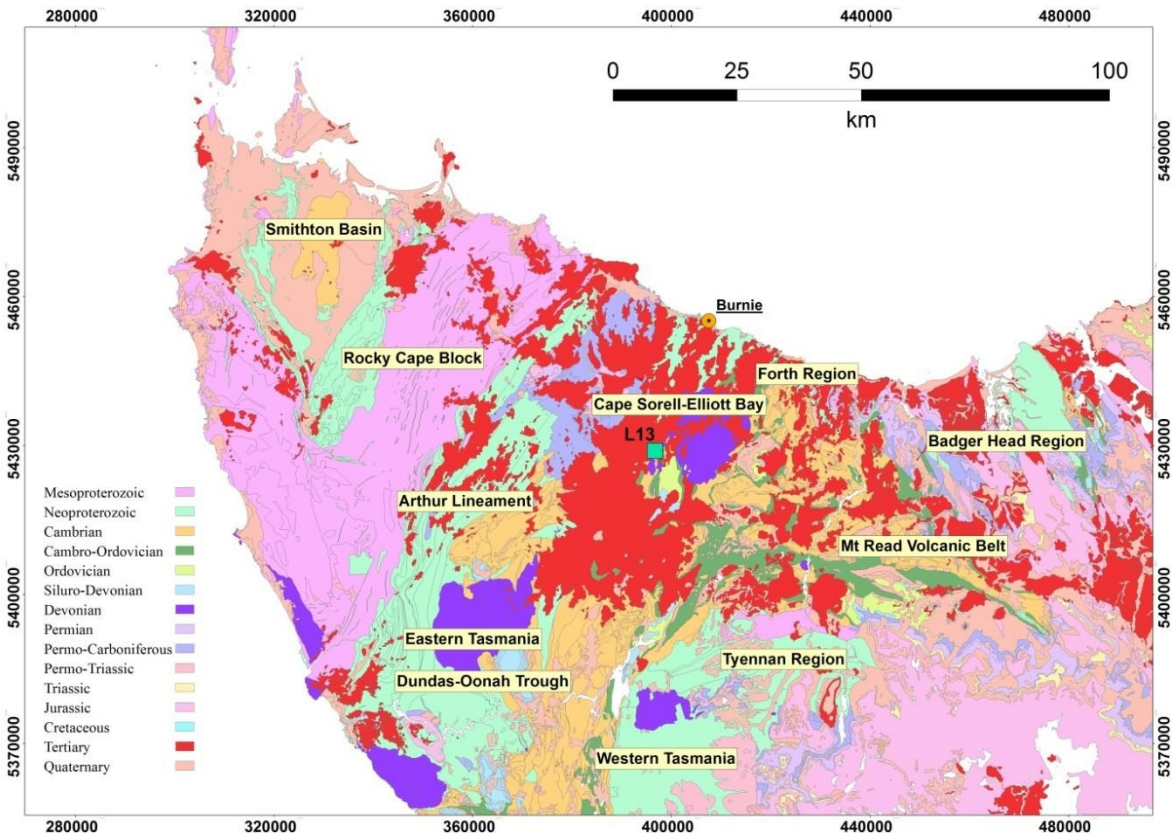

Figure 2-1: Regional geology of northwest Tasmania.

2.3 Precambrian

The basement Burnie and Oonah formations are made up of interbedded quartzose lithic wake, pyllite and some minor dolomite. (Spry 1957) estimates the Burnie formation can be up to 1.5 km thick. It is also noted by Spry, Blissett et al. (1962) that the Burnie and Oonah formations are very similar in nature; with angular quartzite grains and rock fragments and a variable sericitic matrix present throughout both formations. Graded bedding, flow casts, scour, flame and slump structures are all features of the Burnie and Oonah quartzites.

2.4 Cambrian

Uncorformably overlying the Precambrian basement rocks are the Crimson Creek and Success Creek Formations. The Crimson Creek Formation is made up of mafic volcanics and volcano-sedimentary units while Success Creek contains siliceous sandstone, mudstone, dolomite and breccia. The Success Creek Formations interbedded rocks contained within contact metamorphic areoles have been metamorphosed into hornfels, marble and skarn.

2.5 Odovician-Early Devonian

The Ordovician to Early Devonian Warawina Supergroup has been divided into the Tiger, Gordon and Denison Groups by Banks and Baillie (1989). The Denison Group has been further divided into the Moina Sandstone and Owen Conglomerate in the area surrounding L13. These units are the lowest stratigraphic levels of the Wurawina Supergroup and consist of conglomerate, sandstone, siltstone and argillite. The Gordon Group (also called Gordon Limestone) contains both pure and impure carbonates and limestone. These shallow water sediments once covered the majority of western and central Tasmania during the Ordovician period. The Tiger Group is the highest stratigraphic level of the Wurawina Supergroup and is made up of limestone fragment bearing quartzite (Singoyi, B. and K. Zaw 2001). Carbonates within the Gordon Group are the major hosts for skarn mineralisation associated with the emplacement of the Housetop Granite.

2.6 Devonian

The Housetop Granite is a red granite pluton that crops out over 157 km^2 in central northern Tasmania (Bottrill 2005) and is one of a number of granite bodies which intruded the northwest of Tasmania during the Devonian period. The surface and subsurface extent of these granite bodies can be identified in the regional gravity image due to their lower density compared with the surrounding rocks. The intrusion mechanism has been interpreted as passive with an upwards displacement (Gee and Groves 1971). Mineralisation in carbonate replacement deposits is attributed to the intrusion of these

bodies which are generally found within 1-1.5 km of the deposits (Leaman and Richardson 1989). Rb/Sr dating by Williams, McClenaghan et al. (1989) gives an age range of 319±10 Ma to 367±10 Ma, Sawka, Heizler et al. (1990) places the age at 369.4 Ma using $^{40}K/^{39}Ar$ dating. Aeromagnetic data suggests an east-northeast trend of Devonian granite bodies local to the Housetop Granite. Leaman, Richardson et al. (1980) propose that these are part of a larger north-northwest trending zone spanning the entire state from the south to King Island.

2.7 Tertiary

Tertiary basalt, sand and gravel units cover the older geological units along with Quaternary transported and insitu gravel to clay materials. There were multiple basalt flows throughout the Tertiary period; Knights and Matthews (1976) propose four major flows located in the Burnie area separated by sediment bands greater than 1.5m thick. Basalt layers can be more than 360 m thick in places which has proved problematic for drilling programs searching for mineralisation in underlying Palaeozoic strata. The upper surface of these volcanics weather evenly and easily due to its vesicular nature resulting in the nutrient rich red soil of northwest Tasmania.

2.8 Magnetite Skarn Deposits

Magnetite forms when there is an abundance of iron and oxygen in an environment with low oxidation conditions. Oxygen can be added to the system as dissolved gas within magmatic water or to a lesser extent as the by-product of carbonation reactions (Emerson 1986). The Kara deposit has a resource of approximately 3.3Mt of magnetite, with more than 30% iron. The bulk of the magnetite has been extracted for use in coal washing. The mines lifetime is estimated to span another 18-34 years as of January 2013 (Ltd, T. M. (2013)). The majority of the ore is found within the Wurawina Supergroup between the Moina Sandstone and Gordon Limestone. Lesser skarn deposits have been found within Cambrian sediments thought to have developed within calcareous horizons. Magmatic fluids heated during the intrusion of the Housetop Granite cause a replacement chemical alteration within the carbonates (Singoyi and Zaw 2001) resulting in the magnetite ore.

2.9 L13 Geology

There is very little outcrop in the L13 area and no drilling making the geological boundaries somewhat speculative. Tertiary basalt dominates the cover to the north of the L13 prospect and surrounds outcrops of Wurawina Supergroup and Tyndall Group sediments (figure 2-2). The heavily forested southern half of the L13 area is mostly Owen Group conglomerate with interbedded sandstone. A thin zone of Cambrian Tyndall Group

sediments borders the Owen Group rocks to the west. This change in rock type partially explains a change in the vegetation between dense forest and open button grass plains. The cleared forestry land in the northern half of L13 is on Tertiary basalt although there are no clear outcrops over the site due to thick soil and vegetation cover. Some old logging roads within the forest show exposed rock, however it is difficult to determine whether this rock is insitu, material brought in for road building or loose rock brought up in the root systems of fallen trees. Further investigation was not carried out at these sites due to time pressure to complete the gravity survey. Intruding granite plutons of the Housetop Granite are located to the south and southwest of the L13 tenement.

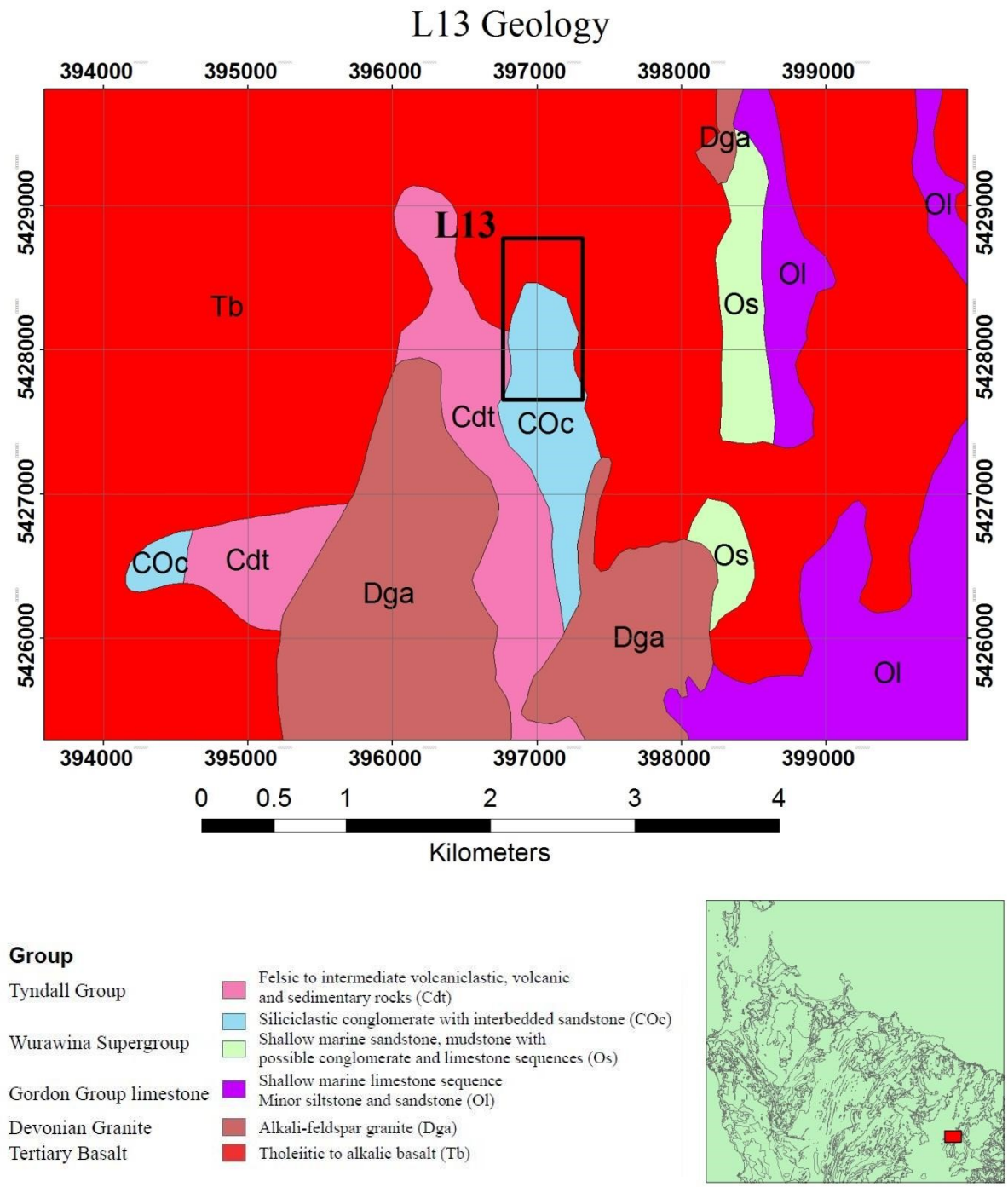

Figure 2-2: L13 local geology

Chapter 3 Potential Fields

3.1 Magnetics

There are three different types of magnetic particles; ferromagnetic, diamagnetic and paramagnetic, all of which occur naturally. However diamagnetism and paramagnetism do not contribute significantly to measured magnetic anomalies in most geological situations (Clark and Emerson 1991). Ferromagnetic particles have a high magnetic

susceptibility this results in a magnetic field being formed in the material parallel to the direction of the external inducing field it is placed in. The inducing field in exploration geophysics is the
Earth's magnetic field, the integral properties of which are the field's strength and direction. Induced magnetization is the predominant mode of magnetization for coarse grained magnetite and is the major type of magnetisation recorded in most magnetic surveys due to magnetite's high magnetic susceptibility.

Susceptibility can be specified in cgs units or SI units. A simple conversion factor of 4π is used to adapt formulas to be compatible with software such as potent and the UBC Geophysical Inversion Facility (UBC-GIF).

$$1\ (SI\ unit) = 4\pi(cgs\ units) \qquad \text{(equation 3-1)}$$

Induced magnetization is often considered a direct indication of the magnetite content of the rock. Magnetite is widely distributed and has a much higher magnetic susceptibility than all other minerals with values three to seven times greater than the next highest; titano-magnetite and pyrrhotite. Average susceptibility for pure magnetite is 6 in SI units but has a range of 1.2 to 19.2 SI (Telford, Geldart et al. 1990). The combination of inducing field, magnetic susceptibility and the geometry of the causative body together dictate the form of an induced magnetic anomaly.

For induced magnetism the strength of the magnetic field can be calculated from the magnetic susceptibility (k) multiplied by the intensity of the inducing field (H).

$$M_i = kH \qquad \text{(equation 3-2)}$$

The total magnetic field strength is denoted as:

$$M_t = M_r + M_i \qquad \text{(equation 3-3)}$$

M_t is the total anomalous field strength, M_r is the strength of the remanent field and M_i is the strength of the induced field (Girdler and Peter 1960). The ratio of remanent magnetism to the induced field is known as the Koenigsberger ratio (Q value). As an example black shales have Q values of 10-100 while magnetite has a Q value less than five (Hyvönen, Airo et al. 2012), (Clark and Emerson 1991).

Remanent magnetism is a 'frozen' magnetism which has strength and direction independent of the Earth's field at the time of the survey. In some cases remanence can

be ignored as it is much weaker than the induced field but determining the relative contributions of remanence and induced magnetisation can be difficult in many situations. The direction and strength of remanent magnetism can be measured from core samples or in situ outcrop. No samples or outcrop are available for the L13 prospect so assessing the relative contribution of remanence is difficult. Remanent magnetism is most pronounced in rock containing fine-grained magnetite (<20µm). In coarse grained magnetite remanent intensities have low amplitudes and decay rapidly with exposure to the Earth's field.

3.1.1 Magnetite Grain size

In his study on titanomagnetites ($Fe_{3-x}Ti_xO_4$, $0 \leq x \leq 1$) Clark (1997) presents susceptibility has a strong reliance on the grain size of the mineral. Variations of 2.5 (in SI units) for a grain sizes varying between 1µm and 120µm is stated but a formula for this relationship is not provided. After samples from L13 have been collected and tested grain size and variation should be measured to properly constrain the model.

3.1.2 Measuring the Field

A magnetic field can be measured in a variety of ways; older methods timed the oscillations of a compass needle while newer digital devices (proton precession and alkalivapour) measure changes in electron energy levels caused by applied magnetic fields. L13 was surveyed with a three axis fluxgate magnetometer. Fluxgate sensors are unidirectional hence the need for a three axis model to measure all components of the magnetic field. External fields parallel to the internal sensors induce a voltage in the coils of the sensor from which the amplitude of the applied field can be calculated.

3.2 Gravity

Variations in the composition of the Earth's crust lead to subtle changes in the Earth's gravitational field. The strength of the field is proportional to the subsurface mass and hence the density of the crust it is also inversely proportional to the distance from source to observer squared (equation 3-4). For common geological scenarios, the surface variations in the gravity field due to subsurface mass variations are extremely small and sensitive gravimeters are required to detect lateral changes in crustal density.

$$F_g = \frac{Gm_1m_2}{r^2} \qquad \text{(equation 3-4)}$$

F_g is the gravitational force between two objects of mass m_1 and m_2 separated by a distance r and G is the gravitational constant (6.67×10^{-11} Nm^2kg^{-2}). In a geophysical gravity survey the two masses are the Earth and the spring-loaded mass within the gravimeter. To find the exact value of this force requires an absolute gravity measurement. Absolute measurements taken by Geoscience Australia average over 2000 measurements in a single location over a 24 hour period to obtain a measurement (Dando & Tracey 2008). Relative gravity measurements can be made much faster and linked to a site where the absolute gravity is known. For a geophysical survey the standard unit of measurement for the gravitational field is the milligal which is equivalent to $10^{-5}ms^{-2}$ in SI units.

3.3 Regional Geophysics

3.3.1 Regional Magnetic

No single magnetic survey covers the whole of Tasmania and composite images have been produced from multiple surveys by Geoscience Australia and MRT. Surveys for northwest Tasmania were conducted by the Bureau of Mineral Resources under the Australian Geological Survey Organisation (AGSO) with line spacing ranging from 400 to 800 m. Commercial magnetic survey data obtained at greater resolutions has been added to create the composite image (figure 3-1).

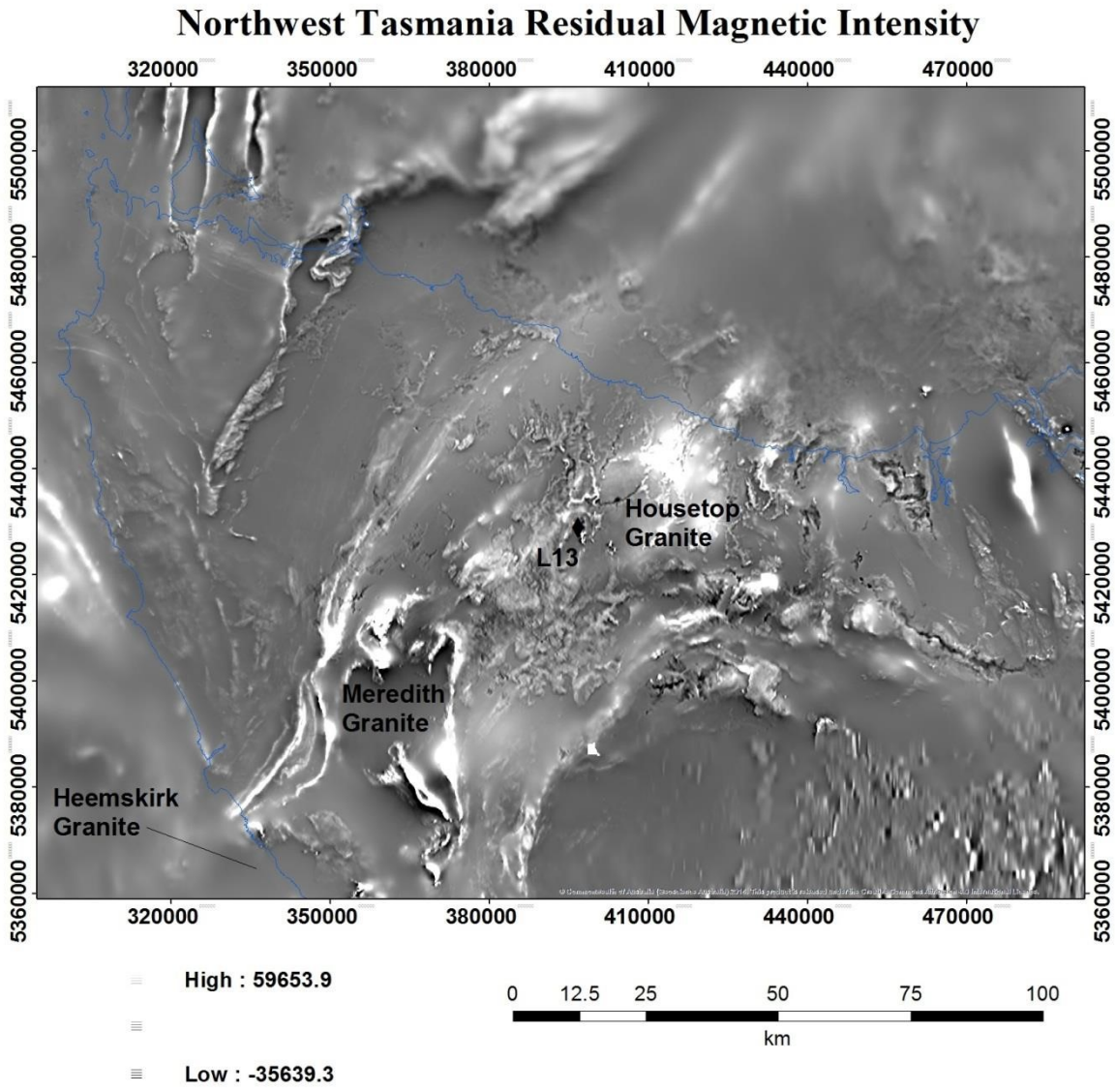

Figure 3-1: Residual magnetic image of northwest Tasmania (units of nT).

There are numerous high amplitude high frequency features surrounding the L13 tenement within a 40 km radius, enclosing the Housetop granite to the northeast. These high amplitude magnetic features represent a combination of magnetite skarn mineralisation formed during intrusion of the Housetop granite and the covering of Tertiary basalt.

At a regional scale (Figure 3-2) magnetite skarn deposits are shown by high intensity, high frequency localised anomalies. Irregular high spatial frequency anomalies that may be either positive or negative result from surface Tertiary basalt

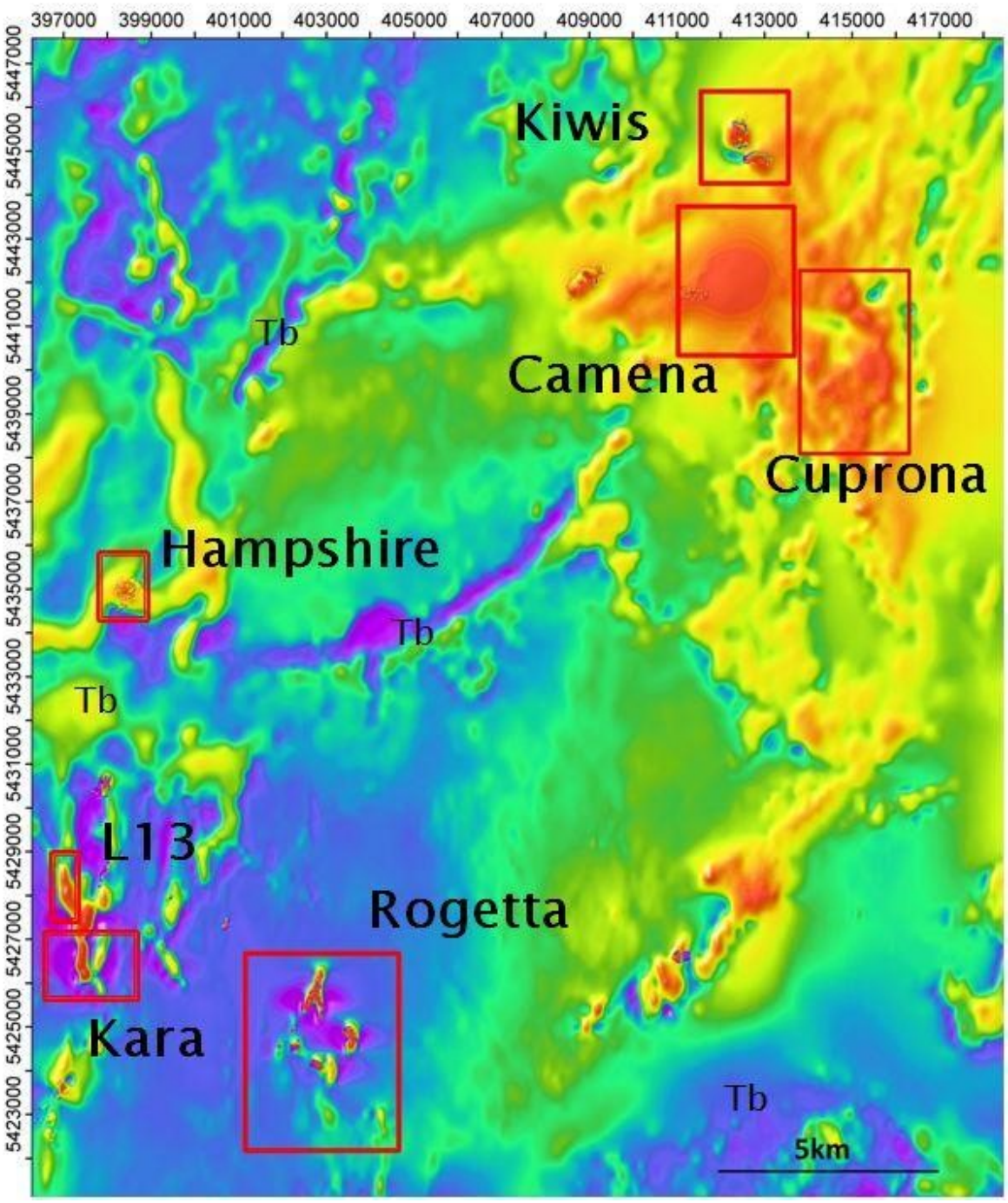

Figure 3-2: Regional magnetic data for magnetite prospects. Tb➔ Tertiary basalt.

3.3.2 Gravity

Gravity data in western Tasmania has been compiled from multiple sources by Mineral Resources Tasmania and is available for download from their site as Bouguer anomaly and residual Bouguer anomaly data. A detailed gravity survey of Tasmania's north-west was conducted in 2012/2013 by Atlas Geophysics Pty. Ltd adding to the MRT database. Measurements were taken along existing roads and forestry paths every kilometre tying in to base stations at Waratah and Smithton (Fotsyth 2013). This survey included measurements

taken in the region of the L13 site. Station spacing is too large to show details of a possible magnetite skarn mineralisation.

Figure 3-3 shows the residual Bouguer gravity data of northwest Tasmania calculated from the Bouguer anomaly. Corrections are made using MANTLE-09 and correct for mantle topography and surrounding water bathymetry. These newer corrections also take into account formations in Bass Straight enabling corrections for surveys conducted on King and Flinders Islands (Leaman 2009).

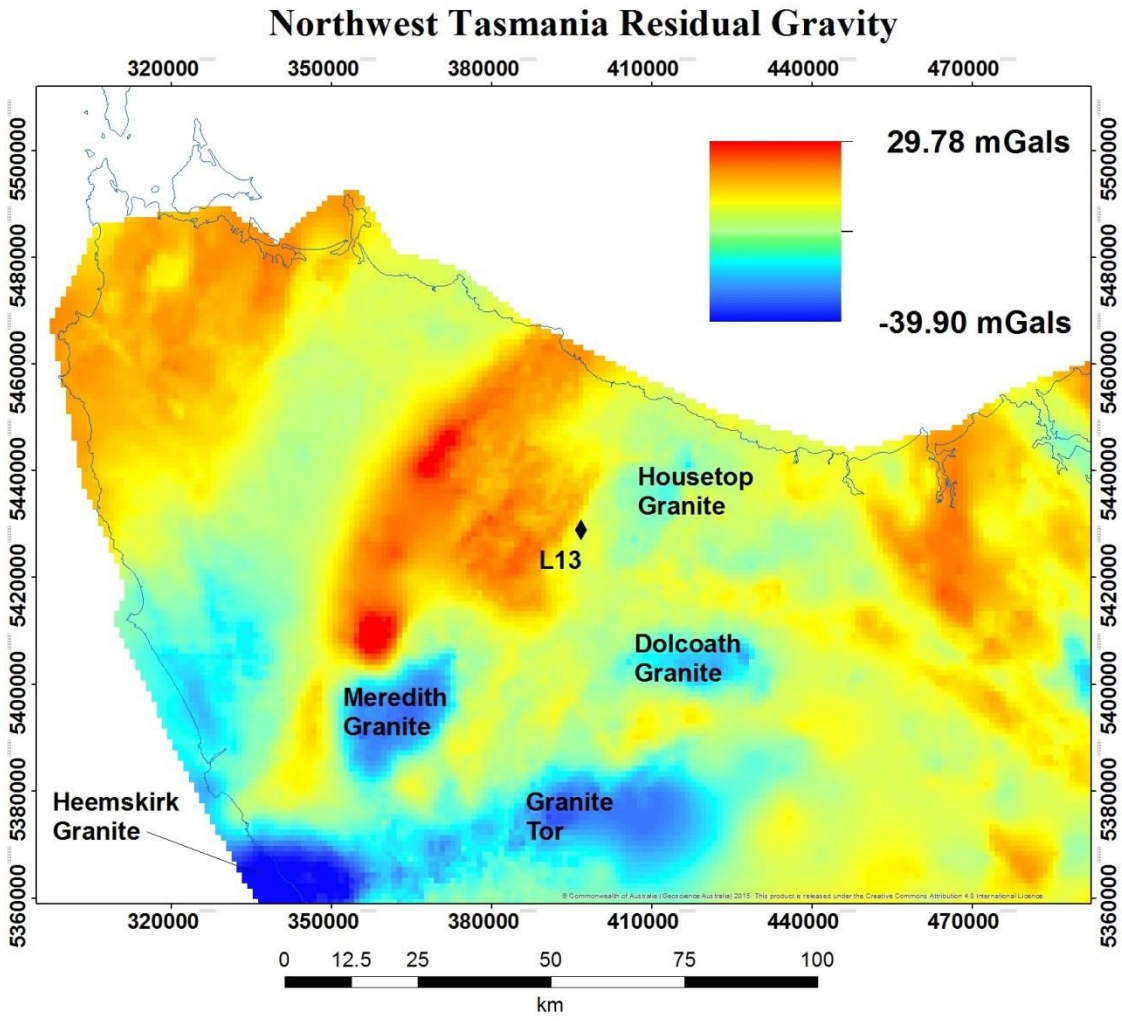

Figure 3-3: Residual gravity of northwest Tasmania (as of June 2013).

The L13 tenement is located between a low anomaly to the east and a high to the west on the residual gravity map (figure 3-3). The low gravity region is inferred to result from the Housetop Granite, one of the Devonian granitoid bodies which can be identified by the low density features in Figure 3-3.

3.3.3 Homogeneous Densities of Hampshire Lithologies

Duffett, Bombardieri et al (2013) compiled a list of densities for rock groups found in northwest Tasmania (Table 3-1). Sedimentary units have a similar density to the average continental crust density of 2.67gcm^{-3}. The Housetop granite has a density less than this (2.62gcm^{-3}) resulting in the low gravity response seen in figure 3-3.

Age	**Unit**	**Density (gcm^{-3})**
Devonian	Housetop Granite	2.62
Ordovician	Gordon Group	2.67
Cambrian	Owen Group	2.74
Cambrian	Crimson Creek	2.79
Cambrian	Success Creek	2.66
Precambrian	Oonah Formation	2.74

Table 3-1: Homogeneous densities for Hampshire lithologies. Adapted from (Duffett, Bombardieri et al. 2013)

Chapter 4 Geophysical Data Acquisition and Processing

4.1 Introduction

Magnetic data covering the L13 prospect were collected by Rada Engineering Pty. Ltd using a three axes fluxgate magnetometer mounted on a multirotor UAV X4 drone. Processing of the raw data was also completed by Rada Engineering. Gravity data were collected by the author using two gravimeters; a Scintrex CG-3 and a Lacoste and Romberg G. Location data was collected with a Trimble R10 DGPS with an Omistar XP signal subscription with the heights corrected using LiDAR data. Gravity data processing was conducted using the 1930 gravity formula, the same formula used by MRT allowing the collected gravity data to be compared to the MRT data base. A kriging interpolation algorithm was used in Surfer 12 to grid the gravity data.

4.2 L13 Data Collection

4.2.1 Magnetics

Magnetic data was initially collected by Lottah Mining personnel, traversing L13 on foot with a magnetometer and a handheld GPS. Data acquired using this method became inaccurate within the bush due to the canopy disrupting the GPS signal and the thickness of vegetation making walking in straight lines difficult and time consuming. The decision was made by Lottah to instead collect the magnetic data using a multirotor UAV X4drone from an external contractor; Anton Rada, Rada Engineering Pty. Ltd. Flight lines were flown in an east-west direction separated by 25 metres with tie lines flown perpendicular every 100 metres. Sensor clearance was set to 20 metres and simultaneously collected elevation data with the magnetics, this data was not used for any data processing due to the greater accuracy of the available LiDAR data.

4.2.2 Gravity

Gravity data were collected on a 50 m × 50 m grid over the whole L13 site with a total of 242 stations recorded. A further 33 readings were measured on the surrounding forestry roads, adding to the sparse MRT gravity data to form some context for the wider area. Data were collected with two gravimeters; a Scintrex CG-3 and a Lacoste and Romburg G.

Towards the end of the second day of gravity data collection the CG-3 meter experienced a large tare. The meters relative mGal reading went from 3972.975 to 3979.360 over a distance of 50 m in 5minutes. Average drift rates for the CG-3 meter are in the order of 10^{-4} mGals per minute and the variation across the entire L13 site was found to be less than four mGals. The tare was confirmed as a mechanical error when a reading was taken at the local base station returning a value 3980.250 compared to 3973.075 three hours earlier. Excluding the local base four other readings were taken after the tare on day two, readings at these sites were repeated at a later date with the Lacoste and Romburg G meter. These higher readings continued on day three and for the first four readings of day four. Early on day four the readings jumped back down from 3982.765 to 3972.970 in nine minutes and 50 m. These first four readings were repeated and the CG-3 performed as normal for the remainder of the survey. The temporary tare in the meter corresponded to problems with the battery and electronics of the meter in particular the data recording and levelling functions. After the survey had been completed the battery was replaced and some minor repairs were completed by GHD. This service brought the CG-3 back to working order. A hard copy of the readings was maintained throughout the survey so there was no loss of data. When connected to a computer it was found that none of the data

taken had been saved on the machine including that from before the tare. A test loop was carried out at the university between trips to the L13site to test the tilt and the drift. Results of this test loop were a 0.275 mGal drift over 56 minutes and the digital tilt display showing inconsistencies with the manual level. For these reasons the survey was continued and some earlier stations recalculated with the Lacoste and Romburg G gravimeter.

A total of nine days were spent collecting gravity data over a period of three weeks for the L13 site, this included collecting stations on the surrounding forestry roads for regional context and referencing the local L13 base station (figure 4-1) to the gravity base station at Natone Primary School. The base station tie in was carried out by taking three readings at Natone Primary with a reading at the L13 local base station taken between each. An absolute gravity measurement has been taken at the Natone Primary station. Comparison of readings there with those at the L13 site enable the absolute gravity to be calculated at the L13 base station and hence all of the gravity stations. Each day there were at least two closed loops to the L13 local base, one at lunch and one at the end of the day.

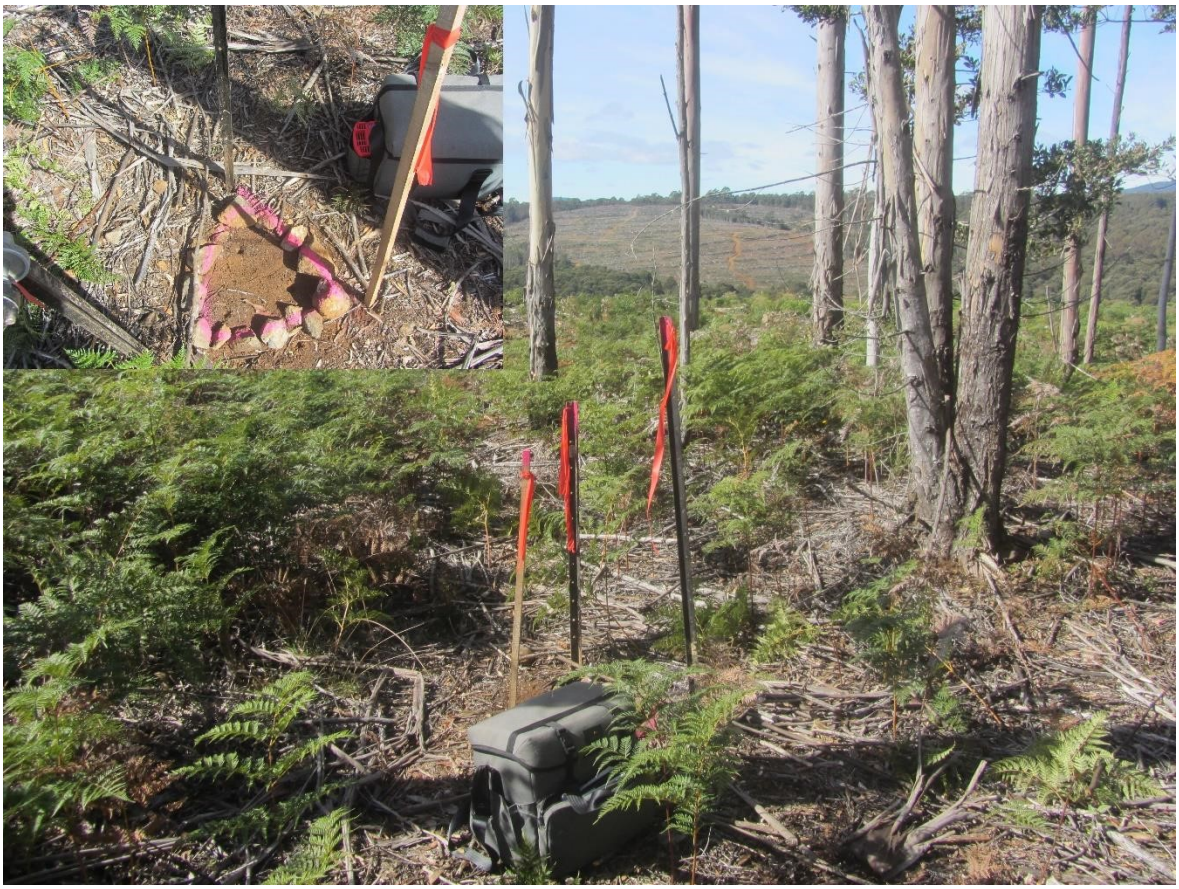

Figure 4-1: L13 local base station location looking east, insert; rock circle for the gravimeter.

4.3 Data Processing

4.3.1 Magnetic Data

Data was provided in three gridded forms; total magnetic intensity (TMI), TMI reduced to the pole (RTP) (figure 4-2) and the first vertical derivative of the RTP data (figure 4-3). The full processing report of the magnetic data from Rada Engineering can be found in appendix B.

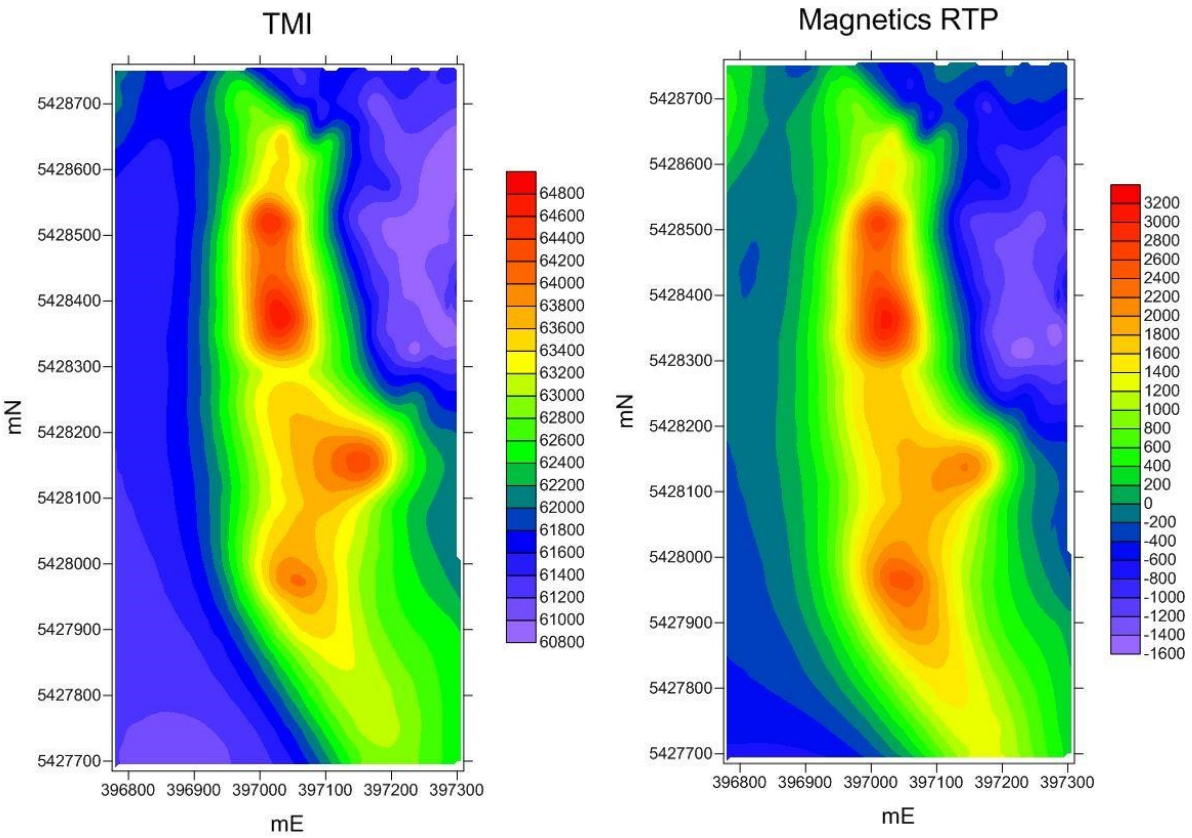

Figure 4-2: TMI (left) and RTP (right) L13 images in units of nT.

The TMI image has a large amplitude (~3000nT) anomaly trending north-south through the middle of the L13 prospect. The anomaly has four distinct peaks, three of which have symmetrical profiles while the eastern most anomaly is skewed to the west. This indicates a near vertical dip for the symmetrical profiles, while a skewedness to the west would suggest a body dipping to the west.

4.4 RTP

Reduction to the pole creates a magnetic image equivalent to data if the observed anomaly was located at the Earth's magnetic pole and therefore was within a vertical magnetic field. RTP provides an image for qualitative interpretation as anomalies are now

positioned above the causative magnetic body rather than skewed due to the Earth's magnetic field direction. At the time of data collection the Earth's magnetic field at the L13 location had a declination of 13.4^{o}, an inclination of -71.5^{o} and total field strength of 61500nT (NOAA 2015).

4.5 1VD

Vertical derivatives are a comparison of data from the same location calculated at different elevations. This technique is applied as a spatial frequency domain transformation used to highlight high frequency features, define the edges of a magnetic body from the rapid change in the vertical (gradient) field. The first vertical derivative refines the position of anomalous features but also amplifies the noise (figure 4-3). Higher order vertical derivatives can be made to further enhance anomalous features. The noise will be amplified as well, meaning vertical derivatives are usually first or second order only.

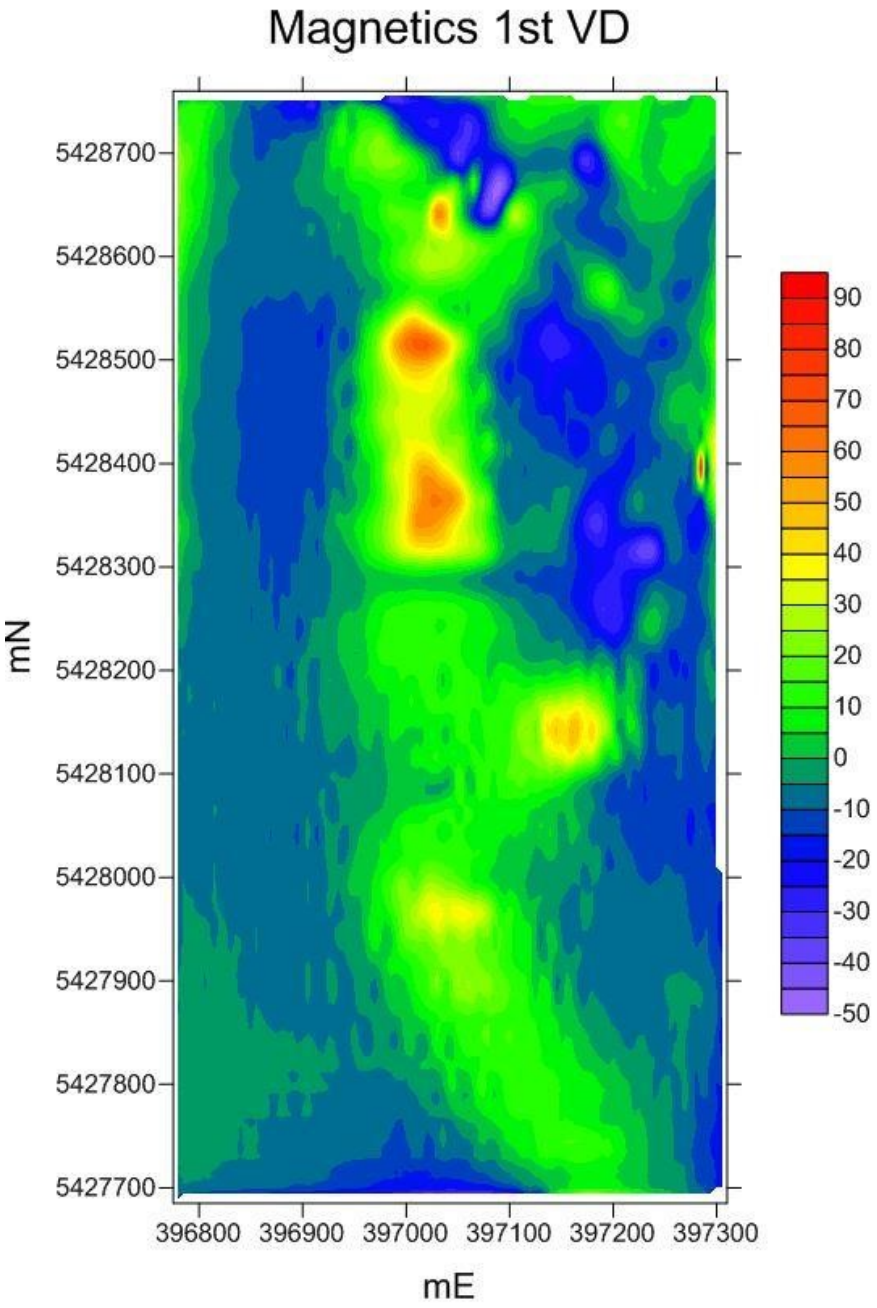

Figure 4-3: RTP 1st vertical derivative of L13, in units of nT/m

4.6 Drift and Simple Bouguer Corrections

Digital gravimeters record data in a format compatible with software such as intrepid while older meters requiring manual recording and need to be correctly formatted into a text document for processing in these applications. Problems with the Scintrex CG-3 meter meant that data was not saved to the device and all data had to be manually imported. Gravity reductions for all stations were processed using Microsoft Excel.

Simple Bouguer corrections based on the 1930 gravity formula were calculated using Microsoft Excel using equations 4-1 to 4-4. The observed gravity (g_{obs}) was calculated

from the relative gravity values obtained from the gravimeter. For the Lacoste and Romberg G relative values need a correction factor of 1.053 multiplied to the readings for conversion to mGals. Drift adjustments correct for the change in readings between the start and finish of each loop at the L13 local base station. The local base station was tied in to the base station at Natone Primary School which has known absolute gravity values for two datums; ISOGAL 65 and ISOGAL84. The ISOGAL 65 value was used to allow a comparison with the MRT gravity survey data.

Normal gravity

$$g_0 = 978049(1 + 0.0052884 \sin^2 \lambda - 5.9 \times 10^{-6} \sin^2 2\lambda\ )\ (mGal)$$

(equation 4-1)

(Ahern 2015)

Free Air correction

$$g_{fa} = 0.3086h\ (mGal)$$ (equation 4-2)

Simple Bouguer correction

$$g_b = 0.04193\rho h\ (mGal)$$ (equation 4-3)

Simple Bouguer anomaly

$$g_{sb} = g_{obs} + g_{fa} - g_0 - g_b$$ (equation 4-4)

A large tare in the CG-3 data occurred during the final loop on day two, with a total drift of 7.175mGal between the local base station in just over three hours. An internal loop recorded a drift of -0.005mGal over one hour, this drift rate was used for the drift corrections of this entire loop.

4.7 Terrain

A Trimble R10 DGPS system was used to record the location and elevation of each gravity station. This DGPS system uses the Omistar XP satellite system and records a horizontal accuracy of ±0.15m. Under the dense tree cover of the southern half of the L13 prospect signal between the DGPS and satellites becomes disrupted resulting in large errors in the recorded elevation. LiDAR elevation data supplied by GHD was therefore used for the simple Bouguer and free air corrections (equations 4-2 and 4-3) LiDAR data was provided in

a XYZ file and gridded in Surfer 12 spacing using a kriging algorithm with a one meter grid. LiDAR heights were obtained for the positions from the DGPS using the Arcmap 10.3 'extract values to point' tool for all but two of the readings taken on the surrounding forestry roads which were outside the eastern boundary of the LiDAR image. Elevation values from the LiDAR data was used due to a greater accuracy than those from the DGPS with discrepancies being as great as 30 meters in the forested area. Average differences between the DGPS and LiDAR heights for readings in open areas were consistently less than 10 centimetres. The DGPS heights were determined to be accurate enough for the points outside the LiDAR image to be included in the final data.

Contour maps were created using a kriging algorithm in Surfer 12, with a grid spacing of 10 m. these gridded files were converted to ers files using ER mapper 7.2 for loading into ArcMap 10.3. The coordinate system for all data was set to MGA Zone 55, Horizontal Datum GDA94.

Terrain corrections for the complete Bouguer anomaly were carried out in two phases. A local scale to 400 m and regional scale to 20 km from the edge of the survey area was used. Local terrain corrections were calculated using the LiDAR heights while the regional correction were calculated from a 25m resolution DEM derived from the 1:25,000 scale topographic mapping. Terrain corrections were undertaken using Fortran code developed by Roach (1994). These two corrections were added to the simple Bouguer anomaly to calculate the Complete Bouguer Anomaly.

Terrain corrections for the simple Bouguer anomaly (figure 4-4) remove some irregular anomalous components, especially in the southern half of the study area where the effect of the steep topography is most dramatic (figure 4-5). Moderate corrections of ~0.6mGal are applied on the east edge in the north half of the field to correct for a steep drop off, sloping to the east. After Complete Bouguer corrections there were four points which appear anomalous compared to surrounding data by at least one mGal. Local variations in the Complete Bouguer Anomaly in excess of 1mGal between 50 m spaced samples are considered as unlikely to be due to geological variations in this environment. These points are interpreted to result from issues with either the primary gravity data or the elevation/location data used to correct the readings and these four points have been removed from the data (figure 4-6). The moderate resolution gravity survey of the area

surrounding the L13 prospect (figure 4-7) displays a significant regional variation of three to four mGals across ~1.5 km, increasing from the east to the west. This regional trend could results from deep mass variations, likely related to the subsurface distribution of low density granitic rocks of the Housetop Granite.

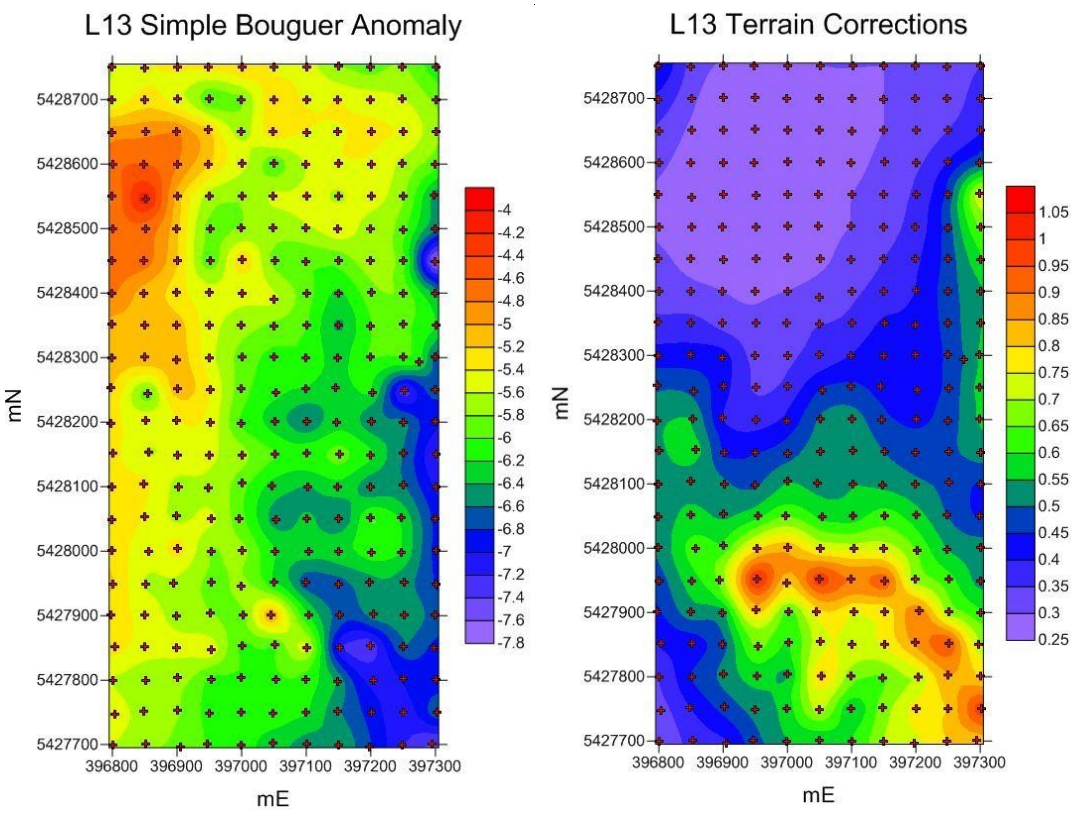

Figure 4-4: Simple Bouguer (left) and terrain corrections (right) gravity stations marked with red crosses, units of mGal.

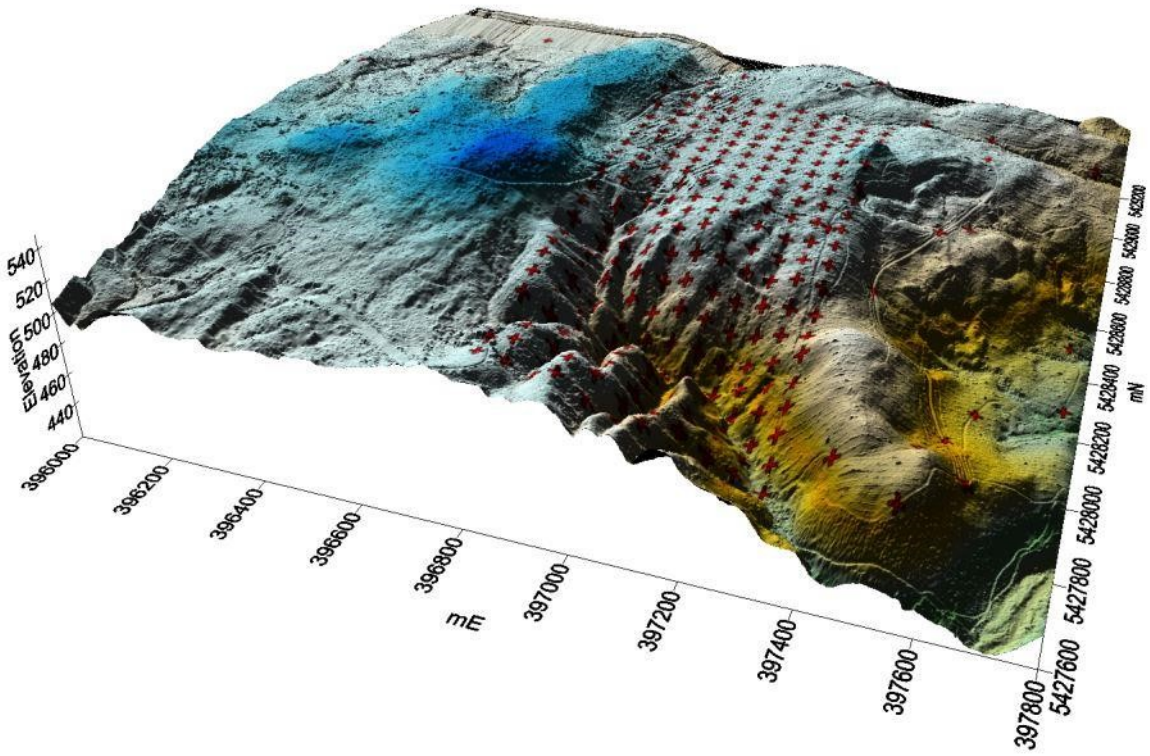

Figure 4-5: LiDAR elevation surface of L13 and the surrounding area, red crosses mark the gravity survey points.

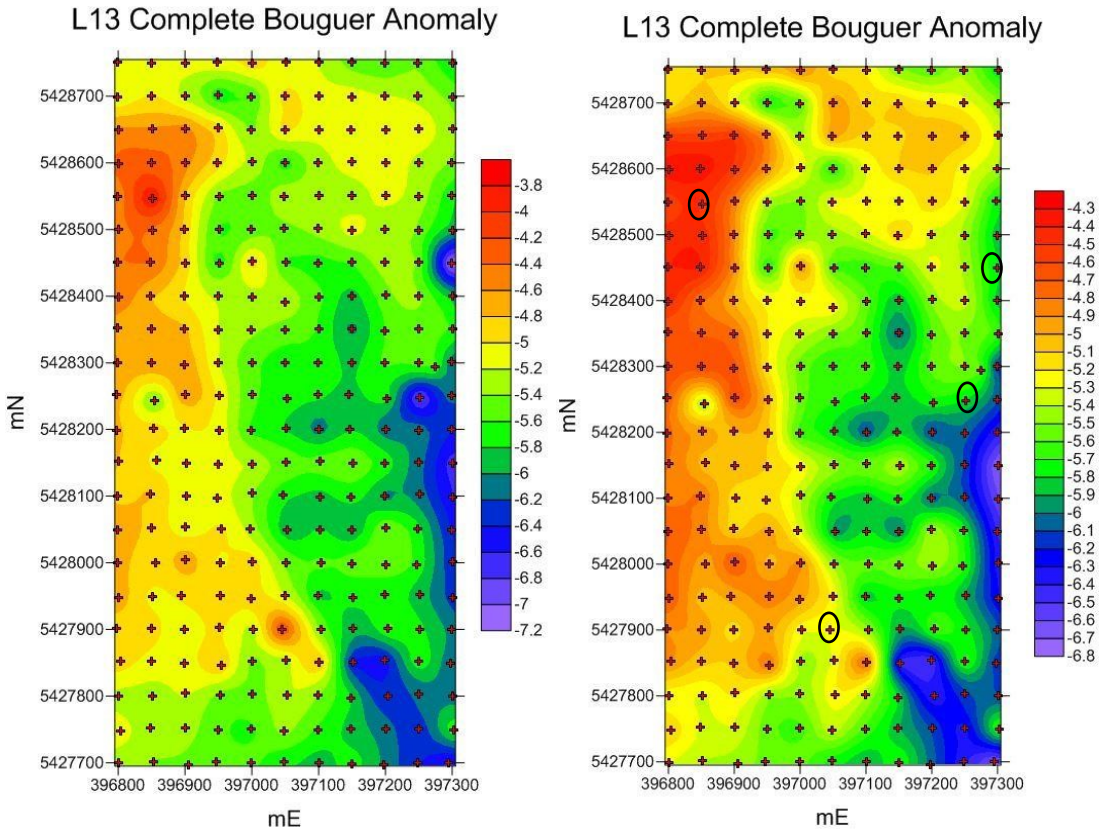

Figure 4-6: Complete Bouguer Anomaly (left), outlying points (circled in black) removed (right), units of mGals

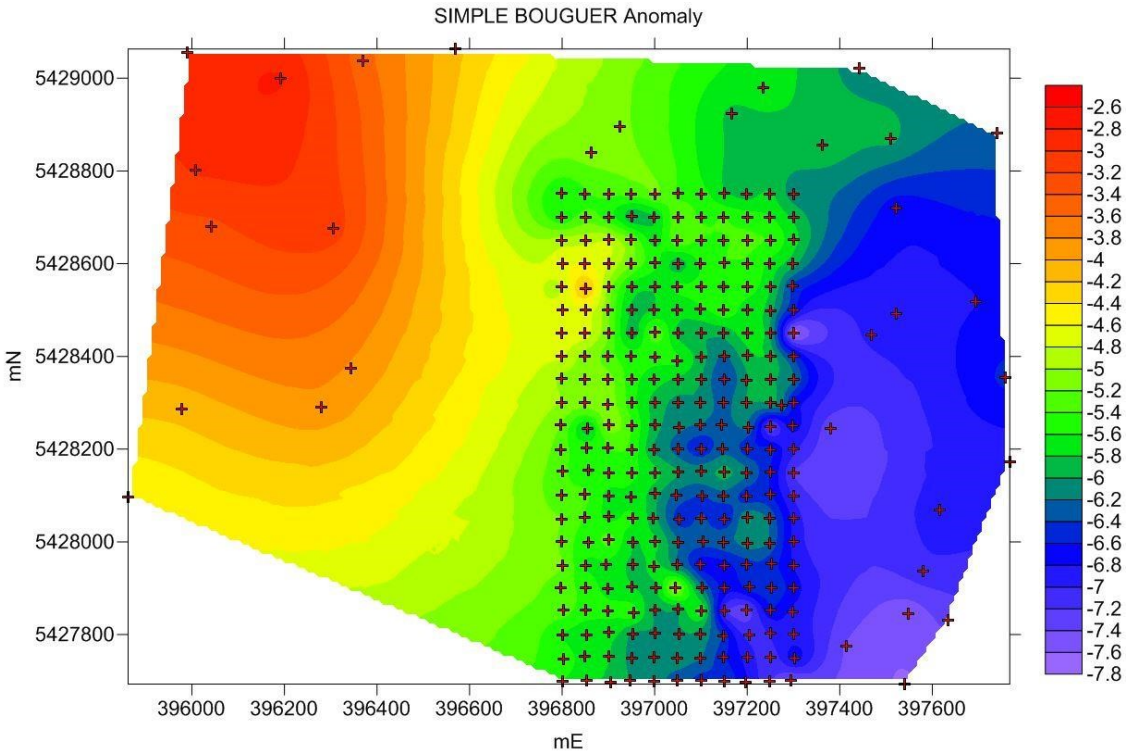

Figure 4-7: Simple Bouguer anomaly of L13 and the surrounding area (in mGal) with overlying post map of the gravity survey points.

The regional trend in the Bouguer anomaly data was removed through regional residual separation by gridding a polynomial regression of the gravity data and subtracting this from the gridded survey data. Polynomial regression fits a simple analytic surface to the whole data rather than fitting each point individually. A bi-linear saddle function (figure 48) of the L13 Complete Bouguer Anomaly data was used for the regional trend removal.

$$z(x, y) = Ax + Bxy + Cy + D$$

(equation 4-5)

A bi-linear surface was chosen as a better representation of the regional trend when compared to a plane surface or quadratic function. The formula (equation 4-5) is simple when compared to the quadratic but has an extra term absent in the plane equation making the contours curve around to the northeast. This curve depicts the regional trend more accurately than the linear contour lines of the planar surface. Removing the regional trend from the Bouguer anomaly amplifies the response of the near surface features. The residual gravity image is better suited to the simple forward modelling being conducted in Potent with the investigation focussing on a single magnetite body.

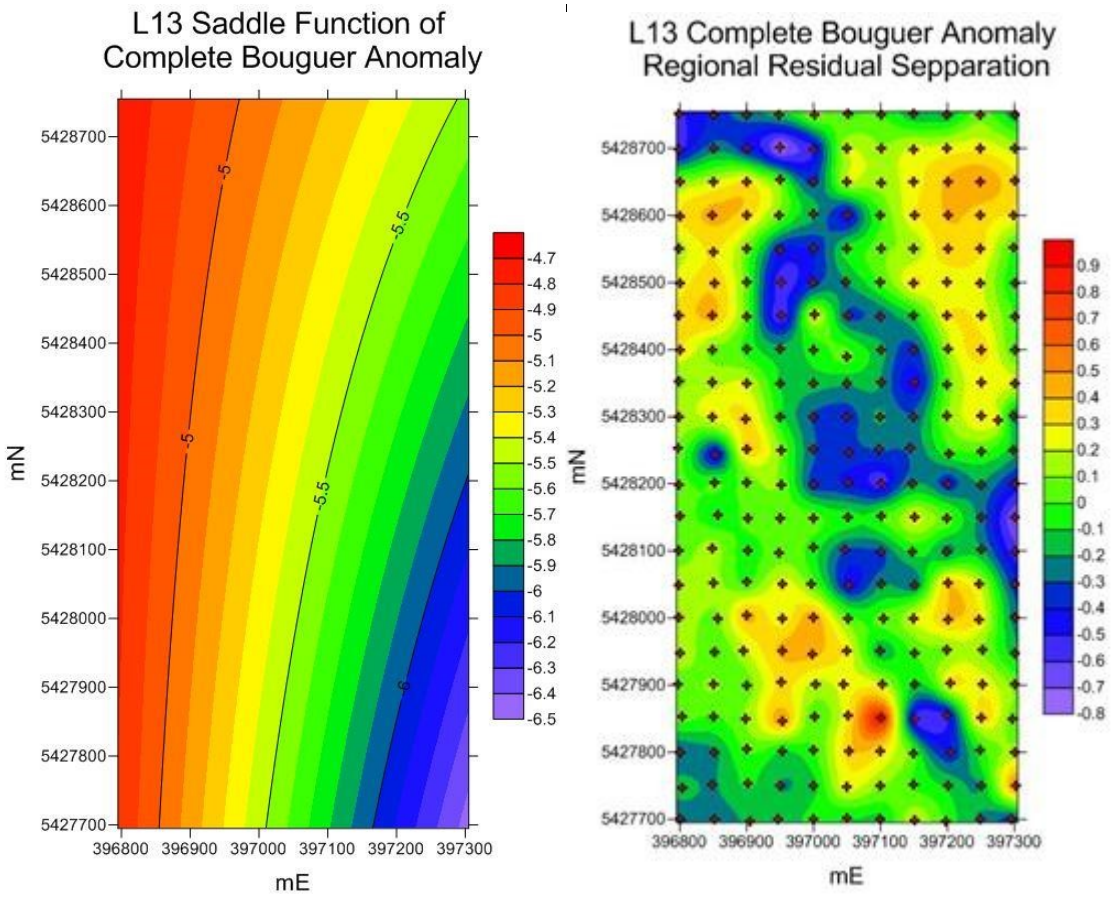

Figure 4-8: Bi-linear saddle regression of L13 (left) residual Complete Bougure Anomaly (right), units of mGals.

There is no single high amplitude positive anomaly in the residual gravity image that correlates with the magnetic anomaly but multiple, high frequency features. Overlying the contours of the TMI image onto the residual Bouguer anomaly (figure 4-9) highlights a slight inverse correlation between the two datasets. The lowest values of the residual Bouguer anomaly are in the centre of the field, bounded to the same area as the high magnetic anomaly. The northeast corner of the L13 site is another good example of this inverse relationship with the lowest magnetic intensity values and some of the highest mGal residual readings. Relationships like this indicate that the material causing the magnetic anomaly have a relatively low relative density. Another possibility is that the magnetite deposit is disseminated rather than a massive skarn body.

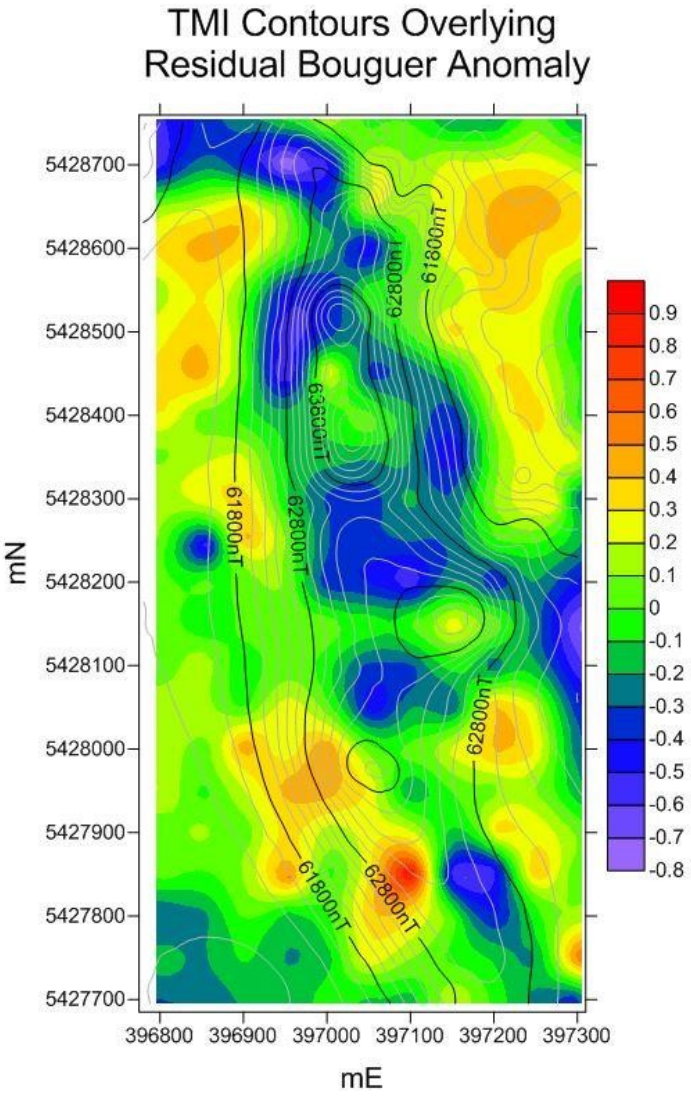

Figure 4-9: Residual gravity map with overlying contours from the TMI image. Gravity image units in mGals.

4.8 Summary

Magnetic data shows a high amplitude feature north-south through the centre of the L13 area. The highest values of this anomaly are the two peaks in the northern half which are amplified in the first vertical derivative image (figure 4-3). Residual Bouguer data displays a low anomaly in the same area as the magnetic high. Variations over the whole area surveyed are less than 2mGals in the residual gravity image and ~3000nT in the TMI. The inverse correlation between magnetic and gravity data can be further explored through forward and inverse modelling, discussed in the next chapters.

Chapter 5 Forward Modelling

5.1 Introduction

At the L13 site there has been no drilling, with the exception of a shallow auger survey in the 1970's (Whitehead 1974), there is also very little outcropping geology from which to obtain petrophysical data. Being able to measure the density and magnetic susceptibility of subsurface material would aid in constraining models of the deposit to use for drill targeting. Forward modelling techniques use physical properties to calculate the response from a model and to compare it with the observed data despite the lack of observed petrophysical data. The TMI image (figure 5-2) has a significant high anomaly of ~3000nT, simple conceptual forward modelling is possible to estimate physical properties and geometry but the results are non-unique. Magnetic data can be used to find a range of possible susceptibilities which can, in turn be used to calculate the percentage of magnetite within the target body. From the inferred magnetite abundance an average density for the body can be calculated and validated by forward modelling and comparison with the observed gravity data.

5.2 Forward Modelling

In the absence of drilling and surface geology there are no petrophysical properties with which to constrain forward and inverse modelling of the magnetic and gravity data. Forward modelling was undertaken using Potent to assess the magnetite body geometry and physical properties. For a specific geometry such as a vertical prism model, it is not possible, without additional information, to simultaneously estimate thickness, susceptibility and depth to top of the body. There are potentially an infinite number of possible solutions which could equally well produce equivalent fits to the observed data. This can often be conceptualised as a "solution cone" in which a discrete observed anomaly could be matched by the response of a diffuse distribution of low susceptibility near to the surface or alternately a higher susceptibility massive zone at greater depth. In this case a range of possible solutions were generated by varying the magnetic susceptibility and dimensions of the target to provide equivalent calculated fields to match that of the observed data. Magnetic susceptibility is related to magnetite volume percentage and hence the average rock density can also be calculated for each model.

These parameters can then be used to calculate a gravity response for each given magnetite model to match the observed Bouguer anomaly.

When adjusting the magnetic susceptibility and density of the target Potent assumes isotropic physical properties. The Earth's magnetic field strength and direction for the

location in question needs to be set to obtain a correct magnetic response for the magnetite body. These were set to IGRF12 values; declination of 13.4°, inclination of -71.5° and a total field strength of 61,517nT (NOAA 2015). Potent by default sets the background TMI or Bouguer anomaly to zero, therefore the magnitude of the calculated model is a result of the added blocks only. For this reason it is necessary to remove the Earth's main field response from the observed data to model anomalous bodies in the subsurface.

5.3 Fitting Calculated to Observed Data

The magnetic image was modelled in Potent to find relationships between the size, depth and magnetic susceptibility of the inferred magnetite skarn body. The TMI image displays a north-south trending magnetic anomaly, within which four high amplitude features can be distinguished. The two northernmost high amplitude zones (figure 5-2) were used in the investigation of a relationship between susceptibility, width and depth to top. These two peaks are approximately symmetrical and therefore a simple vertical dyke model was fitted to each anomaly (figure 5-1). Peaks in the southern half of the anomaly appear to result from one or more dipping bodies which would complicate simple conceptual forward modelling. The Potent invert function enables automated forward modelling and automatically adjusts selected parameters of a body to reduce the difference between observed and calculated responses for the whole data set. To assess relationships between susceptibility and geometry only a simple model can be used. Magnetic data were fitted for single cross sections rather than the whole image.

5.4 Magnetic Data

The magnetic survey conducted by Rada Engineering Pty. Ltd was loaded into Potent as a gridded file. The two anomalies in the north of the survey area were chosen for this investigation, with traverses for modelling extracted through the grid to obtain a two dimensional profile of the anomaly. The inducing field properties were obtained from the National Oceanic and Atmospheric Administration (NOAA) site for the survey day at the centre of L13 (NOAA 2015). Figure 5-1 shows the magnetic profile through magnetic high two (blue) with the inferred background/regional magnetic field value shown in red. This regional value was generated using the extract regional tool in Potent by selecting four points on the "wings" either side of the anomaly (these points are marked in red). A vertical dyke-like body was then added to the model with a vertical extent of 180 m, a length (North South orientation) of 190 m with the centre of the body located at 397010 mE, 5428480 mN, at the approximate centre of the anomaly. For forward modelling of the profile through magnetic high two the vertical extent and length remained the same but the new location updated to

397022 mE, 5428330 mN. These dimensions were chosen as the best fit for the model. The model is unaffected by vertical extent and adding extra vertical extent (depth to base) had little effect. The vertical extent parameter was not investigated in forward modelling. Profiles were extracted through the centre of each anomaly with lines drawn from east to west. The width of data extracted from the grid for these lines was set to 20 metres to ensure the peak of the anomaly was included in the observed data cross section.

Potent provides an option of adding topographic data for forward modelling. However, the small height changes in the Northern half of L13 mean the forward modelling can be calculated without the need to take elevation variations into account.

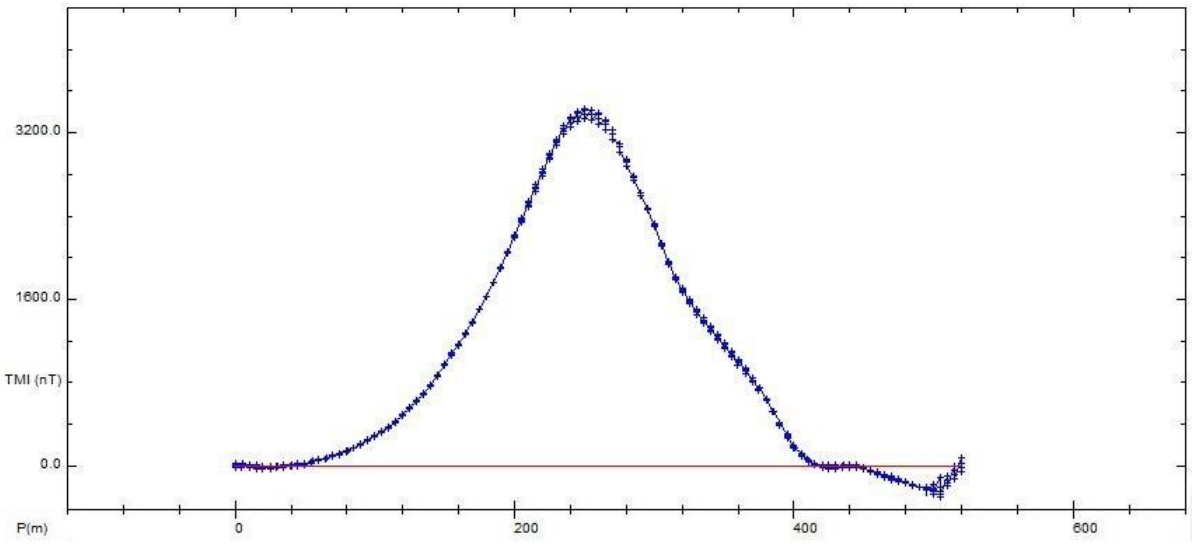

Figure 5-1: Magnetic high 2 with the red line depicting the corrected background level.

Forward models were generated for nine magnetic susceptibilities varying from 0.3 to 3 in SI units with the other parameters were adjusted manually until the observed and theoretical TMI responses matched. The inversion function for Potent was not used in this case as it attempts to fit the entire magnetic image rather than the single traverse of interest. Emphasis was given to fitting the observed to the calculated data in the area of steepest gradient on the flanks of the anomaly. Changing the width of the body had the most significant effect on the amplitude of the anomaly. With depth to top producing relatively small variations. For a dyke model it is only possible to uniquely constrain the product of body width and magnetic susceptibility and not both parameters independently. As the magnetic susceptibility of the body increases in a model, the width decreases in proportion for an equivalent overall fit to the observed data.

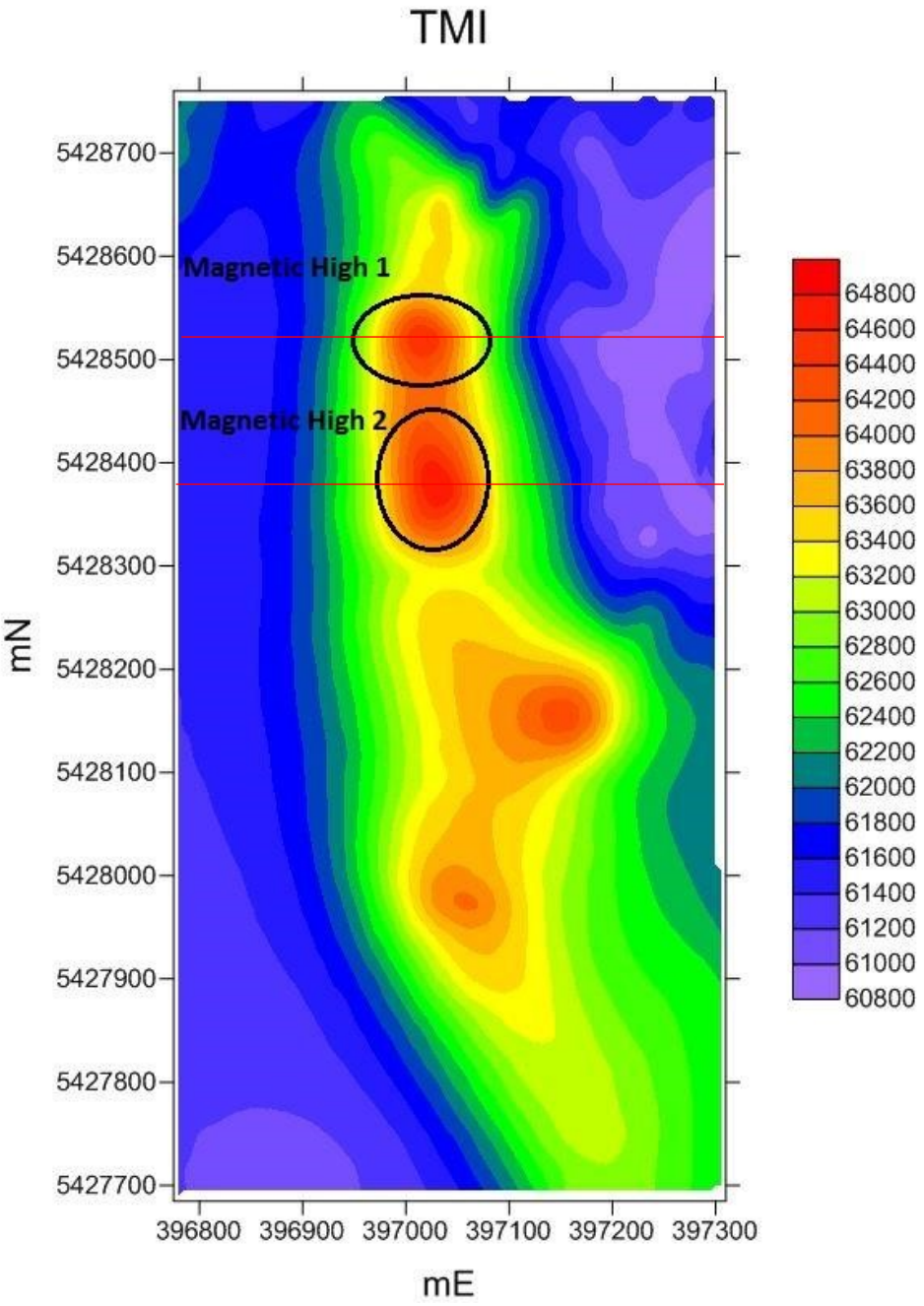

Figure 5-2: Observed TMI image from the drone survey (nT). Magnetic highs investigated circled and profile lines marked in red.

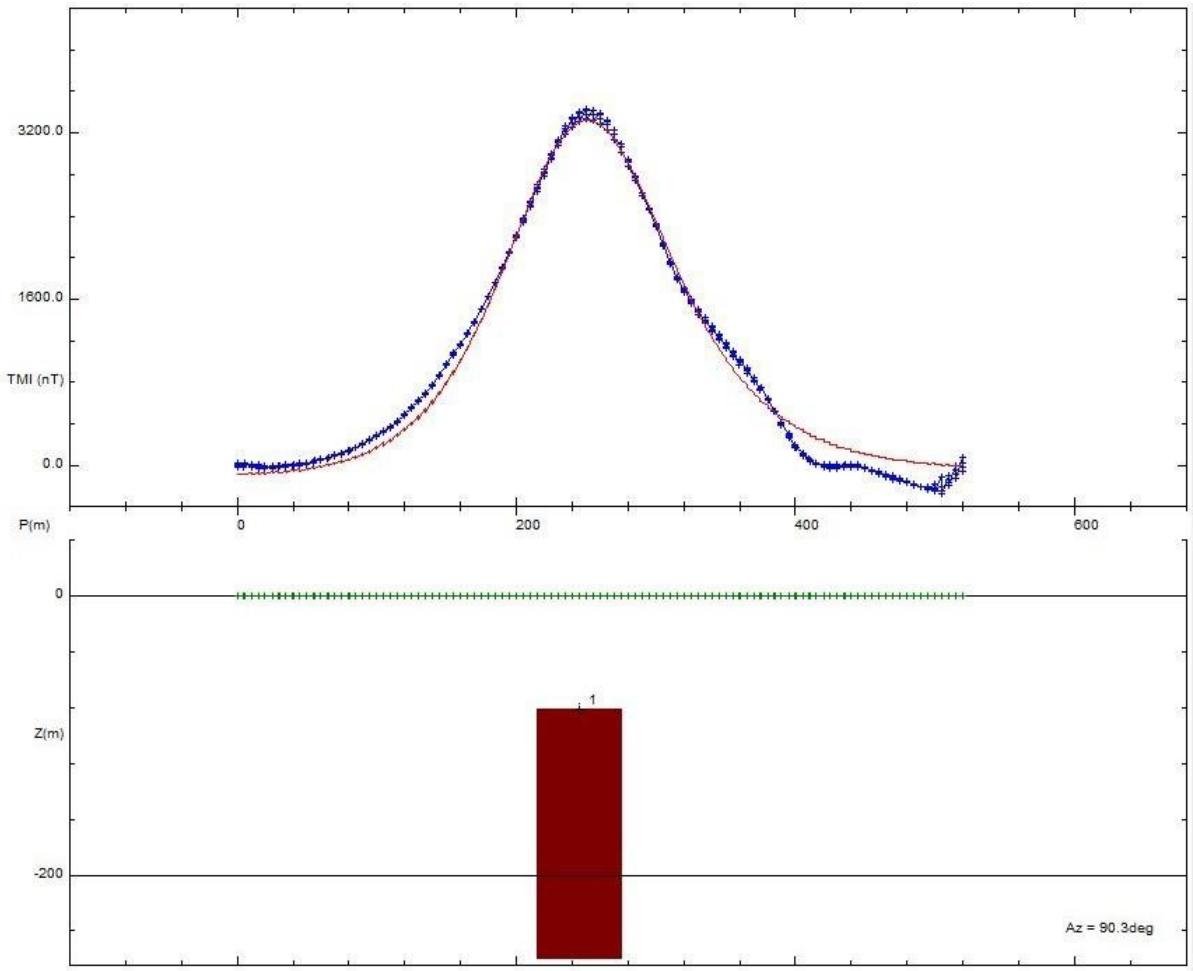

Figure 5-3: Example of calculated data (red) fitted to the observed data (blue).

MATLAB 2014b was used to illustrate combinations of magnetic susceptibility to width and depth to top that produce equivalent fits to the observed data. Exponential curves were fitted to the susceptibility/width and susceptibility/depth to top relationships. These curves had a close fit to each of the data sets except for high susceptibilities and depth to top values for magnetic high two. For both magnetic models the depth to top increases and width decreases with an increase in susceptibility. Three dimensional scatter plots were generated to compare the relationship of all three parameters (figure 5-4 and 5-6)

5.5 Magnetic High one

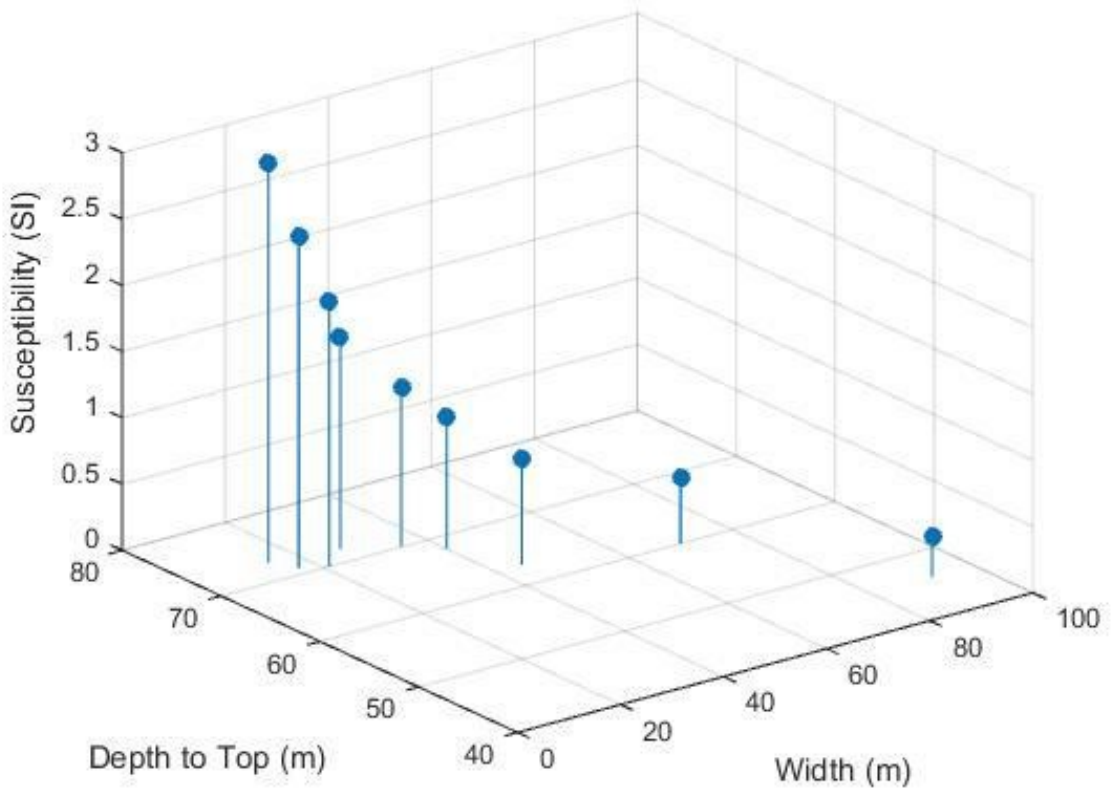

Figure 5-4: Susceptibility, width and depth to top relationships for magnetic high one.

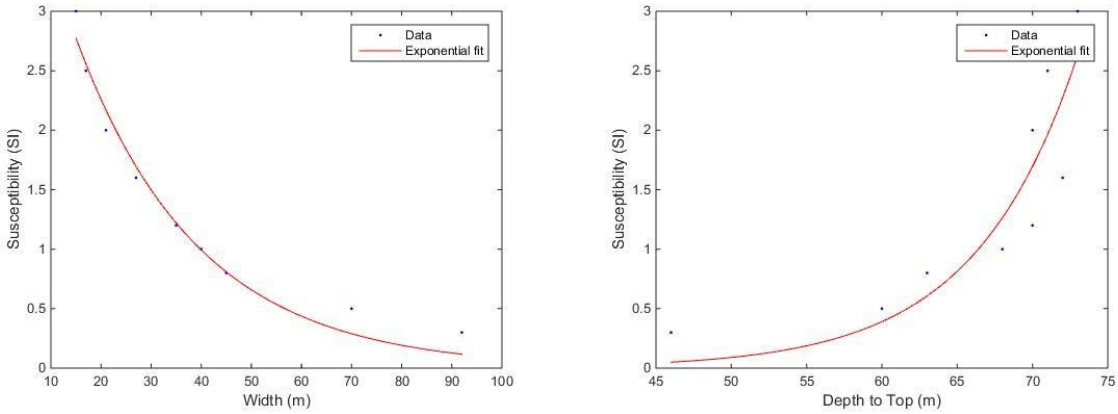

Figure 5-5: Susceptibility vs width (left) and susceptibility vs depth to top (right) with an exponential fit

Susceptibility vs width has an exponential relationship;

$$k = 5.14e^{-0.041w} \qquad \text{(equation 5-1)}$$

Susceptibility vs depth to top has an exponential relationship;

$$k = 5.84 \times 10^{-5} e^{0.15D} \quad \text{(equation 5-2)}$$

Where k is the magnetic susceptibility, w is the width and D is the depth to top.

5.6 Magnetic High two

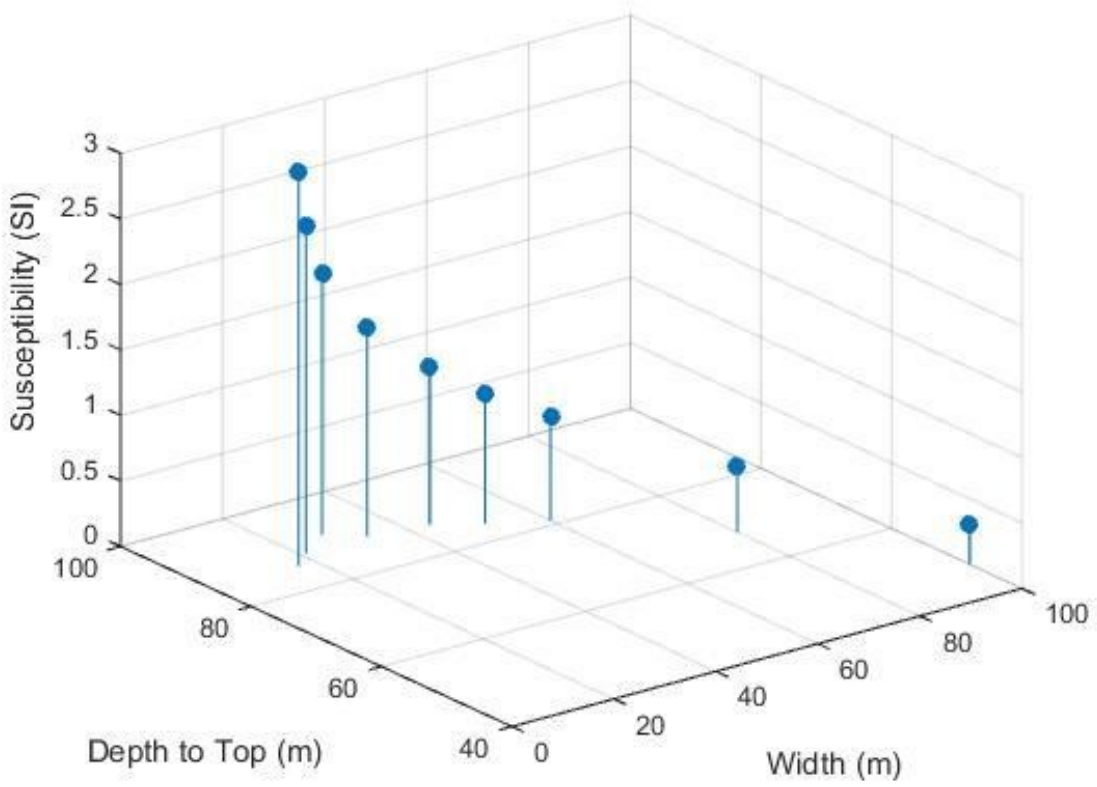

Figure 5-6: Susceptibility, width and depth to top relationship for magnetic high two.

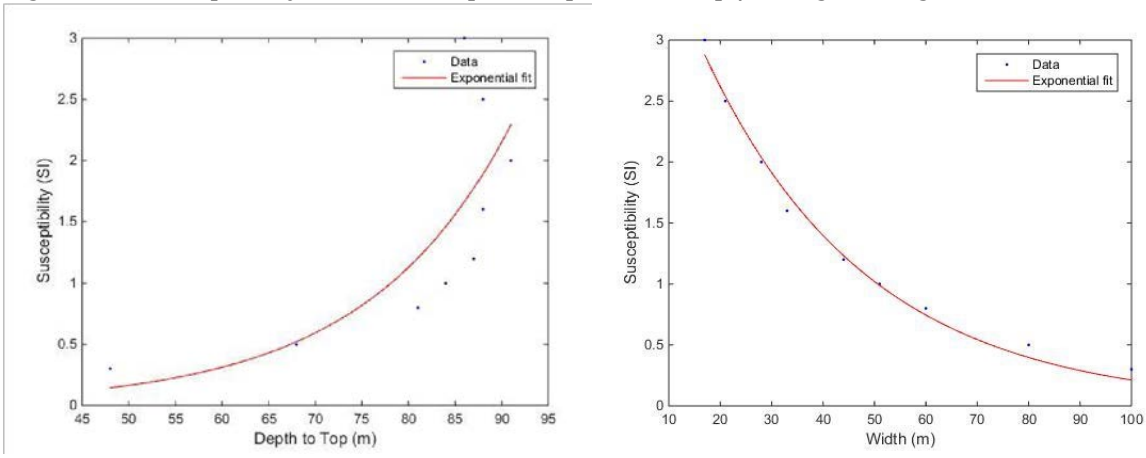

Figure 5-7: Susceptibility vs width (left) and susceptibility vs depth to top (right) with an exponential fit.

Susceptibility vs width has an exponential relationship;

$$k = 4.91e^{-0.031w} \quad \text{(equation 5-3)}$$

Susceptibility vs depth to top has an exponential relationship

$$k = 6.59 \times 10^{-3}e^{0.064D} \quad \text{(equation 5-4)}$$

5.7 Susceptibility,Volume Percent Magnetite Relationship.

Magnetic susceptibility can be used to produce a direct indication of the amount of magnetite present in the rock sample. Therefore the susceptibility of a given body of rock can be used to calculate the percentage of magnetite present. There are a veriety of references in the published literature between magnetite percentage and magnetic susceptibility. Mooney and Bleifuss (1953) provide a linear relationship between the two properties; with k the magnetic susceptibility and $V_{wt\%}$ the volume percentage of magnetite by weight.

$$k = 3000 \times 10^{-6}V_{\%}$$

Formula provided in cgs units, using the conversion factor of 4πcgs=1 SI to be compatible with the Potent software.

$$k = 12000\pi \times 10^{-6}V_{\%}$$

$$V_{\%} = \frac{k}{12\pi \times 10^{-3}} \quad \text{(equation 5-5)}$$

Jahren (1963) suggests a polynomial relationship

$$k = 0.00116V_{\%}^{1.39}$$

Again converting to SI units

$$k = 0.00464\pi V_{\%}^{1.39}$$

$$V_{\%} = \sqrt[1.39]{\frac{k}{0.00464\pi}} \quad \text{(equation 5-6)}$$

Balsley and Buddington (1958) also use a polynomial relationship but state that their formula is only accurate for weight percentages between 0.1 and 10.

$$k = 2.6 \times 10^{-3}V_{\%}^{1.33}$$

Converting to SI units

$$k = 10.4\pi \times 10{-}3V\%1.33$$

$$V_{\%} = \sqrt[1.33]{\frac{k}{0.0104\pi}} \qquad \text{(equation 5-7)}$$

A linear relationship is approximated in Telford, Geldart et al. (1990)for a volume between 0.1 and 35%

$$k = 0.0286V_{\%}$$

$$V_{\%} = \frac{k}{0.0286} \qquad \text{(equation 5-8)}$$

This formula is calculated from two susceptibilities for the quoted weight percentages with no indication of values for other percentages given. A high uncertainty for this data is also quoted. Telford (1990) also states that these relationships are approximations only and data will have significant variation between surveys depending on the samples tested.

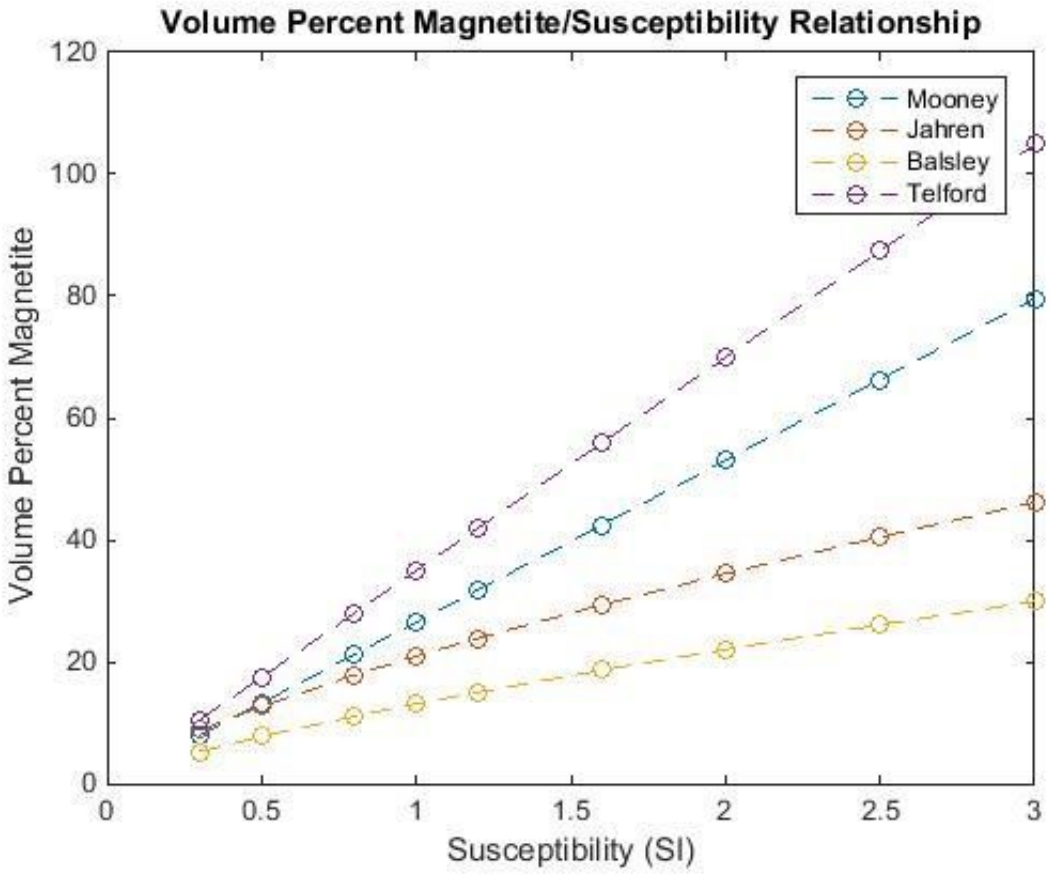

Figure 5-8: Suggested relationships between magnetic susceptibility and weight percent volume magnetite.

The relationship derived by Jahren (1963) was used for further calculations of the volume weight percent magnetite and average density. It is the most recent study of a complete susceptibility/volume relationship and adheres to the approximately linear relationship for volumes less than 10 percent suggested in the literature.

5.8 Average Density

The mass of a rock body (m) is equal to the volume (V) multiplied by the density (ρ).

$$m = V\rho$$

This can be divided into the mass of the magnetite and the mass of the remaining rock (m_R).

$$mT = VM\rho M + VR\rho R$$

The volume of non-magnetite rock (V_R) will be the difference between the total volume (V_T)and the magnetite volume (V_M).

$$V_R = V_T - V_M$$

Substituting this equation into the total mass formula

$$m_T = V_M(\rho_M - \rho_R) + \rho_R V_T$$

The volume percent of magnetite ($V_{\%}$) defines V_M in term of V_T

$$V_M = V\%V\mathrm{T}$$

Substituting this into the total mass equation

$$mT = V\%V\mathrm{T}(\rho M - \rho R) + \rho RVT$$

$$m_T = V_\mathrm{T}(V_{\%}(\rho_M - \rho_R) +$$

$$\rho_R)\ \rho av = V\%(\rho M - \rho R)$$

$$+ \rho_R$$

The calculation uses a background average crustal density of 2.67gcm^{-3} and the density of pure magnetite, 5.2gcm^{-3} (Emerson 1986).

$$\rho_{av} = V_{\%}(2.53) + 2.67 \qquad \text{(equation 5-9)}$$

This formula is independent of the target body size allowing the average density of the block to be calculated from the estimated susceptibility values by substituting in equation 5-6.

$$\rho_{av} = \sqrt[1.39]{\frac{k}{0.00464\pi}}(2.53) + 2.67$$

$$\rho_{av} = 53\sqrt[1.39]{\bar{k}} + 2.67 \qquad \text{(equation 5-10)}$$

Model No.	k (SI)	Volume % Magnetite	Average Density (gcm^{-3})	High One		High Two	
				Depth to Top (m)	Width (m)	Depth to Top (m)	Width (m)
1	0.3	8.8	2.89	46	92	48	100
2	0.5	12.7	2.99	60	70	68	80
3	0.8	17.8	3.12	63	45	81	60
4	1	20.9	3.20	68	40	84	51
5	1.2	23.9	3.27	70	35	87	44
6	1.6	29.4	3.41	72	27	88	33
7	2	34.5	3.54	70	21	91	28

8	2.5	40.5	3.69	71	17	88	21
9	3	46.2	3.84	73	15	86	17

Table 5-1: Model susceptibility, volume percent magnetite and average density (calculated using formula from Jahren (1963)) for varying depth to top and width dimensions.

Table 5-1 compares the properties of each model used in forward modelling. increasing the magnetic susceptibility directly results in an increase in the volume percent magnetite and hence the average density.

5.9 Density Estimations

The obtained average density values are substituted back into the Potent models used for each magnetic susceptibility. To compare to the residual data the background density of the inversion model is set to 2.67 gcm^{-3}. All of the models being tested are within 400 m of the surface allowing for the gravity anomaly of the mineralised body to be compared to the residual gravity image. The rectangular prism target used produces a symmetrical anomaly similar in shape to that of the magnetic image. Interest is in which density will give the best fit to the gravity data. Bouguer anomaly of the model is compared to the residual gravity anomaly to negate the effects of the regional trend (figure 5-9)

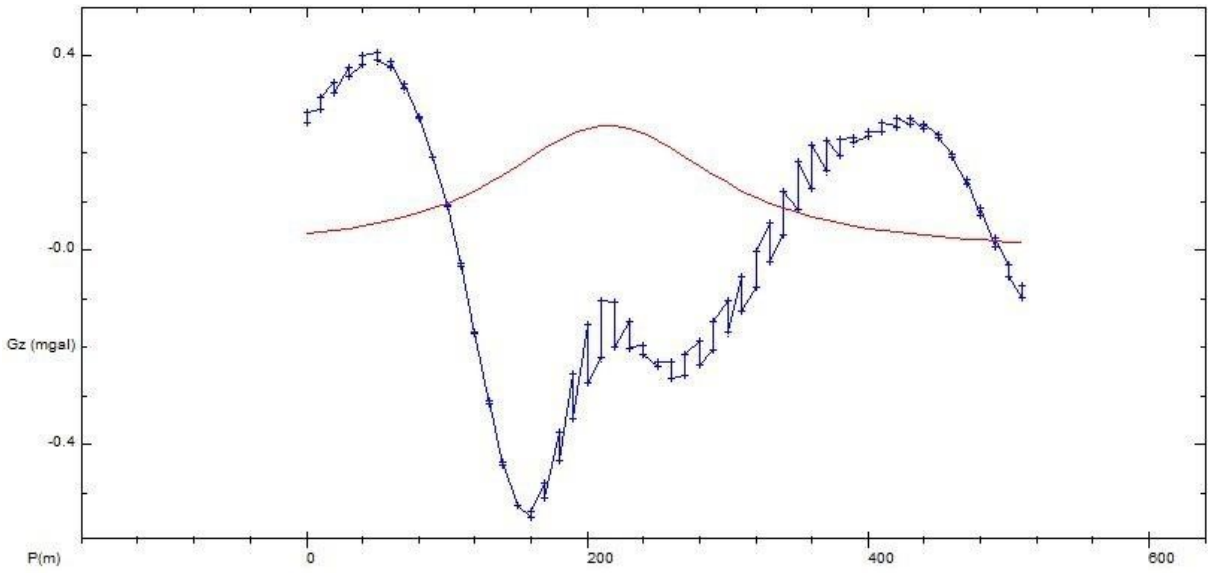

Figure 5-9: Gravity response of model 1 (red) density of 2.89 gcm^{-3}, gravity profile of magnetic profile of high 1 (blue).

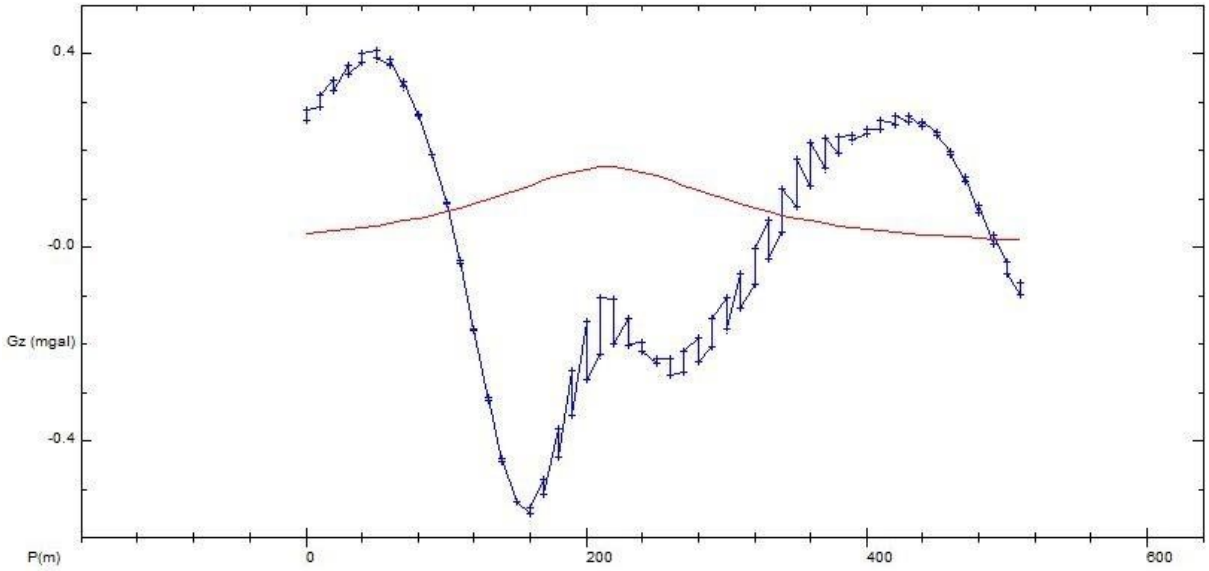

Figure 5-10: Gravity response of model 9 (red) density of 3.84 gcm^{-3}, gravity profile of magnetic profile of high 1 (blue).

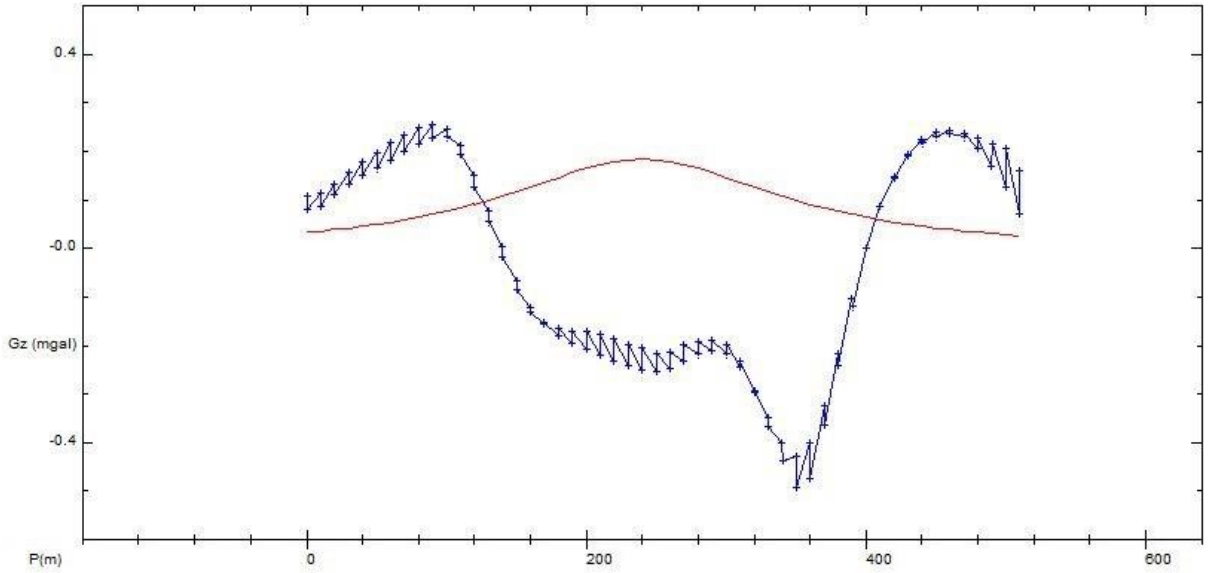

Figure 5-11: Gravity response of model 7 (red) density of 3.54 gcm^{-3}, gravity profile of magnetic high 2 (blue).

Very little variation is seen between the forward modelled density bodies, with differences less than 0.1mGals seen between all models. This indicates magnetite skarn mineralization, which have both a high density and magnetic susceptibility are a likely solution. The nature of the TMI and Bouguer anomaly images suggests multiple, small ore bodies rather than the one larger target used for this exercise.

Chapter 6 Inversion

6.1 Introduction

Creation of a subsurface model from a geophysical dataset is a process known as inversion. The created model is an equivalent source, the response of which (Bouguer or magnetic intensity) matches the observed data. Inversion results are non-unique and affected by the regularisation of the modern software. Without additional constraints provided by surface geology or drill core the validity of the density/susceptibility distributions generated by the UBC-GIF software cannot be assessed. As discussed in Chapter 5 (Forward Modelling) the magnetic and gravity anomalies are interpreted to be caused by multiple, small magnetic bodies near surface, or a massive, high density/high magnetic susceptibility body at depth.

6.2 Depth Weighting

Neither magnetic nor gravity data contains definitive information to determine the depth of the causative body. Computationally the quickest way to reach the achieved misfit for inversion is to concentrate the high susceptibility or density cells close to the observation points. The depth weighting parameter in the UBC inversion software corrects for the tendency of the algorithm to produce a near surface distribution and is defined as a function of the form

$$(z + z_0)^{-\alpha} \qquad \text{(equation 6-1)}$$

Here z is the distance between the observer and the centre of the cell, z_0 and α are constants depending on the survey type. The gravitational force has a $1/r^2$ dependence for a small discrete object while magnetism has a $1/r^3$ relationship. To correct for this α is 2 for a gravity survey and 3 for a magnetic. This process ensures that each cell has an equivalent effect on the survey.

6.3 Mesh File

The mesh file specifies the discretisation of the subsurface model. The mesh size for the L13 inverse models was created with cells of 25m in the x and y directions, half that of the gravity station spacing. The large cell size decreases the computation time without compromising the accuracy of the model. Padding cells are added to the edges of the survey data for both the Easting and Northing directions. Padding is two cells deep, widths of these cells are 100 m and 50 m for the first and second cells from the outside respectively. Cell size increases with depth from 12.5m at the surface for 32 cells to 25 m for another 10 and for the base three layers of cells have a height of 175.85 m. Elevation of the reference cell is set to 560 m to ensure at least one layer of empty cells are above

the topography. For consistency and to aid in comparison between the datasets this mesh size was used for the magnetic and gravity inversions. Comparison of the observed and predicted data from the observed model of the magnetic inversion (figure 6-1) it is clear that the 25 m cell size is small enough to accurately reproduce the observed magnetic data.

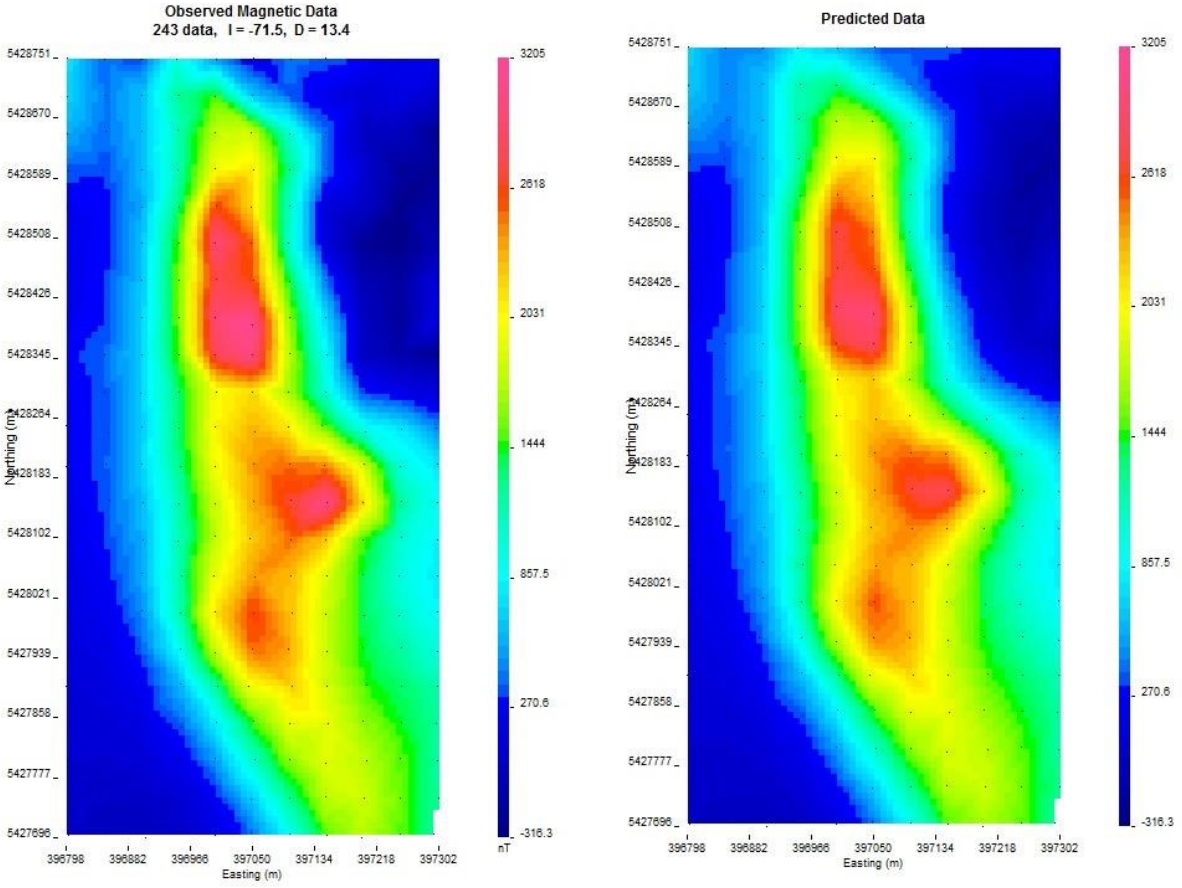

Figure 6-1: Observed (left) and predicted (right) data from an inverted gravity model.

6.4 Magnetic Inversion

6.4.1 Data Pre-Processing

The UBC Mag3D inversion code requires the removal of the regional field and the estimation of error. The regional trend is hard to define for the magnetics as the acquired data covers the L13 area only with no high resolution data for the surrounds. To maintain consistency the regional trend was set to that defined in Potent for forward modelling. This regional value was selected as being ~3,200nT less than the anomaly maximum; approximately 61,200nT. This value was subtracted from the TMI data before loading into Mag3D. Data values for inversion range from -316 to 3205nT 2% of the maximum value (64nT) was set as the absolute error for the imported dataset. Elevation is set to 20 m as

quoted in the survey report from Rada Engineering. Details of the Earth's magnetic field are also required for the time of the survey with the IGRF12 values used; declination of 13.4^{o}, inclination of -71.5^{o} and a total field strength of 61,517nT.

6.4.2 Magnetic Data

Reducing Z_0 causes the cells with a higher susceptibility to be closer to the surface. The bounds on magnetic susceptibility were set to a minimum of -1 and a maximum of 3 in SI units. Cell susceptibilities for all magnetic images are measured in SI units.

Default inversion parameters produce the susceptibility model shown in figure 6-2. The two peaks in the northern half of the L13 area are represented in the inverted model and are shown clearly in the diagonal slice. A large volume of high magnetic susceptibility cells extends from these peaks to the south/south-east edge of the L13 prospect. This is considered to be an unrealistic distribution on geological grades and may result from an incorrect regional-residual trend. High susceptibility cells increase in depth further to the south with the anomaly appearing to continue outside the survey area (figure 6-1). Setting the z_0 value to 0.5 does not completely remove this effect but does show a reduction in the blowing out of the high susceptibility cells. The effect can also be reduced by subtracting a larger regional field from the total intensity.

6.4.3 Regional Field Adjustment

The regional field was chosen as a constant value of 61,200nT to match the value used in forward modelling with Potent. As there is no other high resolution data available this value is a can be adjusted by a small amount without drastic alteration to an inverse model generated after. Increasing the regional field removed from the TMI data by 200nT reduces the amount high susceptibility cells at depth and on the margins of the inverse model. There are still some high value cells outside the bounds of the survey area. These can be interpreted from the continuation of the magnetic anomaly to the south-east seen in the TMI image (figure 6-1).

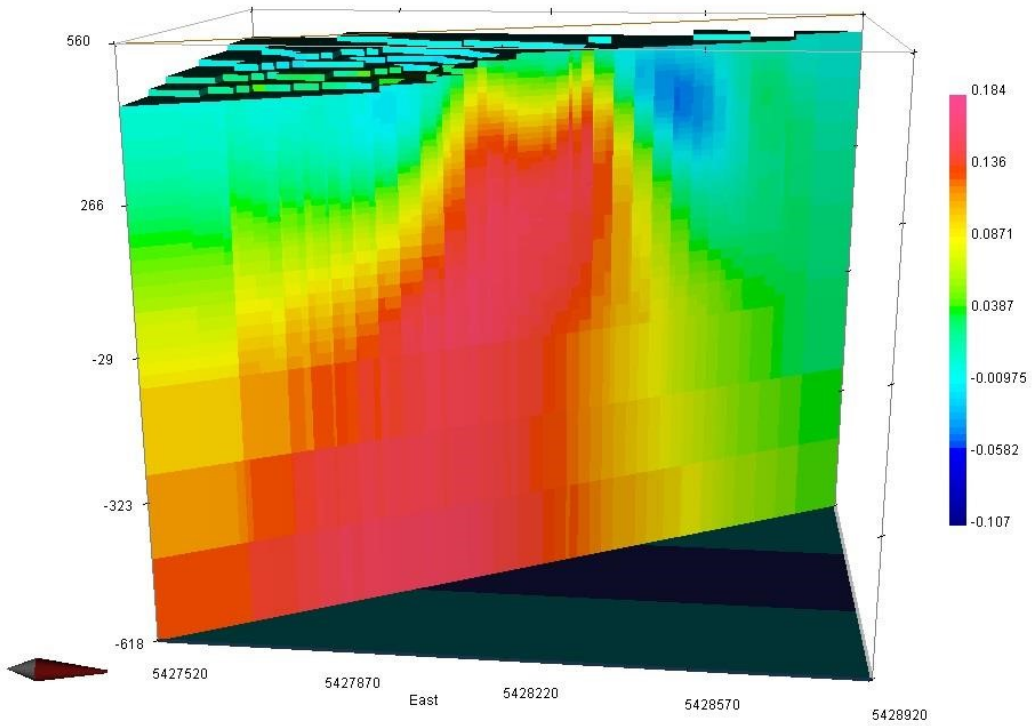

Figure 6-2: Diagonal slice through magnetic susceptibility model.

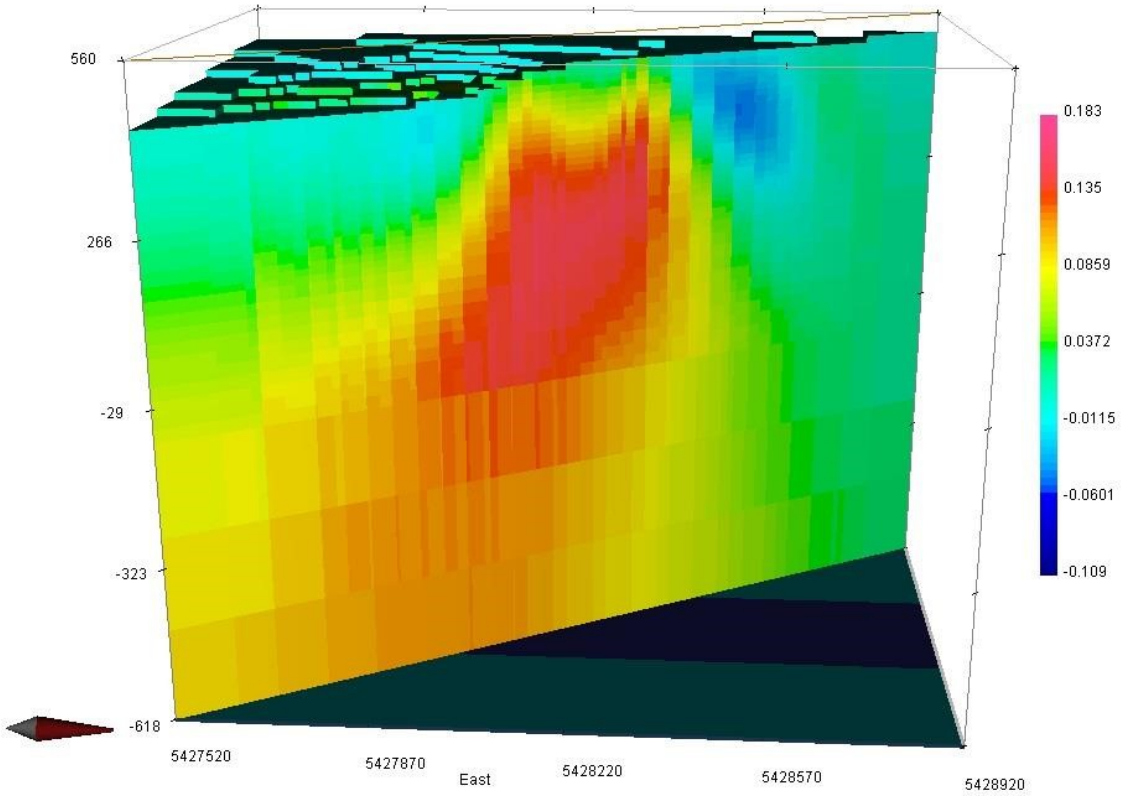

Figure 6-3: Diagonal slice through magnetic susceptibility model for a larger regional field.

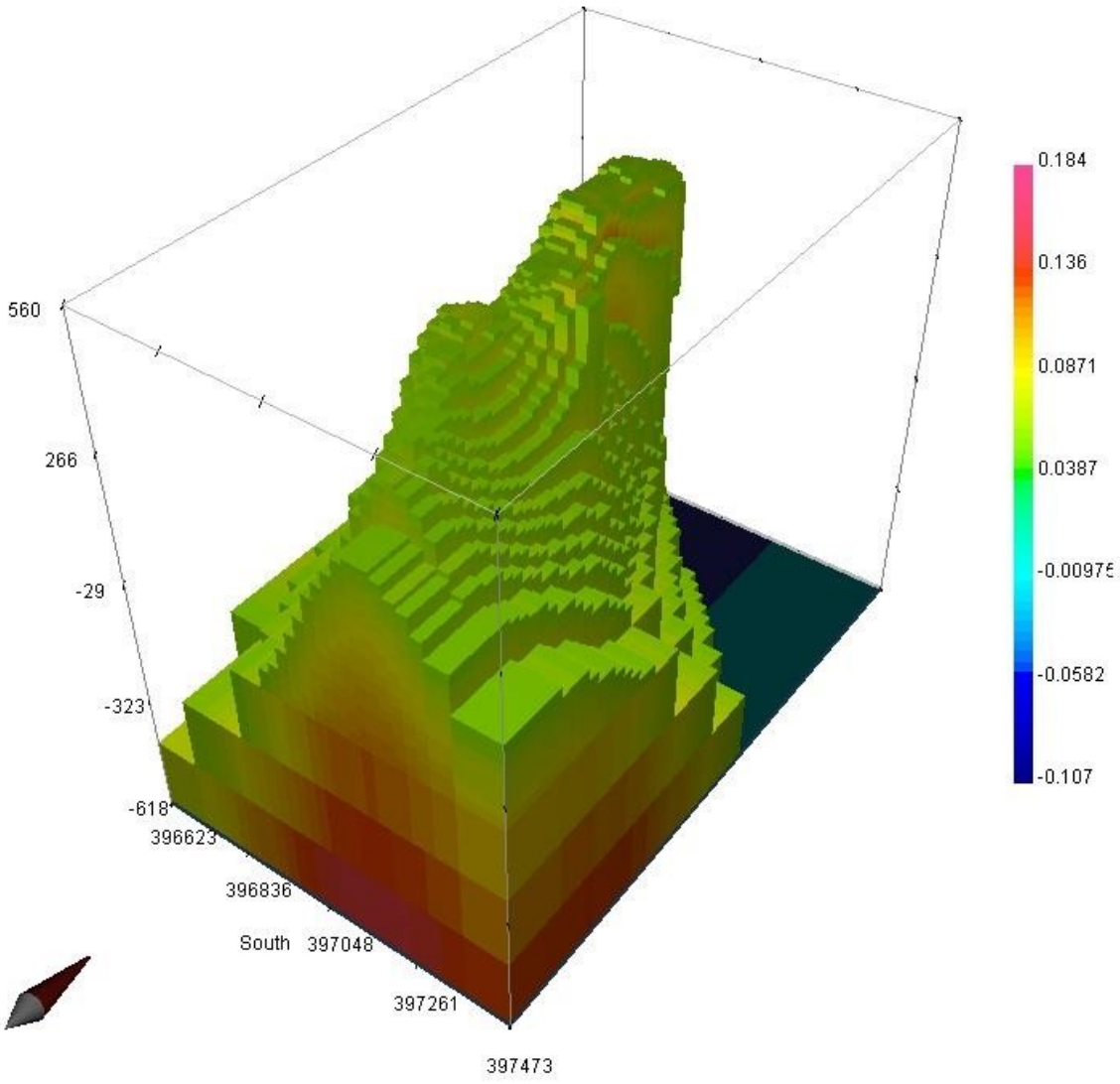

Figure 6-4: Model with magnetic susceptibility below 0.06 (SI) cutoff.

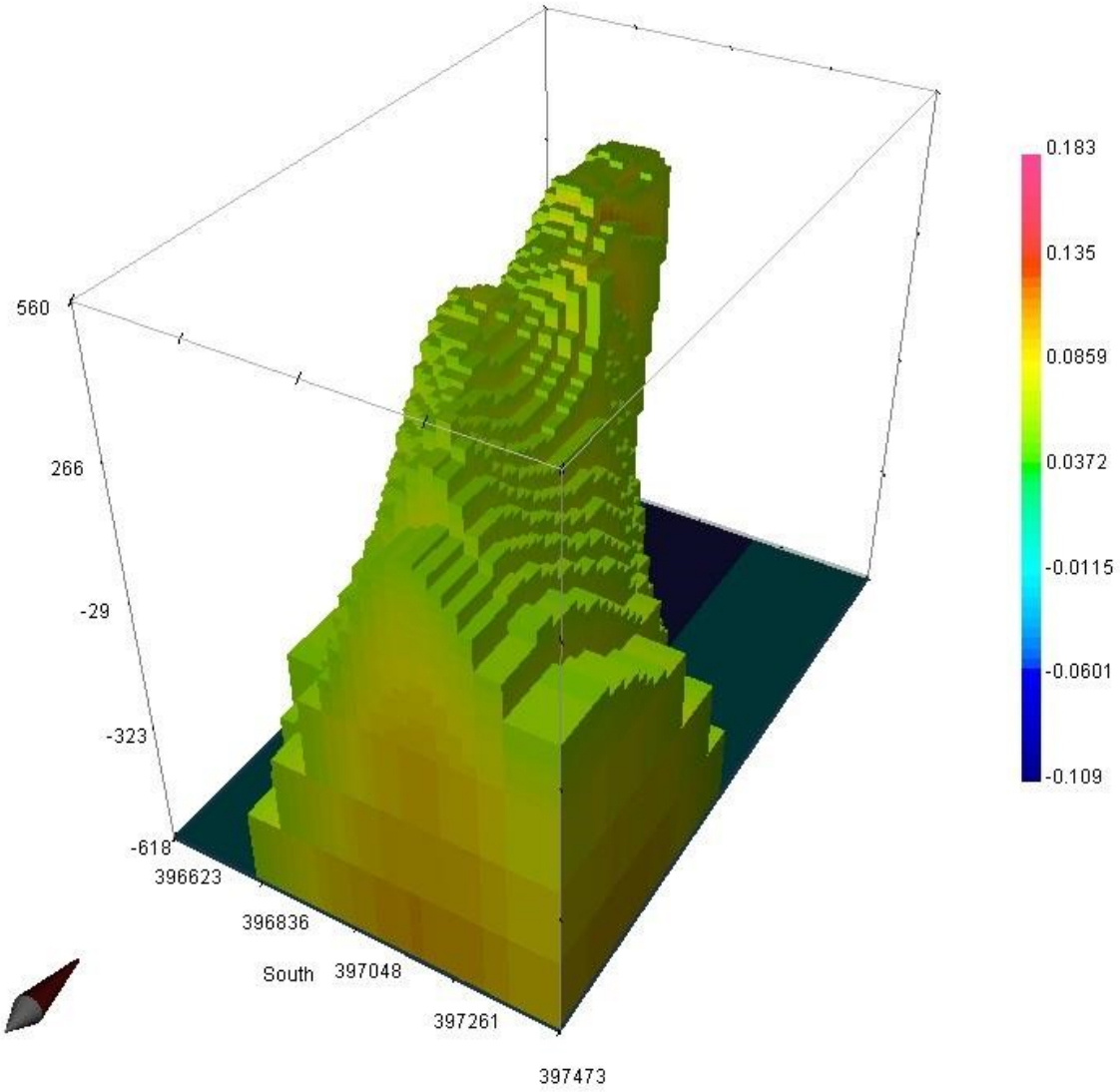

Figure 6-5: Model for larger regional field with magnetic susceptibility below 0.06 (SI) cutoff.

6.5 Gravity Inversion

6.5.1 Data Pre-Processing

The residual gravity image, calculated by subtracting a bi-linear saddle regression of L13 away from the complete Bouguer anomaly (see chapter 4) was used for inversion. Survey height was set to 0.5m and the absolute error set to 0.02mGals approximately 2% of the maximum.

6.5.2 Gravity Data

Qualitative representation of the data suggests an inverse correlation between the magnetic and gravity surveys with areas of high magnetic intensity corresponding to low values in the residual Bouguer anomaly. For this to be the case in the inverted model the high susceptibility cells seen in the magnetic inversion should have a relatively low density

while volumes of low susceptibility correspond to cells with a higher density. All cell density values are calculated in units of gcm^{-3}.

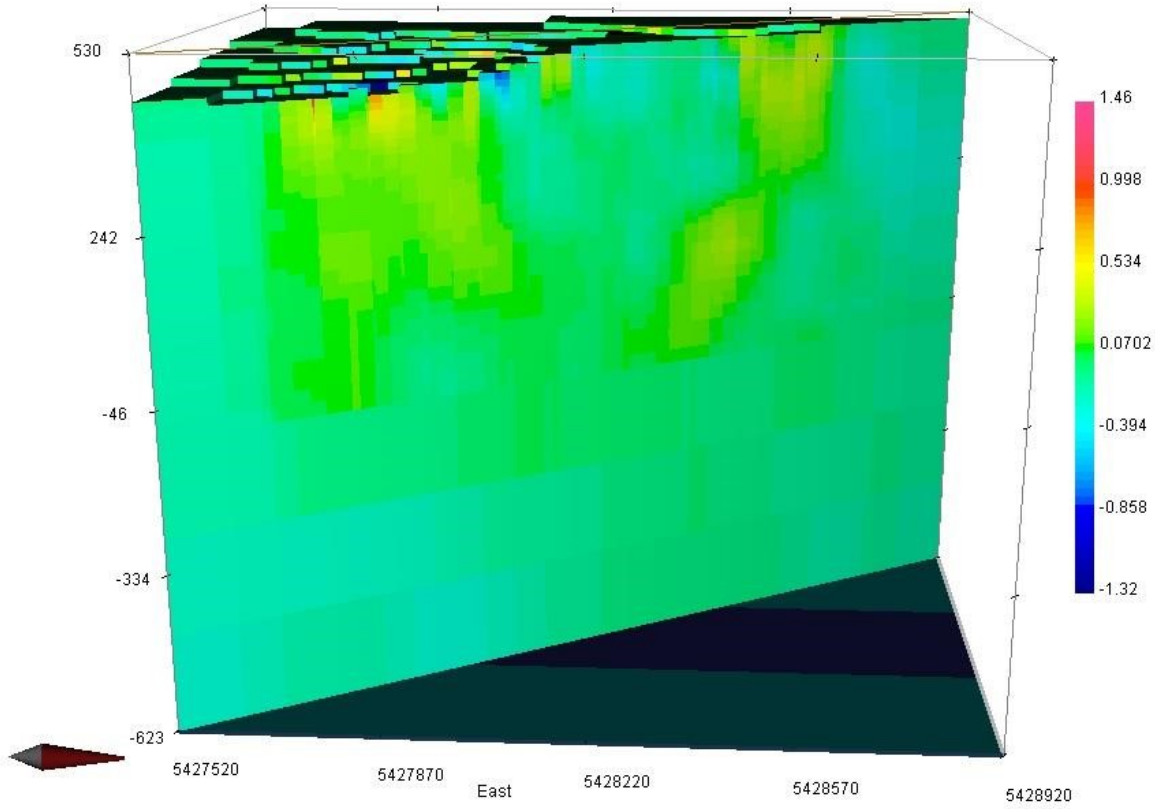

Figure 6-6: Diagonal slice through density model.

The density model from the initial inversion parameters positions the high density cells within the top 150 m. This is emphasised in figure 6-7 where the cells with a relative density less than 0.3 gcm^{-3} have been removed from the model. High density cells are found in small clusters within the top 500 m with the average density of these volumes decreasing with depth.

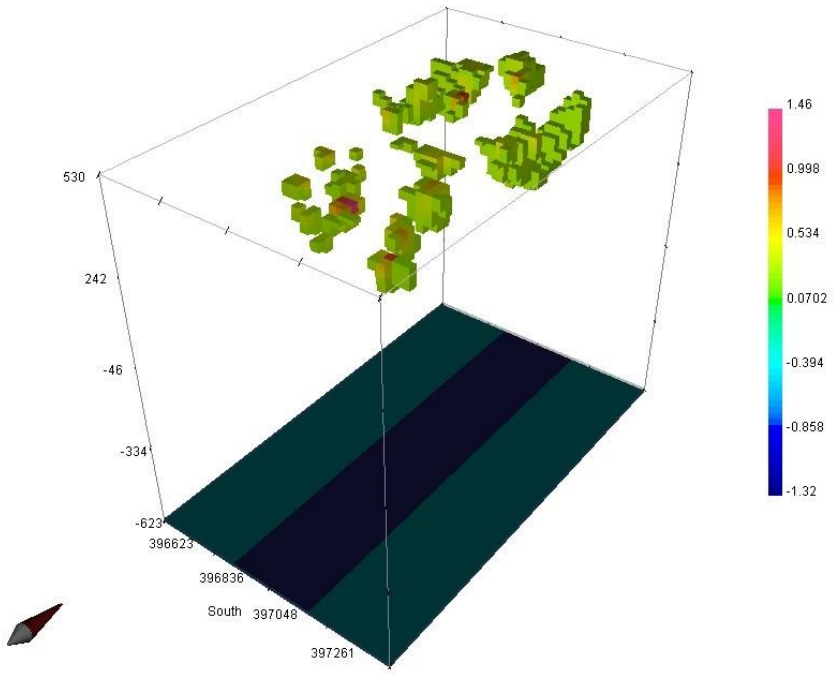

Figure 6-7: Density model for cells of density greater than 0.3gcm-3.

Using a z_0 value of 0.5 for the inversion creates some higher density features deeper in the model. This is shown in figure 6-8 where there is also a greater cell volume of densities greater than 03 gcm^{-3}.

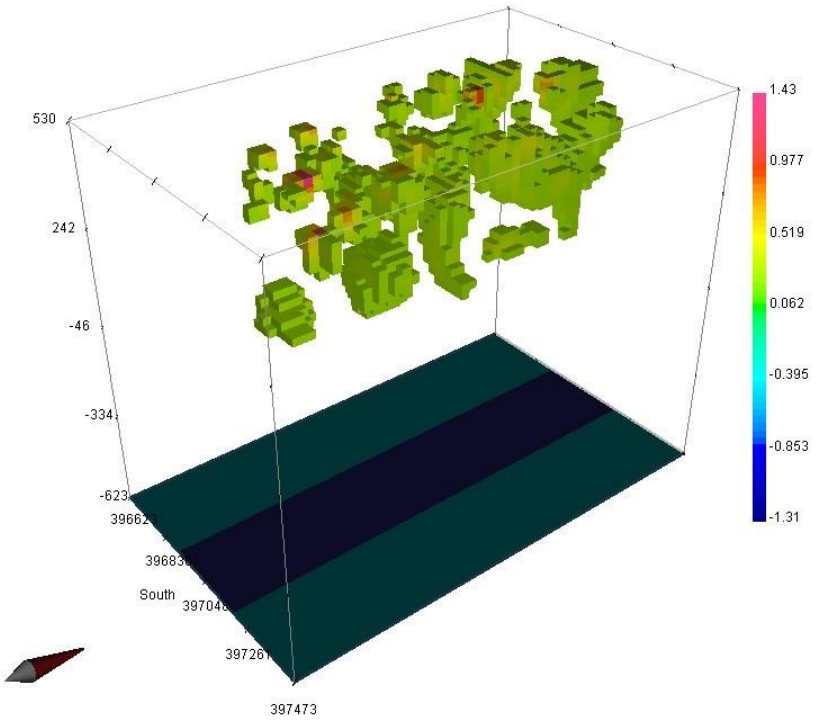

Figure 6-8: z0=0.5 model for density greater than 0.3gcm-3.

6.6 Summary

Maximum cell susceptibility found in the inversion is less than 0.2 in SI units. Substituting this into equation 5-10 yields an average density of 2.84gcm^{-3} and a magnetite volume of 6.6%. This low percentage explains the low north-south trending feature through L13. Densities calculated in inverse modelling have a maximum value of 4.1gcm^{-3}. These do not coincide with cells of high magnetic susceptibility. High density cell distribution indicates a disseminated ore deposit while the magnetic inversion yields a massive magnetite body. The inverse relationship seen between density and magnetic susceptibility indicates that the average susceptibility and therefore magnetite content of the ore body is low while there is a more dense rock separate from the high susceptibility material.

Chapter 7 Discussion and Conclusion

7.1 Overview

Magnetite skarn mineralisation is common in carbonate rocksadjacent to the Housetop Granite in northwest Tasmania. The high susceptibility and density of magnetite result in ready detection of massive magnetite bodies using magnetic and gravity methods. This

study investigated one magnetite skarn prospect known as L13 situated north of the Kara mine near Hampshire. Gravity data was collected by the author over the L13 prospect to complement magnetic data that were aquired by a commercial contractor using a UAV.

The L13 prospect is characterised by a 3000nT magnetic anomaly but does not have a corresponding positive residual gravity anomaly. The lack of subsurface information at L13 means that there are very limited constraints that can be applied to numerical interpretation of the geophysical datasets.

This chapter provides a summary and discussion of the geophysical data of L13 including interpretation, limitations and recommendations for future exploration.

7.2 Magnetic and Gravity Calculations

Magnetic and gravity investigations provide high resolution geophysical images of the L13 site. The magnetic anomaly in the centre of the field has amplitude of ~3000nT above the regional field. The two main peaks of the anomaly are symmetrical on east-west profiles suggest a near vertical dip/plunge for the source. These profiles were used for forward modelling in which a range of prismatic models with variable magnetic susceptibility depth and dimensions were tested to match the observed profile. In the absence of external constraints it is not possible to uniquely specify magnetic susceptibility, width and depth to top for a causative prismatic body and a range of equivalent solutions are possible.

Susceptibilities tested ranged from 0.3 to 3 in SI units. For each tested susceptibility a best fit model was found providing a wide range of plausible alternative models. The volume percent of magnetite in each model was calculated using the relationship provided by (Jahren 1963) and this was then used to estimate the average density of the prism for forward gravity modelling. The calculated Bouguer anomaly for each magnetic prismatic model was then compared with the observed residual gravity anomaly. There were no clear correlations between the calculated forward model profiles and the observed data. A difference of less than 0.1mGal was apparent for all calculated profiles.

Inverse modelling of the residual magnetic and gravity fields was also undertaken. For magnetic inversion the contribution of high susceptibility at depths in the models is in part affected by the choice of background field value. However, the upper surface of the inverse models is relatively insensitive to this parameter. Magnetic data can readily be reproduced with subsurface models that comparatively low maximum magnetic susceptibility (<0.2SI).

7.3 Interpretation

Inverse modelling suggests maximum susceptibilities of less than 0.2 (SI units) which are equivalent to less than 7% magnetite by volume and hence that magnetite may be distributed as disseminated material or as veins. Although isolated peaks of more massive magnetite may be present, the lack of a clear positive gravity anomaly coincident with the magnetic anomaly suggests that massive magnetite is not present in large volumes near the surface. The magnetic anomaly is actually associated with a subtle relative negative residual Bouguer anomaly, suggesting that the mineralised zone has a net mass deficit. In the absence of subsurface data, this is most readily explained by assuming that the high density magnetite that produces the magnetic anomaly in within an envelope of low density material that may be due to alteration.

7.4 Further Study

Lottah Mining had not commenced their drilling program on the L13 site at the time of writing and core from other prospects that had been collected in the vicinity of L13 were listed as “location unknown” in the Mineral Resources Tasmania online core library. The biggest limitation on this study is the absence of petrophysical data with which to constrain the forward modelling and inversion process. Drilling is set to take place in late 2015 at L13. Data from core needs to be tested for density and magnetic susceptibility as a priority and these values then used to constrain the numerical interpretation of the geophysical data and hence provide better understanding of the extent of the magnetite deposit and for drill targeting.

7.5 Conclusion

Magnetic data indicates a subsurface body of high magnetic susceptibility material at L13 but this is not matched by a corresponding positive residual gravity residual gravity anomaly. While numerical interpretation is affected by lack of constraints and hence significant ambiguity, it is considered unlikely that a large volume, high grade magnetite body exists at shallow depths at L13. Magnetite mineralisation is more likely present as small pods, veins or disseminated with an envelope of alteration.

References

Anonomous. "GRAVITY SURVEY CORRECTIONS." Retrieved May, 2015, from http://epsc.wustl.edu/~epsc454/grav-corrections.html.

Anonomous (1959). Magnetic survey of the Natone/Blythe River-Cuprona, and Highclere iron ore deposits, north-western Tasmania, Geoscience Australia, Canberra, A.C.T., Australia.

Anonomous (2005). "The historical development of the magnetic method in exploration." GEOPHYSICS 70(6): 33ND-61ND.

A., P. D., et al. (2014). "Remote remanence estimation (RRE)." Exploration Geophysics 45(4): 314-323.

Ahern, J. L. "International Gravity Formula." Retrieved May, 2015, from http://geophysics.ou.edu/solid_earth/notes/potential/igf.htm.

Baillie, P., et al. (1986). "Geological Atlas 1: 50 000 Series. Sheet 36 (8015N). St Valentines." Department of Mines Tasmania.

Banks, M. and P. Baillie (1989). "Late Cambrian to Devonian." Geology and Mineral Resources of Tasmania 15: 182-237.

Barrett, D. (1980). Geology, Mineralogy and Conditions of Formation of the Kara Scheelite skarn. Unpub, Honours thesis, Univ. of Tasm.: 194pp.

Bottrill, J. T. a. R. S. (2005). Devonian granites and associated mineralisation in northeast and northwest Tasmania. Tasmanian Geological Survey. M. R.
Tasmania.

Clark, D. (1997). "Magnetic petrophysics and magnetic petrology: aids to geological interpretation of magnetic surveys." AGSO Journal of Australian Geology and Geophysics 17: 83-104.

Clark, D. A. and D. W. Emerson (1991). "Notes on rock magnetization characteristics in applied geophysical studies." Exploration Geophysics 22(3):
547-555.

Collins, P. L. F. (1978). The geology and mineralisation of north-west Tasmania.
Geology and mineralizaton of NW Tasmania; a symposium; abstracts, Geological Society of Australia, Tasmanian Division and Specialist Group in Economic Geology, Hobart, Tasmania, Australia.

Corbett, K. and T. Lees (1987). "Stratigraphic and structural relationships and evidence for Cambrian deformation at the western margin of the Mt Read Volcanics, Tasmania." Australian Journal of Earth Sciences 34(1): 45-67.

Dando, N. and R. Tracey (2008) "Absolute Gravity Obsertvation at the National Measurement Institute." Record 2013/30, Geoscience Australia.

Duffett, M., et al. "Next generation 3D geological and geophysical modelling, West Tasmania." ASEG Extended Abstracts 2013(1): 1-4.

Emerson, D. W. (1986). "Physical properties of skarns." Exploration Geophysics 17(4): 201-212.

Emilia, D. A. and R. L. Massey (1975). "Magnetization-inclination estimation from prism-like anomaly profiles." GEOPHYSICS 40(3): 443-450.

Fotsyth, A. a. M., LR (2013). North West Tasmania Gravity Survey. GPCR2013_01, Atlas Geophysics Pty Ltd.

Gee, R. (1968). A revised stratigraphy for the Precambrian in north-west Tasmania.
Papers and Proceedings of the Royal Society of Tasmania.

Gee, R. and D. Groves (1971). "Structural features and mode of emplacement of part of the Blue Tier Batholith in northeast Tasmania." Journal of the Geological Society of Australia 18(1): 41-55.

Girdler, R. and G. Peter (1960). "An example of the importance of natural remanent magnetization in the interpretation of magnetic anomalies." Geophysical Prospecting 8(3): 474-483.

Gunn, P. and M. Dentith (1997). "Magnetic responses associated with mineral deposits." AGSO Journal of Australian Geology and Geophysics 17: 145-158.

Hyvönen, E., et al. (2012). Airborne geophysical, petrophysical and geochemical characteristics of Palaeoproterozoic black shale units in Finland: applications for exploration and environmental studies. Current Research: GTK Mineral Potential Workshop, Kuopio.

Jahren, C. E. (1963). "Magnetic susceptibility of bedded iron-formation." GEOPHYSICS 28(5): 756-766.

King, J., et al. (1982). "A comparison of different magnetic methods for determining the relative grain size of magnetite in natural materials: Some results from lake sediments." Earth and Planetary Science Letters 59(2): 404419.

Leaman, D. (2009). A New Crustal Gravity Model for Tasmania. Mantle-09, Leaman Geophysics.

Leaman, D. and R. Richardson (1989). "Production of a residual gravity field map for Tasmania and some implications." Exploration Geophysics 20(1/2): 181184.

Leaman, D., et al. (1980). "Tasmania—the gravity field and its interpretation." Unpubl. Rep. Dept. Mines Tasm 36.

Ltd, T. M. (2013). "Kara." Retrieved July, 2015, from http://mininglink.com.au/site/kara.

Morris, B., et al. (2007). "Magnetic remanence constraints on magnetic inversion models." The Leading Edge 26(8): 960-964.

NOAA (2015). "Magnetic Field Calculators." Magnetic Field Estimated Values. Retrieved July, 2015, from http://www.ngdc.noaa.gov/geomagweb/#igrfwmm.

Percival, P. c. (2014). Index of Airborne Geophysical Surveys. Canberra, Geoscience Australia. 14th ed.

Pratt, D. A., et al. The remote determination of magnetic remanence. ASEG Extended Abstracts 2012: 22nd Geophysical Conference: 1-5.

Roach, M. (1994). Terrain Correction. Fortran.

Roest, W. R. and M. Pilkington (1993). "Identifying remanent magnetization effects in magnetic data." GEOPHYSICS 58(5): 653-659.

Sawka, W. N., Heizler, M. T., Kistler, R. W., & Chappell, B. W. (1990). "Geochemistry of highly fractionated I-and S-type granites from the tintungsten province of western Tasmania." Geological Society of America Special Papers 246: 161-180.

Singoyi, B. and K. Zaw (2001). "A petrological and fluid inclusion study of magnetite–scheelite skarn mineralization at Kara, Northwestern Tasmania: implications for ore genesis." Chemical Geology 173(1–3): 239-253.

Solomon, M. (1981). "An introduction to the geology and metallic ore deposits of Tasmania." Economic Geology 76(2): 194-208.

Spry, A. (1957). "The Precambrian rocks of Tasmania, Part I-Dolerites of the North-West Coast." Papers and Proceedings of the Royal Society of Tasmania 91: pp. 81-96.

Spry, A., et al. (1962). "The Precambrian rocks." Journal of the Geological Society of Australia 9(2): 107-126.

Telford, W. M., et al. (1990). Applied geophysics, Cambridge university press.

Tracey, R., et al. AAGD07: A new absolute gravity datum for Australian gravity and new standards for the Australian National Gravity Database. ASEG Extended Abstracts 2007: 19th Geophysical Conference: 1-3.

Whitehead, C. (1974). Auger Hole Reports, Australia and New Zealand Exploration Co. L.13 Prospect: 116-134.

Williams, E., et al. (1989). Mid-Palaeozoic deformation, granitoids and ore deposits. Geology and Mineral Resources of Tasmania, Geological Society of Australia Special Publication 15. 15: 238-292.

Zaw, K. and B. Singoyi (2000). "Formation of magnetite-scheelite skarn mineralization at Kara, northwestern Tasmania; evidence from mineral chemistry and stable isotopes." Economic Geology and the Bulletin of the Society of Economic Geologists 95(6): 1215-1230.

Appendix A

Gravity survey data from L13.

Station No.	Date	Time	Reading (mGal)	Longitude	Latitude	Elevation (m)	Simple Bouguer Anomaly (mGal)
GRAVIMETER Scintrax CG-3 (2015)							

6000	7/4	14:29:00	3973.065	145.77318	-41.29027	511.69	-6.01956
1007	7/4	15:42:00	3972.745	145.77347	-41.29021	510.43	-6.47712
1008	7/4	15:58:00	3972.765	145.77349	-41.28977	512.02	-6.08167
1009	7/4	16:08:00	3972.030	145.77349	-41.28932	513.38	-6.49286
1010	7/4	16:15:00	3971.680	145.77290	-41.28931	518.63	-5.79941
1011	7/4	16:23:00	3972.230	145.77289	-41.28975	515.55	-5.88297
1012	7/4	16:31:00	3972.945	145.77288	-41.29021	512.63	-5.77149
6000	7/4	16:36:00	3972.880	145.77318	-41.29027	511.69	-6.01956
LOOP							
6000	8/4	9:19:00	3973.190	145.77318	-41.29027	511.69	-6.01956
1017	8/4	9:32:00	3970.610	145.77350	-41.28887	515.39	-7.74469
1018	8/4	9:38:00	3971.520	145.77291	-41.28885	520.39	-5.84667
1019	8/4	9:47:00	3971.965	145.77231	-41.28840	518.82	-5.66758
1020	8/4	9:58:00	3972.353	145.77172	-41.28794	517.14	-5.56712
1021	8/4	10:02:00	3972.280	145.77232	-41.28795	518.11	-5.44897
1022	8/4	10:11:00	3971.300	145.77292	-41.28796	521.81	-5.69917
1023	8/4	10:17:00	3971.160	145.77290	-41.28842	521.81	-5.87978
1024	8/4	10:23:00	3970.165	145.77351	-41.28842	524.10	-6.42303
1025	8/4	10:29:00	3969.295	145.77350	-41.28795	528.69	-6.34569
1026	8/4	10:36:00	3971.425	145.77351	-41.28751	520.46	-5.79432
1027	8/4	10:41:00	3972.285	145.77354	-41.28706	516.60	-5.65229
1028	8/4	10:45:00	3972.800	145.77293	-41.28706	515.36	-5.37891
1029	8/4	10:51:00	3971.905	145.77292	-41.28750	518.91	-5.61373
1030	8/4	10:58:00	3972.565	145.77234	-41.28750	516.64	-5.39831
1021	8/4	11:06:00	3972.295	145.77232	-41.28795	518.11	-5.41809
1032	8/4	11:14:00	3972.455	145.77171	-41.28840	517.73	-5.37139
1033	8/4	11:22:00	3971.950	145.77230	-41.28885	518.99	-5.66684
1034	8/4	11:27:00	3972.045	145.77230	-41.28929	517.91	-5.82238
1035	8/4	11:35:00	3972.230	145.77227	-41.28977	516.43	-5.96862
6000	8/4	11:40:00	3973.155	145.77318	-41.29027	511.69	-6.01956
LOOP							
6000	8/4	11:40:00	3973.155	145.77318	-41.29027	511.69	-6.01956
1037	8/4	12:17:00	3973.250	145.77346	-41.29067	508.36	-6.59282
1038	8/4	12:24:00	3973.760	145.77345	-41.29111	504.30	-6.91621
1039	8/4	12:31:00	3974.765	145.77345	-41.29157	498.12	-7.16435

1040	8/4	12:36:00	3976.590	145.77345	-41.29202	489.98	-6.97791

1041	8/4	12:41:00	3977.720	145.77343	-41.29247	485.13	-6.84009
1042	8/4	12:51:00	3978.090	145.77344	-41.29291	482.85	-6.95039
1043	8/4	12:59:00	3979.705	145.77342	-41.29338	475.36	-6.84771
1044	8/4	13:22:00	3981.200	145.77341	-41.29382	468.98	-6.63182
1045	8/4	13:30:00	3982.485	145.77337	-41.29427	462.07	-6.74092
1046	8/4	13:35:00	3983.975	145.77339	-41.29472	454.05	-6.86628
6000	8/4	13:50:00	3973.075	145.77318	-41.29027	511.69	-6.01956
LOOP							
6000	8/4	13:50:00	3973.075	145.77318	-41.29027	511.69	-6.01956
1048	8/4	14:09:00	3972.935	145.77227	-41.29020	512.71	-5.95167
1049	8/4	14:16:00	3971.755	145.77167	-41.29020	516.94	-6.29878
1050	8/4	14:24:00	3971.135	145.77170	-41.28974	519.14	-6.44466
1051	8/4	14:33:00	3971.410	145.77170	-41.28930	518.74	-6.20758
1052	8/4	14:40:00	3971.800	145.77170	-41.28884	518.07	-5.90803
1053	8/4	14:50:00	3972.280	145.77111	-41.28838	517.06	-5.58430
1054	8/4	14:55:00	3972.380	145.77113	-41.28793	516.63	-5.52819
1055	8/4	15:02:00	3972.490	145.77113	-41.28749	515.79	-5.54370
1056	8/4	15:08:00	3972.750	145.77115	-41.28705	515.26	-5.34802
1057	8/4	15:15:00	3972.675	145.77174	-41.28749	515.82	-5.35281
1058	8/4	15:20:00	3972.765	145.77173	-41.28704	514.76	-5.43038
1059	8/4	15:27:00	3972.980	145.77174	-41.28661	513.80	-5.36525
1060	8/4	15:35:00	3972.915	145.77235	-41.28705	514.56	-5.31896
1061	8/4	15:45:00	3972.915	145.77234	-41.28660	513.87	-5.41288
1062	8/4	15:51:00	3972.735	145.77293	-41.28660	514.15	-5.53779
1063	8/4	15:56:00	3972.315	145.77355	-41.28662	514.89	-5.81337
1064	8/4	16:03:00	3972.580	145.77356	-41.28617	511.89	-6.09747
1066	8/4	16:08:00	3972.835	145.77294	-41.28616	512.52	-5.71737
1068	8/4	16:15:00	3972.615	145.77235	-41.28615	512.90	-5.86199
1059	8/4	16:21:00	3972.975	145.77174	-41.28661	513.80	-5.36582
6000	8/4	16:53:00	3973.060	145.77318	-41.29027	511.69	-6.01956
LOOP							
6000	9/4	8:32:00	3980.370	145.77318	-41.29027	511.69	-6.01956
1007	9/4	9:10:00	3979.740	145.77347	-41.29021	510.43	-7.02449
1008	9/4	9:16:00	3980.360	145.77349	-41.28977	512.02	-6.07304
1011	9/4	9:21:00	3979.650	145.77289	-41.28975	515.55	-6.10300
1012	9/4	9:26:00	3980.310	145.77288	-41.29021	512.63	-6.07541

6000	9/4	9:30:00	3980.570	145.77318	-41.29027	511.69	-6.01956
LOOP							
6000	9/4	9:30:00	3980.570	145.77318	-41.29027	511.69	-6.01956
1088	9/4	9:49:00	3979.285	145.77108	-41.29019	518.76	-5.91044
1089	9/4	9:56:00	3979.415	145.77049	-41.29018	517.46	-6.03646
1090	9/4	10:00:00	3979.920	145.76990	-41.29018	515.93	-5.83240
1091	9/4	10:08:00	3980.600	145.76931	-41.28972	514.08	-5.47799
1092	9/4	10:21:00	3981.075	145.76930	-41.29018	511.53	-5.54843
1093	9/4	10:29:00	3982.410	145.76869	-41.29020	507.21	-5.06590
1094	9/4	10:36:00	3979.950	145.76810	-41.29016	520.07	-4.99338
1095	9/4	10:42:00	3979.380	145.76750	-41.29015	523.53	-4.88297
1096	9/4	10:53:00	3979.405	145.76810	-41.28970	522.42	-5.03878
1097	9/4	11:02:00	3979.025	145.76750	-41.28968	524.70	-4.96971
1098	9/4	11:11:00	3979.790	145.76811	-41.28926	520.12	-5.06872
1099	9/4	11:17:00	3980.430	145.76871	-41.28926	516.01	-5.23871
1100	9/4	11:24:00	3981.065	145.76870	-41.28971	513.96	-5.04937
1091	9/4	11:30:00	3980.665	145.76931	-41.28972	514.08	-5.42772
1102	9/4	11:37:00	3980.285	145.76931	-41.28927	515.57	-5.47479
1103	9/4	11:41:00	3980.050	145.76991	-41.28929	516.68	-5.49438
1104	9/4	11:49:00	3979.425	145.76990	-41.28973	519.23	-5.65810
1105	9/4	11:55:00	3979.225	145.77050	-41.28974	519.43	-5.82134
1106	9/4	12:01:00	3979.730	145.77050	-41.28937	518.43	-5.48126
1107	9/4	12:06:00	3979.355	145.77111	-41.28930	518.44	-5.84879
1108	9/4	12:11:00	3979.235	145.77110	-41.28973	518.88	-5.92082
6000	9/4	12:17:00	3980.600	145.77318	-41.29027	511.69	-6.01956
LOOP							
6000	9/4	12:17:00	3980.600	145.77318	-41.29027	511.69	-6.01956
1110	9/4	13:12:00	3979.955	145.77053	-41.28883	516.98	-5.87070
1111	9/4	13:17:00	3980.160	145.77051	-41.28837	516.78	-5.69926
1112	9/4	13:23:00	3980.420	145.77052	-41.28793	516.49	-5.49723
1113	9/4	13:29:00	3980.210	145.77055	-41.28748	514.90	-6.02081
1114	9/4	13:36:00	3980.460	145.76995	-41.28703	514.80	-5.79901
1115	9/4	13:45:00	3981.070	145.77054	-41.28703	515.33	-5.14470
1116	9/4	13:57:00	3980.865	145.77055	-41.28659	516.40	-5.18229
1117	9/4	14:05:00	3980.555	145.77058	-41.28613	516.93	-5.40251

1118	9/4	14:11:00	3980.860	145.76998	-41.28613	517.21	-5.08364
1119	9/4	14:17:00	3980.905	145.76935	-41.28612	516.46	-5.22516
1120	9/4	14:23:00	3980.990	145.76879	-41.28611	515.60	-5.34901
1121	9/4	14:28:00	3981.135	145.76818	-41.28611	514.82	-5.39221
1122	9/4	14:40:00	3978.570	145.76757	-41.28609	526.51	-5.73798
1123	9/4	14:49:00	3979.545	145.76756	-41.28656	522.88	-5.58000
1124	9/4	15:08:00	3981.540	145.76818	-41.28656	515.47	-5.17384
1125	9/4	15:16:00	3981.460	145.76877	-41.28656	514.57	-5.48454
1126	9/4	15:22:00	3980.880	145.76936	-41.28656	515.17	-5.98816
1127	9/4	15:28:00	3981.045	145.76995	-41.28658	515.58	-5.78592
1114	9/4	15:32:00	3981.515	145.76995	-41.28703	514.80	-5.53676
1129	9/4	15:46:00	3981.825	145.76995	-41.28747	514.51	-5.41846
1130	9/4	15:55:00	3981.450	145.76994	-41.28792	515.08	-5.78351
1132	9/4	16:00:00	3981.445	145.76935	-41.28792	515.92	-5.65582
1133	9/4	16:07:00	3981.325	145.76934	-41.28837	515.96	-5.85650
1134	9/4	16:19:00	3981.255	145.76992	-41.28837	516.94	-5.81612

1135	9/4	16:23:00	3981.260	145.76933	-41.28882	516.25	-6.01456
1136	9/4	16:27:00	3982.165	145.76993	-41.28881	516.57	-5.07346
6000	9/4	16:36:00	3982.370	145.77318	-41.29027	511.69	-6.01956
LOOP							
6000	9/4	16:36:00	3982.370	145.77318	-41.29027	511.69	-6.01956
1138	9/4	16:53:00	3984.850	145.77552	-41.28892	493.73	-6.95952
1139	9/4	16:59:00	3982.650	145.77621	-41.28646	505.35	-6.65493
1140	9/4	17:04:00	3983.820	145.77432	-41.28523	503.25	-5.79009
1141	9/4	17:09:00	3981.635	145.77198	-41.28458	514.39	-5.72826
1142	9/4	17:14:00	3982.615	145.76909	-41.28481	512.48	-5.14508
1143	9/4	17:19:00	3978.695	145.76707	-41.28360	508.83	-9.67715
1144	9/4	17:25:00	3985.790	145.76489	-41.28325	500.45	-4.20186
1145	9/4	17:29:00	3986.675	145.76248	-41.28346	500.60	-3.30803
1146	9/4	17:35:00	3987.545	145.76037	-41.28378	499.77	-2.63180
1147	9/4	17:40:00	3987.890	145.75798	-41.28325	496.24	-2.93472
1148	9/4	17:47:00	3982.720	145.76834	-41.28531	513.67	-4.86348
6000	9/4	17:56:00	3982.400	145.77318	-41.29027	511.69	-6.01956
LOOP							
6000	10/4	8:50:00	3973.275	145.77318	-41.29027	511.69	-6.01956

1156	10/4	9:00:00	3972.740	145.76752	-41.28926	520.78	-4.67124
1157	10/4	9:04:00	3972.825	145.76751	-41.28879	520.04	-4.68899
1158	10/4	9:11:00	3972.905	145.76755	-41.28836	519.43	-4.68596
1159	10/4	9:18:00	3973.045	145.76754	-41.28790	518.06	-4.77262
1160	10/4	9:26:00	3973.320	145.76756	-41.28746	517.44	-4.57584
1161	10/4	9:34:00	3972.495	145.76756	-41.28701	519.90	-4.87329
1162	10/4	9:41:00	3973.425	145.76814	-41.28746	516.75	-4.59995
1163	10/4	9:50:00	3973.370	145.76817	-41.28700	515.74	-4.80863
1164	10/4	10:00:00	3973.595	145.76876	-41.28701	514.87	-4.74993
1165	10/4	10:05:00	3973.365	145.76935	-41.28700	515.01	-4.95046
1166	10/4	10:19:00	3973.385	145.76933	-41.28747	514.35	-5.09558
1167	10/4	10:26:00	3973.475	145.76875	-41.28747	515.60	-4.75565
1162	10/4	10:32:00	3973.405	145.76814	-41.28746	516.75	-4.59629
1169	10/4	11:14:00	3974.170	145.76815	-41.28795	516.19	-3.96476
1170	10/4	11:25:00	3973.165	145.76875	-41.28791	516.06	-4.98641
1171	10/4	11:32:00	3973.020	145.76873	-41.28836	516.56	-5.07055
1173	10/4	11:41:00	3973.025	145.76873	-41.28882	516.67	-5.08048
1174	10/4	11:48:00	3973.135	145.76811	-41.28880	518.64	-4.57860
1175	10/4	11:54:00	3972.995	145.76815	-41.28836	518.79	-4.64718
6000	10/4	12:04:00	3973.185	145.77318	-41.29027	511.69	-6.01956
LOOP							
6000	10/4	12:04:00	3973.185	145.77318	-41.29027	511.69	-6.01956
1177	10/4	12:34:00	3977.360	145.75813	-41.28553	504.30	-2.87546
1178	10/4	12:38:00	3975.170	145.75851	-41.28664	514.47	-3.16287
1179	10/4	12:43:00	3974.725	145.76167	-41.28670	516.28	-3.25696

1180	10/4	12:48:00	3971.650	145.76207	-41.28943	531.92	-3.49999
1181	10/4	12:55:00	3971.535	145.76129	-41.29017	529.24	-4.20862
1182	10/4	13:00:00	3972.355	145.75770	-41.29016	525.73	-4.07882
1183	10/4	13:05:00	3970.705	145.75627	-41.29187	532.40	-4.56886
6000	10/4	13:20:00	3973.185	145.77318	-41.29027	511.69	-6.01956
GRAVIMETER Lacoste & Romberg G (2015)							
6000	22/4	9:30:00	3944.464	145.77318	-41.29027	511.69	-6.01956
1185	22/4	9:54:00	3943.780	145.77288	-41.29067	508.82	-7.30924
1186	22/4	10:20:00	3945.054	145.77229	-41.29069	508.63	-6.07757
1187	22/4	10:35:00	3944.191	145.77162	-41.29062	512.20	-6.23414

6000	22/4	10:43:00	3944.475	145.77318	-41.29027	511.69	-6.01956
LOOP							
6000	22/4	10:43:00	3944.475	145.77318	-41.29027	511.69	-6.01956
1188	22/4	11:09:00	3943.095	145.77106	-41.29062	517.59	-6.26813
1189	22/4	11:16:00	3942.916	145.77052	-41.29067	519.23	-6.12813
1190	22/4	11:29:00	3944.043	145.76988	-41.29061	514.84	-5.85927
1191	22/4	11:37:00	3945.423	145.76930	-41.29062	510.37	-5.35915
1192	22/4	11:46:00	3946.918	145.76870	-41.29060	505.19	-4.88026
1193	22/4	12:08:00	3944.401	145.76814	-41.29067	512.81	-5.90147
1194	22/4	12:17:00	3943.569	145.76747	-41.29058	520.22	-5.26740
1195	22/4	12:33:00	3943.653	145.76746	-41.29107	519.59	-5.34992
6000	22/4	12:47:00	3944.464	145.77318	-41.29027	511.69	-6.01956
LOOP							
6000	22/4	12:47:00	3944.464	145.77318	-41.29027	511.69	-6.01956
1196	22/4	13:35:00	3945.296	145.77286	-41.29112	505.28	-6.51101
1197	22/4	13:42:00	3945.823	145.77228	-41.29110	502.68	-6.49289
1198	22/4	13:50:00	3945.317	145.77164	-41.29110	506.31	-6.28176
1199	22/4	13:59:00	3943.685	145.77108	-41.29108	513.11	-6.57150
1200	22/4	14:07:00	3943.253	145.77049	-41.29107	516.57	-6.32078
1201	22/4	14:17:00	3944.422	145.76986	-41.29109	511.86	-6.07729
1202	22/4	14:31:00	3945.781	145.76930	-41.29108	508.09	-5.45499
1203	22/4	14:40:00	3946.707	145.76868	-41.29104	504.87	-5.15620
1204	22/4	14:51:00	3946.655	145.76811	-41.29104	504.44	-5.28980
1205	22/4	15:01:00	3944.527	145.76748	-41.29149	514.69	-5.43790
1206	22/4	15:24:00	3947.276	145.76816	-41.29148	500.40	-5.49436
1207	22/4	15:38:00	3946.707	145.76869	-41.29152	503.84	-5.38471
1208	22/4	15:48:00	3946.876	145.76927	-41.29154	502.57	-5.46604
1209	22/4	15:57:00	3946.623	145.76987	-41.29155	503.29	-5.57398
1201	22/4	16:09:00	3944.475	145.76986	-41.29109	511.86	-5.99301
1210	22/4	16:20:00	3945.675	145.77048	-41.29153	505.77	-6.02555
1211	22/4	16:30:00	3945.675	145.77108	-41.29152	505.74	-6.02920
1212	22/4	16:42:00	3947.086	145.77167	-41.29155	499.18	-5.90723
1213	22/4	16:50:00	3947.476	145.77224	-41.29156	496.22	-6.09962
1214	22/4	17:00:00	3946.054	145.77286	-41.29155	500.79	-6.61842

6000	22/4	17:08:00	3944.391	145.77318	-41.29027	511.69	-6.01956

LOOP							
6000	23/4	8:40:00	3944.496	145.77318	-41.29027	511.69	-6.01956
1215	23/4	8:59:00	3948.234	145.77285	-41.29199	490.52	-6.59118
1216	23/4	9:08:00	3948.613	145.77224	-41.29201	489.10	-6.49023
1217	23/4	9:20:00	3948.908	145.77163	-41.29201	488.88	-6.23269
1218	23/4	9:28:00	3947.960	145.77108	-41.29200	493.37	-6.29373
1219	23/4	9:39:00	3947.350	145.77042	-41.29197	496.19	-6.34135
1220	23/4	9:49:00	3948.445	145.76986	-41.29194	492.49	-5.96673
1221	23/4	9:56:00	3947.939	145.76925	-41.29200	496.66	-5.65526
1222	23/4	10:06:00	3947.107	145.76868	-41.29197	500.94	-5.63823
1223	23/4	10:15:00	3946.991	145.76806	-41.29193	501.47	-5.64064
1224	23/4	10:25:00	3944.917	145.76747	-41.29195	513.67	-5.31348
1225	23/4	10:33:00	3944.359	145.76746	-41.29241	517.35	-5.18548
1226	23/4	10:54:00	3947.192	145.76806	-41.29239	503.01	-5.16296
1227	23/4	11:06:00	3947.781	145.76866	-41.29238	496.23	-5.89971
1228	23/4	11:27:00	3949.771	145.76930	-41.29242	488.24	-5.47679
1229	23/4	11:36:00	3950.793	145.76981	-41.29243	480.84	-5.90785
1220	23/4	11:44:00	3948.392	145.76986	-41.29194	492.49	-5.96828
1230	23/4	11:56:00	3948.676	145.77049	-41.29245	488.73	-6.46453
1231	23/4	12:07:00	3949.656	145.77106	-41.29244	484.61	-6.28986
1232	23/4	12:15:00	3950.793	145.77165	-41.29245	477.24	-6.59995
1233	23/4	12:22:00	3951.330	145.77224	-41.29243	478.62	-5.78704
1234	23/4	12:29:00	3950.308	145.77281	-41.29245	481.74	-6.19364
6000	23/4	12:37:00	3944.391	145.77318	-41.29027	511.69	-6.01956
LOOP							
6000	23/4	12:37:00	3944.391	145.77318	-41.29027	511.69	-6.01956
1235	23/4	13:26:00	3951.667	145.77280	-41.29294	474.38	-6.30302
1236	23/4	13:35:00	3953.004	145.77224	-41.29293	468.42	-6.13358
1237	23/4	13:42:00	3953.173	145.77163	-41.29291	467.46	-6.14847
1238	23/4	13:51:00	3952.130	145.77109	-41.29289	472.12	-6.26859
1239	23/4	13:58:00	3952.056	145.77045	-41.29289	472.92	-6.18199
1240	23/4	14:11:00	3952.762	145.76984	-41.29287	471.44	-5.76124
1241	23/4	14:22:00	3951.246	145.76928	-41.29288	477.93	-5.99690
1242	23/4	14:37:00	3950.224	145.76865	-41.29283	488.47	-4.93437
1243	23/4	14:54:00	3946.907	145.76813	-41.29287	502.83	-5.42285
1244	23/4	15:03:00	3944.127	145.76745	-41.29285	518.14	-5.18590

1245	23/4	15:13:00	3944.864	145.76745	-41.29332	515.10	-5.08500
1246	23/4	15:27:00	3946.570	145.76806	-41.29332	504.33	-5.49127
1247	23/4	16:07:00	3948.940	145.76858	-41.29331	492.22	-5.48745
1241	23/4	16:21:00	3951.235	145.76928	-41.29288	477.93	-5.95861
1248	23/4	16:40:00	3952.446	145.76927	-41.29331	471.00	-6.14158
1250	23/4	17:06:00	3954.352	145.77043	-41.29333	461.21	-6.15243
1251	23/4	17:14:00	3953.668	145.77102	-41.29333	460.86	-6.90252

1252	23/4	17:21:00	3954.973	145.77163	-41.29337	455.67	-6.61809
1253	23/4	17:29:00	3953.657	145.77220	-41.29334	463.43	-6.40187
1254	23/4	17:37:00	3952.646	145.77284	-41.29334	467.50	-6.61021
6000	23/4	17:45:00	3944.264	145.77318	-41.29027	511.69	-6.01956
LOOP							
6000	24/4	8:58:00	3944.254	145.77318	-41.29027	511.69	-6.01956
1255	24/4	9:25:00	3953.962	145.77283	-41.29381	462.04	-6.39861
1256	24/4	9:31:00	3955.300	145.77227	-41.29379	454.67	-6.51084
1257	24/4	9:42:00	3953.078	145.77163	-41.29379	466.08	-6.48986
1258	24/4	9:52:00	3952.183	145.77106	-41.29379	472.97	-6.03172
1259	24/4	10:04:00	3952.636	145.77036	-41.29378	476.98	-4.78976
1260	24/4	10:19:00	3949.487	145.76985	-41.29378	487.65	-5.84140
1249	24/4	10:32:00	3951.562	145.76982	-41.29337	477.33	-5.76246
1261	24/4	10:46:00	3951.972	145.76925	-41.29374	475.41	-5.76400
1262	24/4	11:02:00	3948.750	145.76862	-41.29377	492.41	-5.64681
1263	24/4	11:14:00	3948.002	145.76804	-41.29375	497.06	-5.47963
1264	24/4	11:28:00	3945.675	145.76741	-41.29374	509.37	-5.38763
1265	24/4	11:46:00	3947.518	145.76803	-41.29419	500.64	-5.30491
1266	24/4	11:58:00	3947.560	145.76861	-41.29422	499.17	-5.55686
1267	24/4	12:17:00	3950.867	145.76926	-41.29426	483.28	-5.38227
1261	24/4	12:29:00	3951.951	145.76925	-41.29374	475.41	-5.79986
1268	24/4	12:43:00	3948.445	145.76983	-41.29421	492.85	-5.92128
1269	24/4	12:54:00	3951.783	145.77043	-41.29420	476.07	-5.88363
1270	24/4	13:03:00	3953.183	145.77102	-41.29424	470.48	-5.58863
1271	24/4	13:14:00	3951.709	145.77163	-41.29425	471.43	-6.87733
1272	24/4	13:31:00	3954.162	145.77219	-41.29422	456.61	-7.33888
1273	24/4	13:38:00	3955.984	145.77281	-41.29424	450.88	-6.64886
6000	24/4	13:51:00	3944.296	145.77318	-41.29027	511.69	-6.01956

LOOP							
6000	27/4	9:16:00	3944.327	145.77318	-41.29027	511.69	-6.01956
1274	27/4	9:42:00	3955.384	145.77279	-41.29469	453.14	-6.88664
1275	27/4	9:50:00	3953.088	145.77224	-41.29471	464.10	-7.03125
1276	27/4	10:00:00	3951.393	145.77158	-41.29472	475.55	-6.47935
1277	27/4	10:06:00	3952.109	145.77100	-41.29468	474.22	-6.02301
1278	27/4	10:17:00	3951.246	145.77044	-41.29468	477.25	-6.29372
1279	27/4	10:35:00	3947.971	145.76981	-41.29465	494.92	-6.09728
1280	27/4	10:47:00	3947.013	145.76925	-41.29467	500.17	-6.02864
1281	27/4	11:04:00	3947.939	145.76862	-41.29463	497.59	-5.61328
1282	27/4	11:17:00	3945.201	145.76804	-41.29466	511.00	-5.71899
1283	27/4	11:27:00	3948.266	145.76747	-41.29419	498.29	-5.11735
1284	27/4	11:39:00	3946.391	145.76742	-41.29466	505.80	-5.56103
1285	27/4	11:57:00	3945.222	145.76799	-41.29509	511.47	-5.65979
1286	27/4	12:29:00	3945.580	145.76745	-41.29513	510.68	-5.47332
1287	27/4	12:40:00	3945.507	145.76741	-41.29556	510.75	-5.57588

1288	27/4	12:54:00	3945.970	145.76803	-41.29555	507.52	-5.75186
1289	27/4	13:12:00	3948.097	145.76862	-41.29509	498.25	-5.41375
1290	27/4	13:23:00	3945.675	145.76921	-41.29513	507.53	-6.01829
1280	27/4	13:29:00	3947.118	145.76925	-41.29467	500.17	-5.98390
1291	27/4	13:50:00	3946.855	145.76979	-41.29513	500.83	-6.16574
1292	27/4	14:00:00	3950.308	145.77038	-41.29515	483.60	-6.10701
1293	27/4	14:14:00	3950.730	145.77099	-41.29514	481.34	-6.13493
1294	27/4	14:26:00	3951.783	145.77158	-41.29514	473.18	-6.69246
1295	27/4	14:33:00	3953.604	145.77220	-41.29515	462.86	-6.90460
1296	27/4	14:38:00	3954.721	145.77278	-41.29516	456.25	-7.09162
1297	27/4	14:43:00	3957.185	145.77341	-41.29517	446.30	-6.58818
6000	27/4	14:54:00	3944.454	145.77318	-41.29027	511.69	-6.01956
LOOP							
6000	27/4	14:54:00	3944.454	145.77318	-41.29027	511.69	-6.01956
1298	27/4	15:29:00	3954.310	145.77331	-41.29562	456.77	-7.43239
1299	27/4	15:35:00	3953.741	145.77276	-41.29561	461.00	-7.16513
1300	27/4	15:44:00	3951.772	145.77215	-41.29564	472.61	-6.84834
1301	27/4	15:50:00	3952.520	145.77159	-41.29561	471.37	-6.33995
1302	27/4	15:59:00	3949.150	145.77099	-41.29559	487.87	-6.45720

1303	27/4	16:12:00	3949.592	145.77038	-41.29557	486.50	-6.27832
1304	27/4	16:21:00	3948.087	145.76978	-41.29559	494.81	-6.14781
1305	27/4	16:47:00	3945.580	145.76916	-41.29557	508.01	-6.04320
1306	27/4	16:54:00	3946.886	145.76866	-41.29560	502.78	-5.76630
6000	27/4	17:22:00	3944.391	145.77318	-41.29027	511.69	-6.01956
LOOP							
6000	28/4	8:55:00	3944.412	145.77318	-41.29027	511.69	-6.01956
1074	28/4	9:19:00	3943.148	145.77111	-41.28885	517.61	-5.98531
1070	28/4	9:37:00	3943.843	145.77116	-41.28659	516.01	-5.39782
1072	28/4	9:44:00	3943.990	145.77118	-41.28614	514.73	-5.45925
1073	28/4	9:52:00	3943.959	145.77175	-41.28613	513.32	-5.76421
6000	28/4	10:06:00	3944.391	145.77318	-41.29027	511.69	-6.01956
LOOP							
6000	28/4	10:06:00	3944.391	145.77318	-41.29027	511.69	-6.01956
1308	28/4	10:27:00	3948.813	145.77442	-41.29072	482.14	-7.45297
1309	28/4	10:33:00	3953.836	145.77676	-41.29352	459.74	-7.08818
1310	28/4	10:40:00	3955.573	145.77721	-41.29235	453.45	-6.48319
1311	28/4	10:46:00	3957.290	145.77903	-41.29142	442.57	-6.82363
1312	28/4	10:54:00	3956.332	145.77894	-41.28979	448.10	-6.54929
1313	28/4	11:02:00	3951.309	145.77822	-41.28831	472.31	-6.67751
1314	28/4	11:09:00	3947.371	145.77617	-41.28851	491.32	-6.89395
1315	28/4	11:19:00	3953.583	145.77738	-41.29447	460.07	-7.36351
1316	28/4	11:32:00	3950.856	145.77624	-41.29571	474.17	-7.42861
1317	28/4	11:40:00	3951.182	145.77474	-41.29495	473.62	-7.14237
1318	28/4	11:46:00	3950.709	145.77635	-41.29434	474.26	-7.43755
1319	28/4	11:57:00	3947.055	145.77608	-41.28511	495.01	-6.18301
1320	28/4	12:07:00	3949.213	145.77882	-41.28503	484.60	-6.06684
1321	28/4	12:16:00	3946.044	145.77530	-41.28373	501.26	-5.84403
1322	28/4	12:22:00	3944.401	145.77281	-41.28409	511.84	-5.43759
6000	28/4	12:32:00	3944.401	145.77318	-41.29027	511.69	-6.01956

Correction factor of 1.053 has been multiplied to the Lacoste and Romberg readings for display in mGals.

Appendix B

Magnetic survey report from Rada Engineering Pty Ltd

GEOPHYSICAL SURVEY DATA REPORT

Date : 24 May 2015

This readme file describes the equipment and specifications of a geophysical airborne survey conducted by Thomson Aviation Pty. Ltd.

The readme also summarises the data processing parameters and procedures used.

CLIENT DETAILS

Company Flown by : Anton Rada Rada Engineering Pty. Ltd

Company Processed: Anton Rada Rada Engineering Pty. Ltd

Client : Lottah Mining Pty Ltd

Company Job : Thomson 14103

AIRBORNE SURVEY EQUIPMENT:

Aircraft : Multirotor UAV X4

Magnetometer : Fluxgate 3 axes

Magnetometer Resolution : +/- 0.15 nT

Magnetometer Compensation : Post Flight

Magnetometer Sample Interval : 20 Hz, Approx

Data Acquisition : Mike DAQ V1.0

Sensor Number : 845

GPS Navigation System : UBLOX L6 GPS Receiver

AIRBORNE SURVEY SPECIFICATIONS

Area: Hampshire Tasmania L13

Flight Line Direction : 090 - 270 degrees

Flight Line Separation : 25 metres

Tie Line Direction : 180 - 000 degrees

Tie Line Separation : 100 metres

Sensor Clearance : 20 metres (MTC)

Survey flown : May 2015

DATUM and PROJECTION

Datum : Geodetic Datum of Australia 94. GDA94

Projection : Map Grid of Australia. MGA

Zone : Zone 55

DATA PROCESSING : MAGNETIC DATA

MAGNETIC PROCESSING FLOW

The final magnetic data processing was performed using the following processing flow:

- Aircraft magnetic data QC
- Diurnal magnetic data QC
- System parallax removal
- Fluxgate scale, offste, orthogonality calibrations applied.
- Post flight magnetic compensation applied.
- Diurnal variation removal and addition of the mean diurnal base value
- IGRF removal and addition of mean IGRF value.
- levelling using polynomial Tie line levelling,
- Micro levelling if required
- Reduction to the pole.
- Gridding using Minimum Curvature algorithm

MAGNETIC QUALITY CONTROL

The processing of the magnetic data firstly involved the routine quality control in the field of both the aeromagnetic and diurnal data during the acquisition phase. Any data found not meeting the required specifications were reflown.

MAGNETIC PARALLAX CORRECTION

The total magnetic intensity aircraft data was firstly corrected for the effects of system parallax. The parallax parameters were determined and checked from the results of opposing

test line flights.

MAGNETIC DIURNAL CORRECTION

The base station magnetometer data was edited and merged into the main database. The aeromagnetic data was corrected for diurnal variations by subtracting the observed magnetic base station deviations. There were no magnetic storms recorded by the diurnal monitoring station during the survey. The mean value was then added back to the data.

MAGNETIC IGRF CORRECTION

The data was corrected for the regional gradient of the International Geomagnetic Reference

Field (IGRF). The IGRF was calculated for every point along the lines with respect to GPS height using the IGRF Model for 2010 with secular variation applied. The mean IGRF value was then added back to the data.

MAGNETIC PROFILE LEVELLING

The magnetic traverse line data was then statistically levelled from the tie line data using Intrepid polynomial levelling. The steps involved in the tie line levelling were as follows:

- A primary tie line was chosen as a reference tie.
- All other ties were levelled to this tie line using 1st degree polynomial adjustment.
- lines were adjusted individually to minimize crossover differences, using 2nd degree polynomial adjustments.

Any residual flight line effects were removed using Intrepid micro levelling techniques and the resultant line data saved as a separate field.

MAGNETIC GRIDDING

The data was gridded to a cell size of 20% of line spacing using a Spline algorithm.

For further information on the data processing please contact:

Anton Rada at radaengineering@dodo.com.au directly.
